INVESTIGATION OF THE IMPACT OF AGGREGATE SEGREGATION ON RUTTING RESISTANCE OF ASPHALT CONCRETE

A THESIS SUBMITTED TO
THE GRADUATE SCHOOL OF NATURAL AND APPLIED SCIENCES
OF
MIDDLE EAST TECHNICAL UNIVERSITY

BY

AYHAN ÖNER YÜCEL

IN PARTIAL FULFILLMENT OF THE REQUIREMENTS
FOR
THE DEGREE OF DOCTOR OF PHILOSOPHY
IN
CIVIL ENGINEERING

MAY 2019

Approval of the thesis:

INVESTIGATION OF THE IMPACT OF AGGREGATE SEGREGATION ON RUTTING RESISTANCE OF ASPHALT CONCRETE

submitted by **AYHAN ÖNER YÜCEL** in partial fulfillment of the requirements for the degree of **Doctor of Philosophy in Civil Engineering Department, Middle East Technical University** by,

Prof. Dr. Halil Kalıpçılar
Dean, Graduate School of **Natural and Applied Sciences** ________________

Prof. Dr. Ahmet Türer
Head of Department, **Civil Engineering** ________________

Prof. Dr. Murat Güler
Supervisor, **Civil Engineering, METU** ________________

Examining Committee Members:

Prof. Dr. İsmail Özgür Yaman
Civil Engineering, METU ________________

Prof. Dr. Murat Güler
Civil Engineering, METU ________________

Prof. Dr. Mustafa Şahmaran
Civil Engineering, Hacettepe University ________________

Assist. Prof. Dr. Hande Işık Öztürk
Civil Engineering, METU ________________

Assist. Prof. Dr. Elif Çiçek
Civil Engineering, Hacettepe University ________________

Date: 09.05.2019

I hereby declare that all information in this document has been obtained and presented in accordance with academic rules and ethical conduct. I also declare that, as required by these rules and conduct, I have fully cited and referenced all material and results that are not original to this work.

Name, Surname: Ayhan Öner Yücel

Signature:

ABSTRACT

INVESTIGATION OF THE IMPACT OF AGGREGATE SEGREGATION ON RUTTING RESISTANCE OF ASPHALT CONCRETE

Yücel, Ayhan Öner
Doctor of Philosophy, Civil Engineering
Supervisor: Prof. Dr. Murat Güler

May 2019, 212 pages

In this study, effect of aggregate segregation on rutting resistance of asphalt concrete is investigated using laboratory compacted specimens. A procedure to determine inhomogeneity level is proposed using 2-dimensional cross section images of asphalt concrete specimens. A redistribution algorithm is developed to assess the aggregate distribution characteristics and inhomogeneity index of the cross sectional images. In order to simulate field conditions, specimens are produced in two different groups: (i) with the same compaction effort and (ii) at the same density corresponding to 4% air void. Unbiased and segregated specimens at two levels are produced for each group using the Superpave gyratory compactor. Repeated creep test is conducted to measure rutting resistance of specimens. Digital images are then produced using a flatbed scanner from the vertical cut sections taken at midpoint of the test specimens. Generated images are processed and analyzed for the analysis of aggregate distribution to compute the specimens' inhomogeneity levels. The prepared specimens are classified according to their inhomogeneity test results as homogenous, medium level segregated and high level segregated. A number of parameters characterizing the rutting performance of specimens are calculated and the results are statistically analyzed for possible relationships with the inhomogeneity level of the test specimens.

Results of statistical analyses show that flow number and loading cycles at 5% permanent deformation are highly correlated with the computed inhomogeneity levels. The outcomes of the study indicate that aggregate segregation significantly affects the rutting resistance of asphalt concrete specimens and the proposed image based method can successfully determine the inhomogeneity level of specimens.

Keywords: Inhomogeneity Index, Asphalt Mixture Segregation, Digital Image Processing, Rutting Resistance, Repeated Creep Test

ÖZ

AGREGA SEGREGASYONUNUN ASFALT BETONU TEKERLEK İZİ DİRENCİNE ETKİSİNİN İNCELENMESİ

Yücel, Ayhan Öner
Doktora, İnşaat Mühendisliği
Tez Danışmanı: Prof. Dr. Murat Güler

Mayıs 2019, 212 sayfa

Bu çalışmada, agrega segregasyonunun asfalt betonu tekerlek izi direncine etkisi laboratuvarda sıkıştırılan numuneler kullanılarak incelenmiştir. Segregasyon seviyesinin, asfalt beton numunelerin iki boyutlu kesit görüntüleri kullanılarak belirlenmesini sağlamak için bir yöntem önerilmiştir. Agrega dağılım karakteristikleri ve kesit görüntüleri segregasyon indeksinin değerlendirilmesi için bir yeniden dağıtma algoritması geliştirilmiştir. Saha koşullarını simüle edebilmek için iki farklı grupta numuneler üretilmiştir: (i) aynı sıkıştırma enerjisi uygulayarak ve (ii) %4 hava boşluğuna karşılık gelen yoğunlukta. Superpave yoğurmalı pres kullanılarak her bir grup için ön koşulsuz ve iki seviyede segregasyona uğramış numuneler üretilmiştir. Daha sonra, numunelerin tekerlek izi direncini ölçmek için tekrarlı sünme deneyi yapılmıştır. Test numunelerinin orta noktasından alınan düşey kesitlerden, masaüstü tarayıcı kullanılarak dijital görüntüler elde edilmiştir. Numunelerin segregasyon seviyesini hesaplamak için, üretilen görüntüler işlenmiş ve agrega dağılımını belirlemek amacıyla analiz edilmiştir. Hazırlanan numuneler, segregasyon test sonuçlarına göre homojen, orta seviye segrege ve yüksek seviye segrege olarak sınıflandırılmıştır. Numunelerin tekerlek izi performansını karakterize eden çok sayıda parametre hesaplanmış ve sonuçlar, numunelerin segregasyon seviyesi ile

muhtemel ilişkileri için istatistiksel olarak analiz edilmiştir. İstatistiksel analiz sonuçları, akma yükleme sayısı ve %5 kalıcı deformasyona karşılık gelen yükleme sayısının hesaplanan segregasyon seviyeleri ile yüksek derecede ilişkili olduğunu göstermektedir. Çalışmanın sonuçları, agrega segregasyonunun asfalt betonu tekerlek izi direncini önemli derecede etkilediğini ve önerilen görüntü tabanlı metodun numunelerin segregasyon seviyelerini başarılı bir şekilde belirleyebildiğini göstermektedir.

Anahtar Kelimeler: Segregasyon İndeksi, Asfalt Karışımı Segregasyonu, Dijital Görüntü İşleme, Tekerlek İzi Direnci, Tekrarlı Sünme Deneyi

To my family

ACKNOWLEDGEMENTS

Foremost, I would like to express my sincere gratitude to my supervisor Prof. Dr. Murat Güler for his guidance, advice, endless patience and insight throughout the research.

Besides my advisor, I would like to thank the rest of my thesis committee: Prof. Dr. İsmail Özgür Yaman, Prof. Dr. Mustafa Şahmaran, Asst. Prof. Dr. Hande Işık Öztürk and Asst. Prof. Dr. Elif Çiçek for their help, valuable advices and insightful comments.

I want to thank my dear friends Yalçın Karakaya, Oruç Altıntaşı, Reza Shabani, Başak Varlı Bingöl, Farshad Kamran, Laleh Sorkhi, Ömer Can Pamuk and Meltem Tangüler Bayramtan for their friendship and support. I also want to thank METU Transportation Laboratory technician Ahmet Sağlam for his support during my experiments.

Last but not least, I would like to thank my family for supporting me throughout my life.

TABLE OF CONTENTS

APPENDICES

LIST OF TABLES

TABLES

LIST OF FIGURES

FIGURES

LIST OF ABBREVIATIONS

2D : 2-dimensional

3D : 3-dimensional

AC : Asphalt Concrete

AASHTO : American Association of State Highway and Transportation Officials

ASTM : American Society for Testing and Materials

CCD : Charge-Coupled Device

CDF : Cumulative Distribution Function

DIP : Digital Image Processing

dpi : Dot Per Inch

ESAL : Equivalent Single Axle Load

FN : Flow Number

LVDT : Linear Variable Displacement Transducer

MAPE : Mean Absolute Percentage Error

NCHRP : National Cooperative Highway Research Program

SGC : Superpave Gyratory Compactor

SHRP : Strategic Highway Research Program

Superpave : Superior Performing Asphalt Pavements

TIFF : Tagged Image File Format

TGDH : Turkish General Directorate of Highways

VFA : Voids Filled with Asphalt

VMA : Voids in Mineral Aggregate

LIST OF SYMBOLS

E **:** Expected aggregate area

$\boldsymbol{\mathcal{E}_p}$ **:** Permanent Strain

k **:** Number of macro blocks positioned within section image

n **:** Number of aggregate size fractions

O **:** Observed aggregate area

p **:** Area fraction

$\boldsymbol{P_e}$ **:** Normalized percent retaining

$\boldsymbol{P_f}$ **:** Excluded particle percentage from the image analysis

$\boldsymbol{P_i}$ **:** Retaining percentage calculated in the image analysis

r **:** Representative aggregate area

$\boldsymbol{T_{eff}}$ **:** Effective rutting test temperature

CHAPTER 1

INTRODUCTION

1.1. Background

Aggregate segregation can occur during the mixture production and construction phase of asphalt concrete pavements. Past studies indicate that mixture's inhomogeneity due to segregation has a major impact on the service performance of asphalt concrete pavements (Cross & Brown, 1993; Khedaywi & White, 1995; Gardiner & Brown, 2000; Cross et al., 1998; Peng & Sun, 2009; Sun, 2016). Asphalt concrete pavements produced from segregated mixtures are highly prone to reduced performance life and increased distresses due to early degradation in mechanical performance. Previous studies show that segregation results in a decrease in the fatigue life, moisture resistance, indirect tensile strength and unit weight of asphalt concrete. It also increases the maintenance costs by requiring frequent rehabilitation of pavements. Field experiences indicate that segregation occurs as a result of non-uniform distribution of coarse and fine aggregates during batching, mixing and compaction operations. In addition to asphalt concrete pavements, segregation can also be a critical factor for laboratory samples used to determine mixture performance properties. It is well known that specimens produced from segregated mixtures can lead to high variability or even incorrect outcomes in performance tests causing serious deficiencies in the structural design of pavements. It should be expected that poor performance prediction is almost inevitable when the mixture mechanical properties do not meet the specification requirements due to mixture related problems such as aggregate segregation developed during the production stage of asphalt concrete. Therefore, determination of the degree of inhomogeneity for both laboratory and field cored samples is important not only for quality control/quality assurance of the produced mixture but also for the service life prediction of asphalt concrete pavements.

Inhomogeneity of asphalt mixtures is evaluated based on distribution of its components which are aggregate, binder and air void. Aggregates are the major component of the asphalt mixture and control the distribution of other constituents. Aggregate distribution is generally used to test inhomogeneity of mixtures although some studies have been conducted to evaluate air void distribution in asphalt mixture specimens. There are a number of methods proposed to evaluate asphalt mixture segregation in the field. Nondestructive methods such as permeability and nuclear density measurements and destructive methods such as asphalt content, gradation and density measurements have been used for many years; however, image based segregation analysis methods are also widely used nowadays parallel to the development in digital imaging technologies. Many studies have been conducted to characterize microstructure of asphalt concrete using 2-dimensional (2D) cross sectional images because it is more practical and cost effective to use 2D images as compared to 3-dimensional (3D) imaging methods. Besides, 2D methods have been proved to produce results that are comparable to the those of 3D analyses. Even though the techniques to study mixture inhomogeneity using digital imaging technology have increased significantly in recent years, none of these studies, however, proposed a method to quantify the overall mixture segregation based on statistical distribution of aggregates coupled with aggregate shape parameters extracted from the digital image analysis of aggregate particles. Since aggregate segregation is related to the quality of manufacturing process for asphalt mixtures, determination of segregation level in an effective manner is one of the popular topics of research area in the microstructural characterization of asphalt concrete.

Segregation in the field and its effect on the performance have been investigated extensively so far; however, studies about segregation in laboratory compacted specimens and the effect of segregation on the mechanical performance are limited and more in-depth studies are necessary to understand the micro-structure of segregated mixtures. Several studies conducted on laboratory compacted specimens show that segregation has an important effect on the mechanical performance of asphalt concrete. The outcome of these studies proved that variability in the mechanical test results is increased by high level of segregation while it is decreased with better homogeneity of mixtures. The type of mechanical test performed is also important, so that the selected test procedure can reflect the influence of specimen segregation on mechanical performance. A mechanical test that is sensitive to aggregate distribution such as simple performance tests should be selected for this purpose. To obtain segregated specimen in the laboratory, combining fine and coarse fractions with different percentages and placing the portions to the mold in layers are applied in sequence before starting the performance tests.

1.2. Research Objectives

The objectives of this research can be summarized as follows:

(1) Develop a method to evaluate aggregate segregation in asphalt concrete based on 2-dimensional cross sectional images.

(2) Assess the effect of inhomogeneity on rutting resistance of asphalt concrete specimens using the proposed inhomogeneity test method.

Using the image analysis and rutting test results on laboratory compacted specimens, the proposed method to identify inhomogeneity will be verified. It is also aimed that the effect of parameters describing the rutting resistance will be investigated using laboratory specimens prepared as homogenous and segregated during the fabrication process.

It is expected that the outcome of this study will be utilized in future studies to enlighten the relationship between cross sectional structure of mixture and its performance under loading. The procedures developed in the scope of this study can be easily used to assess aggregate distribution characteristics of field cored and laboratory compacted asphalt mixture specimens. The developed index enables one to determine the inhomogeneity level of mixtures without any personal judgement or empirical approach. In this way, it will be possible to identify the source of variability introduced to the results of performance tests whether by testing operator or due to mixture's inhomogeneous structure.

1.3. Scope

The thesis study was conducted in two main phases. In the first phase, an index was developed to evaluate asphalt mixture inhomogeneity based on 2D cross sectional images. For this purpose, four different design mixtures were produced by varying aggregate type and gradation at two levels in the laboratory. The test samples were prepared using the Superpave gyratory compactor with a 150 mm diameter mold. Specimens were produced from the compacted samples by cutting in three vertical sections using a diamond saw and sectional images were obtained from the three surfaces using a flatbed scanner. To convert the sectional images into binary images, a series of image processing techniques was implemented. After the image binarization, image based gradation estimations were implemented based on an appropriate aggregate shape parameter. To see aggregate distribution characteristics and assess change in the inhomogeneity index under different aggregate distribution combinations, an aggregate redistribution algorithm was developed. This algorithm detects all particles in a cross section and then the particles are spatially redistributed with random locations and orientations to obtain synthetic cross sectional images. The proposed inhomogeneity index describes the homogeneity level of specimen's cross section based on percent rating between zero for complete homogeneity and 100% for complete segregation condition. Using the developed redistribution algorithm, cumulative distribution functions were generated for the inhomogeneity indices of synthetic images, and thus it was possible to determine the inhomogeneity levels statistically. Using the developed redistribution algorithm, inhomogeneous synthetic images were generated by restricting the coarser aggregates from upper half of the section. This way, the power of the proposed inhomogeneity test was calculated statistically.

In the second phase of the study, two groups of specimens were produced: (i) specimens compacted under the same gyration effort (group-1) (equal compaction energy) and (ii) specimens compacted at the same density corresponding to 4% air void (group-2). Three sets of specimens were prepared for each group to simulate different levels of segregation. Unbiased homogenous and segregated (biased) specimens at two levels were produced in the laboratory and then repeated creep tests were conducted to measure the rutting resistance of specimens. The unbiased specimens were prepared as homogenous as possible and the biased specimens were segregated intentionally using special laboratory procedure at medium and high levels. The repeated creep tests were implemented and the results were processed to obtain the important test parameters for rutting resistance. After the testing, digital images were obtained from the vertical cut sections taken at midpoint of the test specimens and inhomogeneity levels were determined accordingly by using the proposed image based method. Finally, rutting test parameters and inhomogeneity levels were analyzed together to assess possible relationships between them. In this way, classification of specimens according to their inhomogeneity levels was achieved and the outcomes for each segregation level were analyzed to reveal the accuracy of the proposed method. In the final step, the effect of segregation on the rutting resistance of asphalt concrete specimens was determined.

1.4. Outline of Research

Chapter 2 presents a literature review relevant to researches on image based microstructural characterization and asphalt mixture segregation. There are three main topics discussed in this chapter. The first topic includes the microstructural characterization of asphalt mixtures and previously proposed image based homogeneity test methods. The second topic deals with the necessary tools and methods of digital image processing used in the study. In this section, basic image processing operations and some important filters are discussed. The final topic explains Superpave mix design basics and the details of the repeated creep test.

Chapter 3 presents the details of the proposed inhomogeneity index. The image processing steps are described and the details of aggregate redistribution algorithm are presented. Statistical analysis for the power of the proposed method is also given in this chapter.

Chapter 4 covers the specimen preparation and the repeated creep test details. In this this chapter, steps for the preparation of two groups of asphalt mixture specimens with 3 different segregation levels are explained. Material properties and the design details are discussed in detail. Volumetric results of unbiased and biased (medium and high level segregated) specimens for both groups are illustrated. Repeated creep test setup and specimen preparation in accordance with specification requirements are explained. Finally, the repeated creep test results are analyzed and discussed in this chapter.

Chapter 5 covers the image analysis of tested specimens and determination of inhomogeneity levels of all specimens. Inhomogeneity levels s are determined by using the proposed method. In this chapter, rutting test results and inhomogeneity levels are also evaluated together to discuss possible relationships between inhomogeneity and rutting resistance.

Chapter 6 includes conclusions and future recommendations for the study.

CHAPTER 2

LITERATURE REVIEW

2.1. Introduction

This chapter presents a review of literature on two dimensional image based microstructural characterization of asphalt concretes. Previously proposed homogeneity test methods are discussed in terms of weak and strong points. Digital image processing (DIP) techniques used to characterize asphalt mixtures are reviewed in detail. The studies conducted about effect of inhomogeneity on mechanical performance of asphalt concrete are also summarized. In the final section, Superpave mix design method and the repeated creep test are explained.

2.2. Microstructural Characterization of Hot Mix Asphalt

One of the first studies to characterize asphalt mixture microstructure was conducted by Yue et al. (1995). The authors performed digital image processing analyses to quantify orientation, distribution and shape of the aggregates in asphalt concrete mixtures. Cut sections taken from asphalt mixture specimen in horizontal and vertical directions were scanned using a flatbed scanner to obtain 2-dimensional (2D) digital images. To determine aggregate boundaries, a manual technique was adopted as the image analysis software did not give satisfactory segmentation result for the mixture components. The analyses conducted using vertical and horizontal cross section images showed that major axis of the aggregates have a tendency of lying horizontally within the mixture's cross sections. Using ferret diameter as a shape parameter, actual gradation was predicted by using the area of particles. The actual gradation curve was predicted successfully by eliminating particles smaller than 2 mm due to the fact that smaller size fractions were difficult to extract accurately from the cross section images. They concluded that the gyratory compactors can produce specimens with uniformly distributed coarse aggregates as compared to Marshall compactors and roller compactors.

Masad et al. (1999) proposed several parameters to measure aggregate orientation, aggregate gradation and air void distribution in asphalt mixtures. In this study, computer automated image analysis procedures were implemented to determine the parameters characterizing the evolution of internal structure of asphalt concrete mixtures during laboratory and field compaction. X-ray tomography images were generated to determine air void distribution of cored samples.

Using imaging technology, the capability of Superpave gyratory compactor to simulate the microstructure of asphalt pavements and the effect of different field compaction patterns on the internal structure were investigated by Tashman et al. (2001). Computer automated image analysis techniques and X-ray CT images were used for the evaluation of aggregate and air void distribution. They found that the internal structure of the asphalt pavements can be simulated by changing the gyration angle and specimen height in the Superpave gyratory compactor. In parallel with the developments in the imaging technologies and the processing techniques, many other studies have also been conducted on internal structure characterization and homogeneity testing that are summarized in the following sections.

2.3. Determination of Aggregate Shape Parameters and Gradation Based on 2D Images

After obtaining sectional images from the cut surfaces of asphalt mixture specimens and converting the images into binary format, the next step is to determine of aggregate shape parameters for microstructural characterization and estimating aggregate size distribution for the further analyses. Some of the aggregate shape parameters used in the previous studies can be counted as particle area, perimeter, center coordinate, major axis length, minor axis length, maximum ferret diameter, major axis orientation, etc. Summation of the pixels available within particle boundary is defined as particle area and summation of the boundary pixels of a particle is named as perimeter. The maximum Feret diameter is the length of the longest line connecting two border points on the particle perimeter.

In previous studies, a number of parameters have been used for the analysis of particle size distribution using the sectional images of asphalt concrete specimens. Yue et al. (1996) used minor axis length, ferret diameter and major axis length parameters to predict aggregate gradations based on the two dimensional cross section images of asphalt concrete samples. The particles with at least 2 mm ferret diameter were included in the gradation analysis. Vertical and horizontal cross section images were obtained from specimens using a flatbed scanner. The results of this study showed that aggregate particles on the horizontal cross sections are greater than those on the vertical sections.

Masad et al. (1999) used the Feret diameter as a shape parameter to predict coarse aggregate gradation based on 2D vertical sectional images. Feret diameter is defined as the equivalent circle diameter with the same area as the aggregate. Only for particles with Feret diameter of 4.75 mm or higher were considered in the analysis. Superpave gyratory compacted specimen were cut into three vertical sections and only two specimens were used for the gradation analysis. The results produced acceptable results for the coarse aggregate gradation.

By applying geometrical transformation to cross sectional images, major and minor axis of the ellipse were determined by Bruno et al. (2012). The method assumes that the minor axis of ellipse corresponds to the diameter of a particle. Three horizontal slice faces for each cored specimen were obtained using a diamond saw blade. In their study, four core samples were analyzed to find the size distribution of aggregate particles. Results of analyses indicate that there are small differences exist between the actual and the estimated gradations.

Moon et al. (2015) used equivalent circle diameter as a shape parameter to estimate the aggregate gradation. The resolution of images was set to 720 dpi and this resolution allowed particle detection as small as 0.075 mm. The diameter of each particle was calculated using the particle areas. To conduct gradation analysis, 60 images for each set of samples were used. The digital pictures of small beams were captured using a flatbed scanner. A total of 20 mixtures with different nominal maximum aggregate sizes and three percentages of reclaimed asphalt pavement were evaluated. The actual and estimated size distributions were compared statistically. The estimation results were successful for coarse particles for particles larger than 4.75 mm. However, poor estimations were obtained for aggregates smaller than 2.38 mm.

Adhikari et al. (2013) used average polygon diameter as a shape parameter to determine aggregate gradation based on the cross section image of asphalt mixture specimens. Wu et al. (2011) used Feretmeter as a shape parameter. Feretmeter is equivalent circle diameter and this shape parameter can be calculated using aggregate area in a section. Different aggregate shape parameters were compared to determine the particle size distribution of aggregates from cross sectional images of concrete specimens by Ozen & Guler (2011). Six different mix designs with different aggregate types, gradation and maximum aggregate sizes were prepared for this study. Specimens cut into 4 equal pieces using a circular diamond saw and three cut sections were obtained for each specimen. A desktop type flatbed scanner was used and the resolution of the scanner was set to 150 dpi. The available shape parameters in the literature for the image based particle size distribution were compared in this study. These selected parameters were particle area, maximum Feret diameter, equivalent circle diameter and equivalent ellipse major axis. Particle area is the summation of pixels within the aggregate boundary. Maximum Feret diameter is the longest line that connect two border points. Equivalent circle diameter is the diameter of a circle having the same area as aggregate particle. Equivalent ellipse major axis is the length of an ellipse with the same area and the same perimeter as the aggregate. After the necessary image processing operations on cross section images, passing aggregates for each sieve were determined for all mentioned parameters using the standard and the diagonal sieve sizes. Because of the resolution limitation, particles smaller than 2.38 mm were not included in the analysis, hence a correction was applied to the results of particle analyses. According to the statistical tests conducted, maximum Feret diameter resulted in the best approximation to the actual gradation. The use of diagonal sieve opening together with the maximum Feret diameter were suggested by the authors.

2.4. Available Indices for Homogeneity Testing

Inhomogeneity of aggregates within asphalt mixture specimen occurs during batching, mixing, placement and compaction processes. Aggregates with different size fractions may not be mixed thoroughly; therefore, it can result in fine and coarse aggregate agglomerations in the compacted asphalt mixtures. When segregation occurs, coarse and fine particles are concentrated in different regions of mixture (Khedaywi & White, 1996).

There are some methods to evaluate asphalt mixture inhomogeneity based on digital images of cross sections obtained from asphalt concrete samples in the literature. Asphalt concrete comprises of three phases: aggregate, asphalt binder and air void. Aggregates constitute the major part of asphalt mixture, so that asphalt mixture homogeneity mostly depends on aggregate distribution. Most of the studies in the literature have measured inhomogeneity level based on the aggregate distribution. Homogeneity tests were conducted based on the frequency of particles, the distances between center of particles and the area of particles. Each group of indices represents different physical property of tested materials. The frequency-based indices evaluate concentration of components in the image area. The distance-based indices evaluate spatial distribution of particles. The amount of material is measured using the area-based methods (Azari, 2005). The available methods to measure inhomogeneity are discussed in the following part.

2.4.1. Random Quadrat Test

In general, the quadrat test is used to measure homogeneity based on a frequency-based statistic (Cressie, 1992). The test statistic is developed based on the number of aggregate centroids located in each quadrat. This index has been utilized to evaluate homogeneity of asphalt mixture specimens based on section images (Masad et al., 1998).

To implement the proposed procedure, each specimen is cut three vertical slices with equal intervals as shown in Figure 2.1. The method does not include aggregates smaller than 2.36 mm. The centroids of aggregates which is larger than 2.36 mm are determined. Square quadrats are located randomly in the cross section a hundred times. Quadrat length and the small dimension of the cross section ratio of 1/30 is used in the study. The number of aggregates in each quadrat positioning is recorded. The frequency distribution of the number of aggregates in each quadrat is compared with a Poisson' distribution. The high level deviation from a Poisson distribution shows non-uniformity.

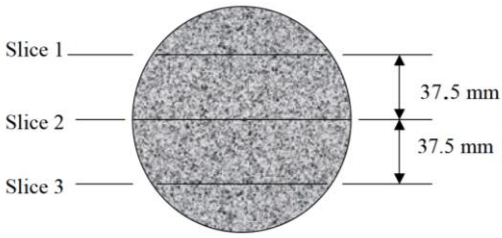

Figure 2.1. The cut positions for random quadrat test (Azari, 2012)

For a specimen, the homogeneity index is calculated using three slice faces as shown Equation 2.1.

$$S_r = \frac{1}{3}\sum_{i=1}^{3}\frac{s_i^2}{x_i} - 1 \qquad (2.1)$$

Where s_i^2 is the variance, and x_i is the mean frequency of the one hundred quadrats on the ith slice face.

The one of the most important disadvantages of this method is that a very small quadrat size is used for homogeneity testing. In some cases, aggregate size may be greater than the quadrat size. The other drawback is that the quadrats are positioned within a cross section randomly, hence estimated frequency may not represent the population because of the sampling of the small portion of slice faces. Generally, this method is not recommended for well-graded aggregates.

2.4.2. Quartered Quadrat Test

Quartered quadrant test measures the variations in the mean aggregate diameters in the four quadrants of the specimen slice face (Masad et al., 1998). Similar to random quadrat test, specimens are cut to obtain three slice face with 37.5 mm intervals (Figure 2.1). The location and the size of each aggregates which are greater than 2.36 mm are detected. To implement the test, each vertical section image is divided into four rectangular quadrats. Mean aggregate diameters are calculated for each quadrant. The average and the standard deviation of the mean aggregate diameters on four quadrants are calculated. The coefficient of variation is calculated four each slice face then the segregation index is equal to the average of the coefficient of variations of the three slices.

In this method, the quadrat locations are known, so that segregation patterns in the cross section can be detected. Because the average and the standard deviation of the aggregate diameters are known, the variation in aggregate size in each quarter can be determined. In the random quadrat test, all cross sections may not be sampled by quadrats due to random positioning; however, the quadrants completely cover the slice face in quartered quadrat test.

The most important drawback of this method is that there is no critical value to distinguish homogeneity and inhomogeneity conditions. Also, because of the averaging of the diameters, the variation in diameters within each quadrat is lost.

2.4.3. C_V Quadrat Test

N panels with the same sizes are placed over the specimen middle section and the number of aggregates in each panel positioning is determined in C_V quadrat test (McCuen & Azari 2001). The mean and the standard deviation of number of particles are counted for the N panels. The coefficient of variation (C_V) which is equal to the ratio of the standard deviation to the mean is used as the test statistic. To determine the decision criterion, a Monte Carlo simulation is used to determine distributions of test index for homogenous and inhomogeneous specimens. The power of the test depends on the panel size and panel number. Accuracy of the test rises with the higher number of panels and the larger panel size. The most important advantage of this method is that the measured statistic can be compared with the critical values obtained from simulations. Because of random positioning, form of inhomogeneity cannot be determined. Also, the entire cross section may not be sampled due to the randomly positioning of quadrats.

2.4.4. Eccentricity Test

To measure vertical inhomogeneity using the horizontal section images of asphalt concrete specimens, eccentricity test was proposed by Yue et al. (1995). The eccentricity index is calculated for each cross section, which is equal to the ratio of the distance between the center of aggregates and the geometric center of the horizontal section image. The center of aggregates and geometric center should coincide in a completely homogenous section and there should be no variation between the eccentricity values in vertical section images. The disadvantage of this study is that even if eccentricity value is equal to zero, fine or coarse aggregates packing at the specific region in the mixture might happen.

2.4.5. Moment of Inertia Test

This test evaluates vertical homogeneity of asphalt mixture specimens based on horizontal section images (Yue, et al. 1995). This index uses the moment of inertia of aggregates and the moments of inertia with respect to x and y axes that should be equal in all cross sections for an ideal homogenous distribution. Similar to the eccentricity test, even if the moment of inertia with respect to x and y is equal, fine or coarse aggregates packing might still happen.

2.4.6. Runs Test

The runs test is used to evaluate vertical homogeneity of asphalt mixture specimens (McCuen & Azari, 2001). In this test, the vertical slice faces are divided horizontal layers with equal thicknesses and the number of aggregates in each layer are counted. For a homogenous specimen, each layer is expected to contain the same number of particles. To determine inhomogeneity level, the overall median frequency is compared with the frequency in each layer. The disadvantage of this method is that the size of aggregates is not taken into account.

2.4.7. Average Depth Test

The average depth test was developed to evaluate vertical inhomogeneity by McCuen and Azari (2001). This method detects all particles by considering size fractions and then the distance between the top of specimen and the center of specimen is measured and mean distances are saved for each size fraction. The means are expected to equal to zero for a homogenous specimen. Both sizes and locations are considered in this method.

2.4.8. Nearest Neighbor Distance Test

This method was proposed for the evaluation of vertical homogeneity by McCuen and Azari (2001). The face of the middle slice of specimen is divided into upper and lower halves and the average distance between the nearest neighbor particles located on each half are computed. In this method, the means should be equal in both halves for the better homogeneity.

2.4.9. Inner-Outer Average Diameter

To measure radial inhomogeneity, this method was proposed by Tashman et al. (2001). The diameter of particles in the inner and the outer part of section are compared (Figure 2.2). Particles smaller than 2.36 mm are not included in the analyses. To conduct this study, three vertical slice faces for each specimen are used. The most important weakness of this method is that the test cannot distinguish top or bottom concentration of the coarse particles.

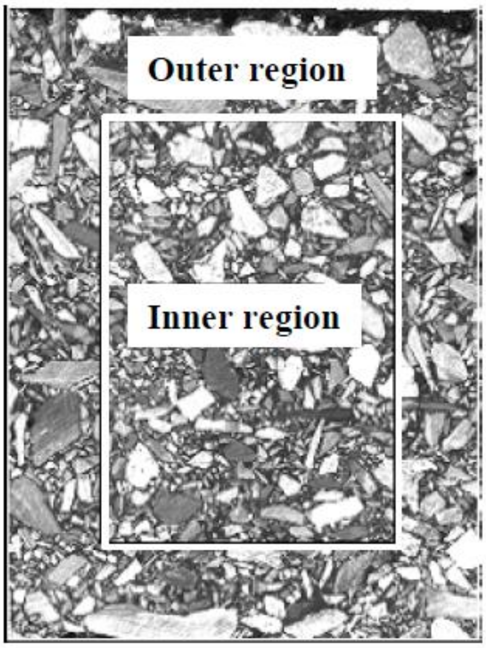

Figure 2.2. Inner-outer regions for the average diameter test (Tashman et al., 2001)

2.4.10. Index Proposed by Peng and Sun

Peng and Sun (2009, 2011) conducted studies to investigate asphalt mixture homogeneity index using digital image processing. In the scope of this study, authors developed and categorized a homogeneity index and they evaluated the main factors affecting the homogeneity index. The proposed method measures an overall homogeneity of a specimen in addition to horizontal and vertical homogeneities by using multiple sectional images. According to their study, aggregate gradation, asphalt content, compaction effort and experiment temperature have effects on the computed index value.

In their method, the frequency of aggregates within a specific area and distances between the centers of aggregates are considered. The first parameter in the index is the distance related a coefficient that is calculated by comparing the geometrical center of a specimen and the center coordinates of aggregate particles retained on the corresponding sieve. It is assumed that the center of aggregates retained on the same sieve should coincide with the geometry center of cross section in a homogenous section. The second parameter is about frequency of aggregates determined by dividing cross section into four sectors and counting the number of aggregates retained on each sieve in each sector is counted. For the perfect homogeneity case, each sector should contain the same number of aggregates retained on the same sieve. The index of homogeneity of a cross section was calculated combining these two parameters. Because each size fraction has a different effect on homogeneity, an area coefficient was also adapted to the index. To determine the homogeneity of the asphalt specimen, horizontal and vertical cross sections were considered. Three vertical and three horizontal slice faces were used for the index calculations. They also classified the index of homogeneity according to the degree of segregation. The segregation classes were determined as no segregation, low, medium and high level segregation.

2.4.11. Visual Particle Cross Sectional Area (VSA) Test

Hunter et al. (2004) proposed the visible particle cross sectional area (VSA) method to evaluate the segregation of laboratory compacted asphalt concrete samples. The cross sectional images were taken using a digital camera and then the weighted circumferential orientations were calculated for various particle area ranges. In that study, two different segregation types were considered which are sector based (radial segregation) and inner-outer regions based (regional segregation). Horizontal surface images were used for both segregation testing.

2.4.12. Aggregate Area Ratio (AR) Test

Zhang et al. (2017) developed indices to evaluate the aggregate distribution uniformity of asphalt concrete. Horizontal slice faces of asphalt concrete cores were used for the uniformity testing. Horizontal section and sample homogeneity were tested based on the distribution of coarse aggregates. The horizontal sectional CT image was divided into four quarter regions and coarse aggregate ratio was used for the evaluation. In this study, the coarse aggregates were determined as particles larger than 2.36 mm diameter. The coarse aggregate area ratio AR is equal to the ratio of coarse aggregate area to the specimen sectional area.

In the scope of the study three indices were proposed which are D_H, D_{V1} and D_{V2}. D_H is the horizontal uniformity coefficient and it measures the variation of coarse aggregate area ratio in the four quarter regions of a specimen section. D_{V1} is the vertical uniformity coefficient and it evaluates the coarse aggregate distribution in vertical direction of asphalt concretes. D_{V1} is determined using different sectional images of one core sample. D_{V2} also measures the vertical uniformity by using different approach. The coarse aggregate composition proportion (SCA) was used in this index. The most important disadvantage of this method is that the indices do not take into account the gradation distribution in sections and specimens.

2.4.13. Indices Developed by Azari (2005)

Several statistical test indices were proposed to test vertical and radial homogeneity by Azari (2005) by following six steps of hypothesis testing. The main purpose of the hypothesis testing is the comparison of the sample value and population value. The distributions of the test statistics for homogeneity and inhomogeneity conditions were determined for evaluation.

The first step of the hypothesis test was the formulation of null hypothesis and thus the null hypothesis and the alternative hypothesis were formed based on the aggregate shape or distribution properties and they reflect the homogeneity and inhomogeneity. The next step was to determine the test method, which computes the test statistic and its distribution. Here, the power of the test statistic is critical since it is expected that the test should detect the homogeneity and the inhomogeneity cases. The third and the fourth steps were determined as the level of significance to estimate the test statistic. The region of rejection and the test statistic were defined in the fifth step. In the final step, the test statistic was compared with the critical value and the null hypothesis was accepted or rejected.

In the literature, there are also indices developed to evaluate vertical and radial homogeneity of asphalt concrete samples. The summary of the test methods used to determine vertical and radial homogeneity is given below.

-*Vertical segregation based on horizontal section images*

The proposed test was adopted from statistical tests. The Chi-square and t-test were done for aggregate frequencies. The t-test was also conducted for aggregate areas and mean nearest neighbor distances. Geometric properties of coarse aggregates in the lower and upper portions of the specimens are compared to compute test statistic. The difference between the aggregate properties in the lower and upper parts of the specimen was evaluated using the statistical test. Locations of the cut sections are given in the Figure 2.3.

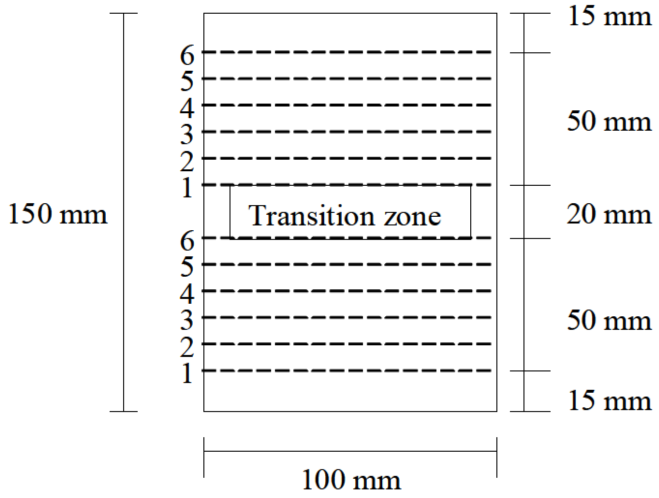

Figure 2.3. Horizontal cut section positions (Azari, 2005)

Six slices from the upper part and six slices from the lower part were taken for the testing as shown in the figure. The statistical test parameters were obtained from these cut sections and tests were conducted to assess difference between the upper and the lower portions.

-*Vertical segregation based on vertical section images*

To assess vertical inhomogeneity, the vertical section images of the specimens were divided into two regions as the upper and the lower portions. Statistical testing was conducted to see the difference between aggregate properties in these portions. The four vertical slices for both sides of the middle slice were taken with 10 mm intervals as shown in Figure 2.4.

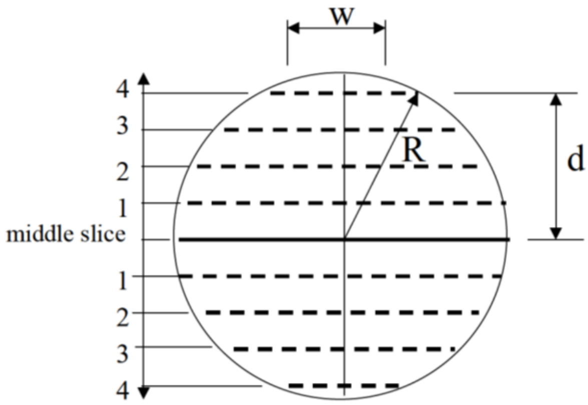

Figure 2.4. Vertical cut section positions (Azari, 2005)

where, R is equal to 50 mm. To test vertical inhomogeneity, the vertical slice faces of the specimens were divided into two portions as the upper and the lower potions. The statistical testing was conducted to see the difference between the aggregate distribution properties in these portions. A total of eight vertical slices were used for the testing.

-*Three layer vertical segregation based on horizontal section images*

To measure gradual vertical inhomogeneity this test was suggested. Three groups of horizontal slices were used. The aggregate distribution properties in the bottom, middle and top portions were compared in this method.

-*Radial segregation based on horizontal section images*

The aggregate properties in two portions of the horizontal section images which are the ring and core were compared. Three horizontal sections were used for each specimen.

-Radial segregation based on vertical section images

The vertical section of the specimen was divided into regions as center and ring to test homogeneity. The aggregate shape properties in the center and the ring portions were compared.

2.5. Air Void Homogeneity in Asphalt Mixtures

In addition to the uniformity of aggregate distribution, air void distribution and the effect of distribution characteristics on performance of asphalt mixtures have been studied by many researchers. The motivation behind the investigation of air void distribution is that air void distribution in asphalt concrete is critical for the pavement distresses such as rutting and fatigue cracking (Thyagarajan et al., 2008). Air void distribution in asphalt concrete specimens was generally determined based on the x-ray computed tomography (CT) images in the previous studies (Hu et al., 2012; Masad et al., 1999). The detection of air void in 2D cut section images is difficult because color variation is lost between bitumen phase and aggregate by filling of the voids during the cutting process with dust or mud.

One of the first studies on microstructural characterization of asphalt concrete using image analysis was carried out by Masad et al. (1999). To measure aggregate orientation, gradation and air void distribution, parameters were proposed in this study. X-ray tomography images were used for the characterization of air void distribution. The top and bottom 5 mm of a specimen was not included the analyses to prevent the effect of surface voids. Superpave gyratory compactor was used to produce specimen for the analyses. The result of the study indicated that air void distribution in vertical direction is uniform at low gyrations; however, when the number of gyrations is increased, air void content of the middle section becomes lower indicating further compaction. The laboratory measurements of air void were consistent with X-ray tomography-based measurements. The void distribution in the specimens was non-uniform and voids were concentrated at the top and the bottom of the gyratory compacted specimens.

Hu et al. (2012) conducted a study to evaluate the homogeneity of asphalt mixture based on the air void distribution. In this study, images were obtained via x-ray CT and vertical air void distributions and aggregate gradations were assessed using virtually cut slice images. This study also examined the effect of compaction level using the Superpave gyratory compactor on the homogeneity, and thus in the scope of the study specimens were compacted at 45, 60 and 75 gyrations. Homogeneity was evaluated by comparing the air void distribution and aggregate gradation in different cut sections to find out if they are close or not. It was determined that the air voids are much higher on the top and bottom ends of the sample, and the air voids are lower in the middle part of the sample. Also, it was emphasized that high uniformity improves the air void homogeneity. When the compaction level increases, gradations at different cut slices within a specimen becomes very close to each other. This study shows that there is close relationship between air void distribution and the aggregate distribution at different cut sections of a specimen.

Thyagarajan et al. (2010) investigated the effect of different Superpave gyratory compactors and specimen preparation on air void distribution. Also, the influence of air void distribution on mechanical performance was discussed. Similar to the previously mentioned study, x-ray CT was utilized for the image acquisition. To evaluate the air void distribution in lateral and vertical directions, a heterogeneity index was developed. In this study, four different Superpave gyratory compactors were used and specimens were produced with different diameters and heights. Cores with 100 mm diameter and 150 mm height were taken from the specimens for mechanical testing. The dynamic modulus and the static creep tests were conducted to evaluate heterogeneity effect on performance. According to the uniformity test results, air void distribution along the vertical and lateral directions were non-uniform. Air void heterogeneity in the lateral direction was higher. The dynamic modulus test did not affect the heterogeneity indices; however, the compactor type and the specimen preparation affected the dynamic modulus values significantly. The variations among the replicates were very high in the static creep test, indicating insignificant factors in the statistical analyses.

2.6. Effect of Asphalt Mixture Inhomogeneity on Mechanical Performance

Inhomogeneity of asphalt mixture can have a critical role in the mechanical performance in addition to service life of asphalt concrete (AC) pavements (Cross & Brown, 1993; Cross et al., 1998; Khedaywi & White, 1995; Gardiner and Brown, 2000; Peng & Sun, 2009). Previous studies show that mixture segregation during the fabrication process can considerably decrease the service life of AC pavements due to deterioration in mechanical performance of AC, i.e., fatigue resistance, tensile strength, etc. (Cross & Brown, 1993; Cross et al., 1998). Superpave mixture design method is widely used and specimens are mostly prepared by using Superpave gyratory compactor for the mechanical testing. If segregation occurs during the mixing and compaction process of laboratory compacted specimens, the mechanical tests may give unreliable results. The use of inhomogeneous specimens in the volumetric and mechanical tests also result in incorrect pavement layer designs. Therefore, in addition to the asphalt concrete in the field, homogeneity of laboratory prepared specimens is important for the better performance prediction and correct pavement design.

To assess effect of segregation on performance of hot mix asphalt, a study carried out by Cross and Brown (1993). The authors tried to determine tolerable segregation level, before the raveling occurs. For this research, five different pavements were used and the raveling degree was determined by conducting the sand patch test. As expected, the raveled regions had more surface voids. The degree of segregation was determined based on the aggregate amount passing from the No.4 sieve. The field and laboratory experiments showed that when the variation in the percent passing from the No. 4 is larger than 10%-12%, it can result in significant raveling. The study showed that asphalt content and density in the segregated areas of a pavement are lower than average values of the pavement. On the contrary, if fine aggregates concentrated in a region, the region will have lower air void content and higher asphalt content and these conditions cause rutting and flushing (Cross & Brown, 1993; Williams et al., 1996). Another study conducted by Cross et al. (1998) investigated moisture sensitivity, fatigue life and indirect tensile strength of the field cores taken from segregated and non-segregated areas of four recently constructed pavements. Similar to the previous study, difference between the percent passing No. 4 in segregated and non-segregated sections was used to determine the degree of segregation. Asphalt content, nuclear gage unit weight, core unit weight and macro texture were used to measure segregation. The results showed that asphalt content is the best sign of segregation. Macro texture was determined as the best nondestructive indicator of segregation. To predict pavement performance, core unit weight was suggested as the best parameter. The authors defined four levels of segregation based on the asphalt contents, gradations and air void of the field cores and thus samples were prepared in a laboratory to simulate the four levels of inhomogeneity. The conducted laboratory test indicated that segregation result in a decrease in the fatigue life, moisture resistance, indirect tensile strength and unit weight of asphalt mixture; however, an increase was observed in permeability of asphalt mixtures as a result of segregation. Segregation has more effect on the coarse graded mixtures.

Khedaywi and White (1995) proposed methods to simulate segregation in asphalt mixture. To simulate asphalt mixture segregation, fine and coarse fractions were combined with different percentages and four artificially segregated mixtures and one design control mixture were fabricated in the laboratory. U.S. Corps of Engineers gyratory testing machine and a laboratory linear compactor were used for the compaction. Stability index, compatibility index, rutting potential, moisture susceptibility was determined for each aggregate combination. Results showed that inhomogeneity affects the gradation, stability index, unit weight, air voids, compatibility index, asphalt content, moisture susceptibility, indirect tensile strength and rutting potential of asphalt concrete mixtures.

Because of the rotational movement of the Superpave gyratory compactor, radial inhomogeneity occurs in the specimens. The effect of inhomogeneity on shear properties of asphalt mixture specimens were investigated by Azari et al. (2005). The result indicated that the permanent strain decreases when the level of inhomogeneity increases.

Effect of various level of gradation segregation on warm mix asphalt were evaluated by Li et al. (2018). With one control gradation and six segregated gradations, a total of seven samples were compacted in the laboratory. The S value was defined as the deviation from the design gradation and it shows segregation level. The corresponding S values was selected as lower than 10%, 10-20%, 20-35% and larger than 35%. Three levels were selected for coarse aggregate segregation and three levels were determined for fine aggregate segregation. Binder contents corresponding to each gradation was calculated based on equal asphalt film thickness principle. Coarser aggregate segregation lead to high air void content and low asphalt content. Therefore, coarser aggregate segregation was more prone to moisture damage. Finer gradations result in rutting susceptible mixtures and low temperature cracking performance of the finer gradation was better than coarser gradations. The control gradation gave best result for the indirect tensile strength.

Peng and Sun (2017) investigated effect of horizontal aggregate homogeneity on indirect tensile test of asphalt mixture specimens and a discrete element model to predict indirect tensile (IDT) results was also developed. A proposed index was used to assess aggregate distribution in 2D horizontal cross sections. Results indicated that the correlation between the horizontal aggregate distribution and the average splitting strengths and average maximum horizontal stresses is insignificant. However, there is a significant correlation between aggregate distribution and maximum horizontal stresses and the variations in the splitting strengths. Another study conducted by Peng and Sun (2016) indicated that there is a good correlation between vertical aggregate homogeneity and the variation of penetration strengths. Effect of aggregate homogeneity on the indirect tensile strength was investigated by using three dimensional discrete element models (Peng et al., 2017). Results showed that there is no correlation between specimen homogeneity and IDT strength. On the other hand, the correlation between homogeneity and the variation in the IDT strength was significant.

2.7. Simulation of Asphalt Mixture Segregation in Laboratory

To assess the effects of aggregate segregation on asphalt mixture properties, some techniques were proposed to produce segregated specimens in a laboratory. Khedaywi and White (1995) proposed a laboratory method to simulate asphalt mixture segregation. To produce segregated asphalt mixture specimens, fine and coarse fractions of the design gradation were combined with different percentages and four artificially segregated mixtures and one design control mixture were fabricated in laboratory. The design aggregate combination was sieved over a 10 mm sieve to obtain the coarse and fine fractions. The percentages of the coarse and fine material to obtain the segregated mixtures at different levels are shown in Table 2.1.

Table 2.1. *Combination of coarse and fine fractions*

Mix. No.	**Segregation Type**	**Material Percentage**	
		Retained on 10 mm	**Passing from 10 mm**
1	Very fine	0	100
2	Fine	24	76
3	Mix design	48.3	51.7
4	Coarse	74	26
5	Very coarse	100	0

Mixtures were proportioned for 1200 g aggregate and the US Corps of Engineers Testing Machine was used to compact the mixtures. To conduct Purwheel tracking device test, the weights of mixtures were arranged according to target slab size and more aggregates were used to reach same volume for the fine segregation cases.

Li et al. (2018) designed six trial segregated gradations in addition to the design gradation to compare mechanical properties. In this way, properties of warm mix asphalt (WMA) with different segregation levels could be evaluated. To fabricate segregated specimens, gradations that deviates from the control gradation were calculated and the deviation from the control gradation was defined as the degree of segregation. To measure difference between segregated and the control gradations, S value was used. The S value was given as shown in Equation 2.2.

$$S = \sqrt{\sum_{i=1}^{n}(P_{ij} - P_{aj})^2} \tag{2.2}$$

where, n=number of size fractions and P_{ij} and P_{aj}=percent passing of the segregated and the control gradations, respectively. Four levels of segregation were defined that are no segregation, low level segregation, medium level segregation and high level segregation. The corresponding S values were determined as smaller than 10%, 10-20%, 20-35% and larger than 35%, respectively. Optimum asphalt content was determined according to the target air void for the control gradation. For the segregated gradations, asphalt contents were determined according to the principle of equal thickness of asphalt membrane.

To prepare vertically inhomogeneous asphalt mixture specimens, Haleh (2005) modified the method proposed by Khedaywi and White (1995). The design gradation was separated into two potions over the no.4 sieve as the coarser and finer portions. The coarser gradation was created by blending 75% of the coarser portion and 25% of the finer portion and the finer gradation was created by blending 25% of the coarser portion and 75% of the finer portion. Combination of the coarser and finer gradations were equal to the design gradation. In this study, the mixture with coarser gradation was placed on the lower part of the specimen and the mixture with finer gradation was used for the upper part of the specimen. The optimum binder contents for coarser and finer mixtures were calculated using theoretical calculations and the workability of the mixtures. Sum of the asphalt contents of the finer and coarser portions was equal to design asphalt content. The homogenous specimens were compacted to reach target air void with 4.85% optimum asphalt content; however, optimum asphalt content was calculated as 3.5% and 6.4% for the coarser and finer portions, respectively.

2.8. Digital Image Processing

2.8.1. Introduction

An image is defined as a two dimensional function f(x,y) by Gonzales and Woods, 2002. In this function, x and y are spatial coordinates within an image frame. The amplitude of f at any coordinates (x,y) is named as the gray level or intensity of the image at selected point. Both of these variables are distinct, so image function is digitized before the processing step. A digital image has a finite number of elements called as pixel and each element has a specific intensity and location. Figure 2.5 shows representation of a physical image via a rectangular array. Each pixel has a brightness value and it represents an actual physical image at the corresponding point and this convention operation is named as digitalization.

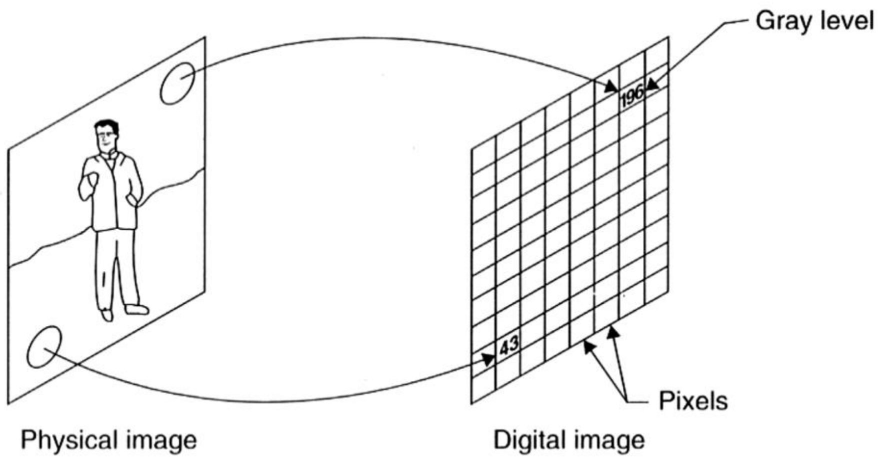

Figure 2.5. A physical image and digitalized image (Castleman, 1996)

Summary of fundamental steps in digital image processing are depicted below (Figure 2.6). These steps are acquisition of the image, preprocessing, segmentation, representation / description, and recognition / interpretation.

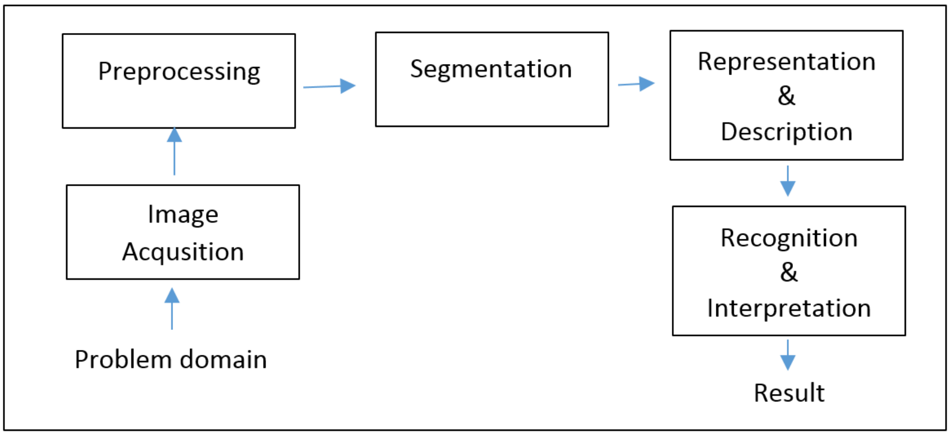

Figure 2.6. Fundamental steps in DIP

First, a digital image should be produced using a CCD camera, scanner or X-Ray tomography. After acquiring the image, the preprocessing phase is applied to improve the image for the success of subsequent processes. Most widely used preprocessing steps are contrast enhancing and noise removal. Segmentation step is conducted to partition an image into its components. To extract the specific features which are basic for differentiating objects, the representation and the description operations are implemented. Image recognition and interpretation steps mean assigning labels to objects and assigning meaning to those labels. In the below section operations used in this study are discussed briefly.

2.8.2. Image Acquisition

The digital image processing starts with transferring the images to the computer memory. Two essential components of the image acquisition are image acquisition device (imaging sensor) and frame grabber which converts the sensor based signal into digital format (Gonzalez & Woods, 2001). The acquisition can be carried on using various types of techniques like scanners, cameras, tomography and optical microscopy.

Flatbed scanners are economical and functional option to acquire images. The working principles of the CCD camera and flatbed scanner are similar. An entire image is captured at once in the CCD camera. However, single row of photosites is moved from the upper edge and moves down across the image by capturing rows in the scanner. The electrical signal produced by imaging sensor is converted into a digital image by the frame grabber. The produced image can be stored and processed by the computer. The working principle of the flatbed scanner is shown schematically in Figure 2.7.

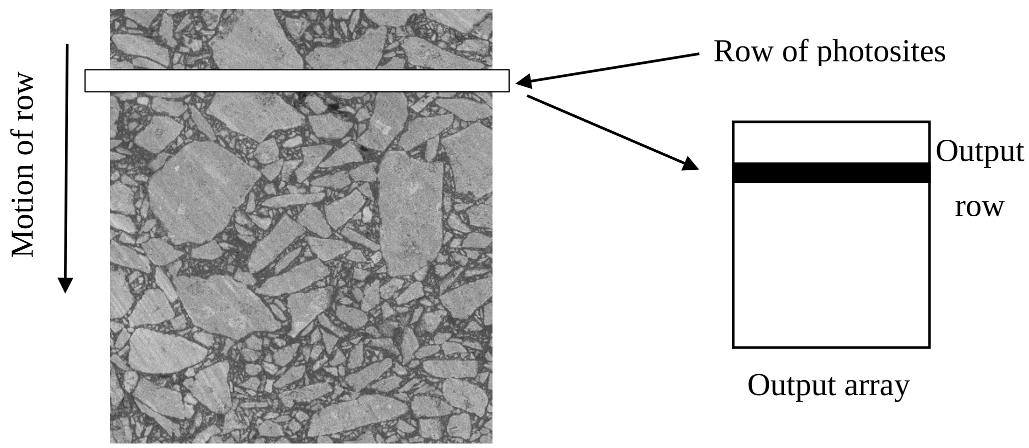

Figure 2.7. Image capturing using a CCD scanner (McAndrew, 2004)

The scanner is useful to obtain 2D surface images of objects. In this study, a flatbed scanner was, therefore, used because it is functional, economical and easy to use for capturing 2D cross sectional images.

The obtained images can be stored using different file formats such as portable network graphics (PNG), joint photographic experts group format (JPEG), tagged image file format (TIFF) and Bitmap (BMP). TIFF format is widely used in the different fields. TIFF uses lossless compression and images can be edited and resaved without any loss in the image quality. Because of advantages of TIFF format, this file format was used in this study.

2.8.2.1. Image Coding

After the image acquisition step, the next step is storing the image in a computer memory. Image coding refers to storing the captured image in the computer memory. The origin (0,0) is located at the bottom left corner in the traditional coordinate system; however, the spatial reference origin (0,0) is located at the top, left corner of the image. Captured image with M rows and N columns can be presented in the array format as the following:

$$f(x,y)=\begin{bmatrix} f(0,0) & f(0,1) & \cdots & f(0,N-1) \\ f(1,0) & f(1,1) & \cdots & f(1,N-1) \\ \dots & \dots & & \dots \\ f(M-1,0) & f(M-1,1) & \cdots & f(M-1,N-1) \end{bmatrix} \tag{2.3}$$

The right side of Equation 2.3 refers to a digital image. Each element of this matrix shows the magnitude of a pixel. The origin of the image is at the upper left corner. In grayscale images, brightness of each pixel is defined by a numerical value between 0 and 255, being 0 as black and 255 as white. A color image can also be represented by three dimensional arrays with Red, Green and Blue layers.

2.8.2.2. Spatial Resolution

Smallest visible detail in an image depends on its spatial resolution. In other words, spatial resolution can be defined as the number of pixel values per inch, and thus images with higher spatial resolution contains more number of pixels. On the contrary, images with low spatial resolution show less details and it is hard to detect small details. Figure 2.8 shows an image with the size of 1024x1024 pixels in the upper-left and subsampling images.

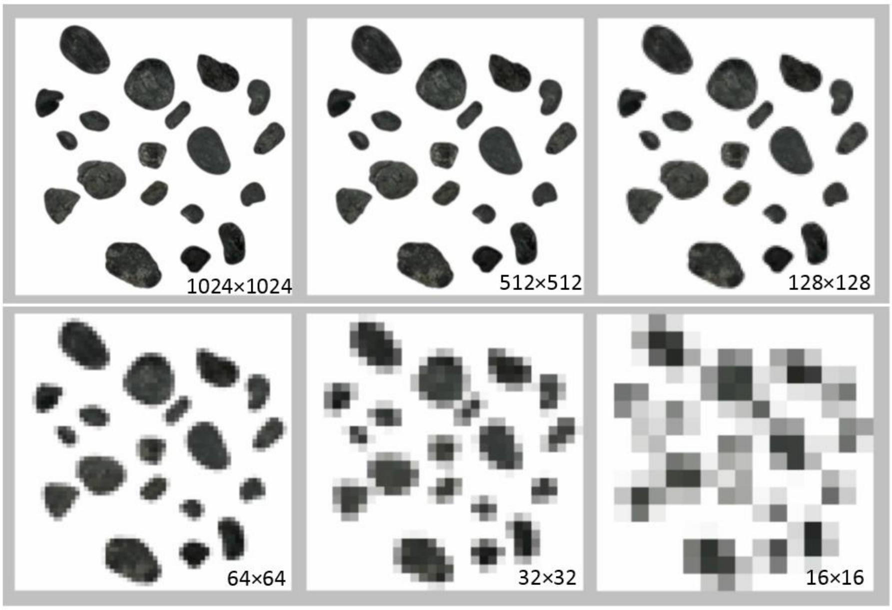

Figure 2.8. The effect of decrease in the spatial resolution in the visual appearance (Onal, 2008)

Resolution is measured in dots per inch (dpi) and the resolution of the images is selected according to smallest piece to be inspected. For example, if the resolution of an image for an area of 25 mm x 25 mm is scanned at 600 dpi, the size of each pixel will be equal to 0.0423 mm.

2.8.3. Preprocessing

After an image is obtained and stored in the computer memory, the next step is the image preprocessing. In order to implement further image operations properly, the preprocessing is the key step. The preprocessing steps can be considered basically as enhancement of image features, noise removal and contrast enhancement.

The dynamic range, contrast and other many properties of an image can be modified by using histogram operations. These techniques are beneficial to improve details and eliminate unwanted effects caused by a digitizer or the display system. The gray level histogram of an image shows number of pixels at each intensity value found in the image. Gray scale images (8 bit) consist of 256 intensity levels, so that the horizontal axis of the histogram extends from 0 (black) to 255 (white) (Shapiro & Stockman, 2001).

2.8.3.1. Smoothing

Smoothing is the most extensively used filter to eliminate random noises from images. Smoothing method works by replacing the pixel values by the average of the neighborhood intensity values. This method blurs the shape edges which is unwanted for particle detection but because the images used in this study have two phases with different intensity ranges, there will be no loss of image information. Smoothing filter is an effective method of reducing noises. Each pixel is replaced with an average of its 3x3 neighborhood. This average value becomes the new intensity value of the corresponding pixel. The method is shown in Figure 2.9.

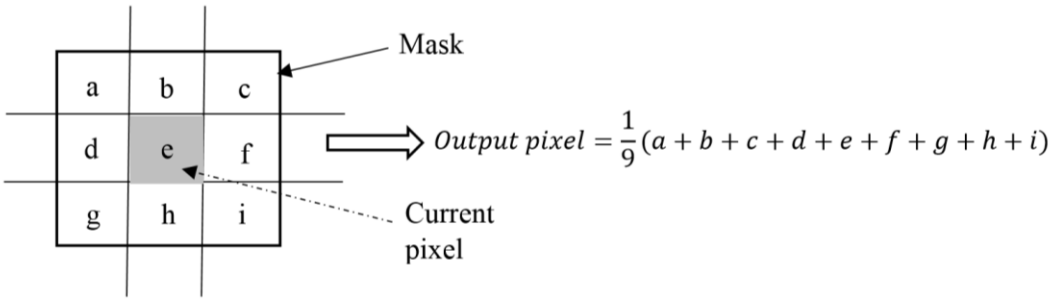

Figure 2.9. Performing the averaging filter

2.8.3.2. Contrast Stretching

If the range of intensity values of the acquired images is very small, contrast stretching (also named as normalization) may be used to improve the contrast by stretching the range of intensity values. In this way, objects are easily distinguished from the background. The initial histogram of an example image and the histogram after the contrast stretching are shown in Figure 2.10.

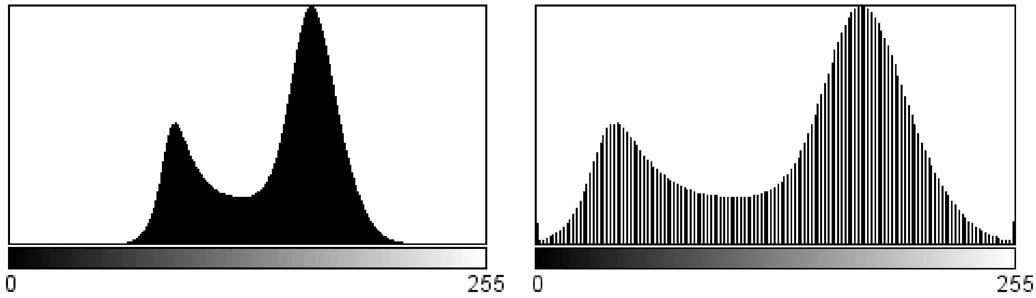

Figure 2.10. Intensity graphs before and after the contrast stretching

In this method, the upper and the lower limits of normalization are specified. For 8-bit gray scale images, lower limit and upper limit can be 0 and 255, respectively. Then, the pixel values are stretched between the determined limits according to the following equation.

$$P_{out} = (P_{in} - c)\left(\frac{b-a}{d-c}\right) + a \tag{2.4}$$

where a and b are the target lower and upper limits, which are generally selected as 0 and 255. The lower and upper pixel values of the original images can be called c and d. Then, each pixel value is mapped from P_{in} to P_{out} using Equation 2.4.

Images of an identical sample before and after contrast stretching operation are given in Figure 2.11.

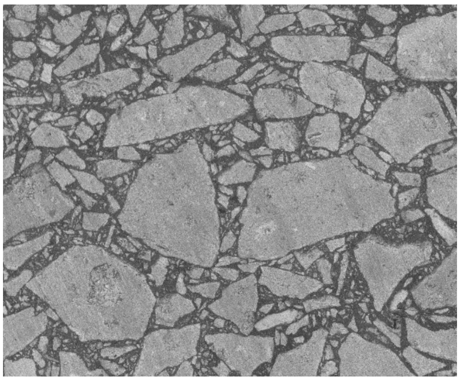
(a)

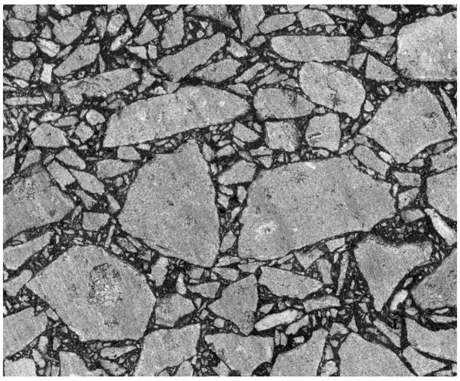
(b)

Figure 2.11. An example of contrast stretching; a) Grayscale image, b) After the normalization

2.8.4. Segmentation

Image segmentation is conducted to divide an image into multiple parts. At the end of segmentation operation, a binary image is obtained with separated object and background parts. There are two pixel values in a binary image which represent object pixels by 1 and background pixels by 0. After the segmentation step, all shape properties of an image can be extracted.

2.8.4.1. Binary Image

Binary image is a two-phase image of black and white color entities (such as aggregates with white color objects and binder matrix with black color background) and it is obtained after a series of filtering operations. By selecting a reference intensity value as threshold, the upper and lower intensity values are converted to black or white phases. In addition to the manual threshold selection, there are many methods of automatically determining the threshold value. The user may follow trial and error method to obtain a reasonable threshold value. However, in order to decrease the human factor, automatic thresholding methods have been developed recently. In this study, cross sectional images were analyzed by an automatic thresholding algorithm proposed by Schneider et. al. (2012). It is an iterative procedure that detects the two parts of an image as objects and background. After determining the initial threshold, the averages of the pixels lower and higher than the threshold are computed. The averages of these two groups are first computed, and the threshold is incremented until the threshold is larger than the combined average. Figure 2.12 shows the histogram of an example image in which the threshold value separates the object pixels from the background pixels.

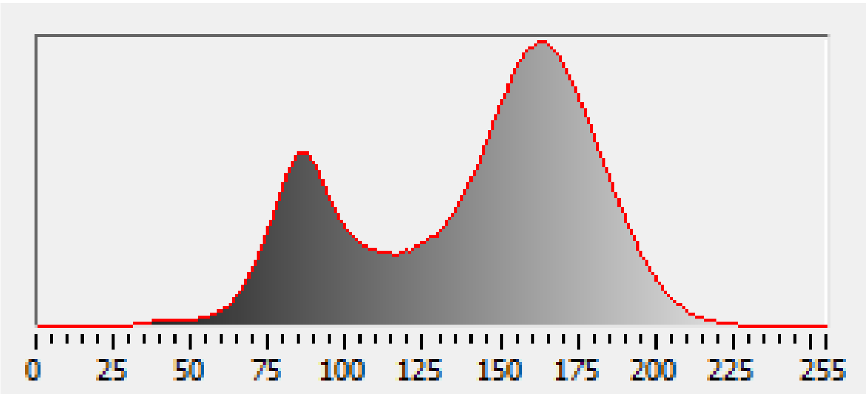

Figure 2.12. Location of the threshold value on histogram

In binary images, there are two pixel values, 0 (black) and 1 (white), one of them for objects and the other one is for background. Thresholding operation is implemented based on a simple approach as shown in below equation.

$$g(x,y) = \begin{matrix} 1 \; if \; f(x,y) > T \\ 0 \; if \; f(x,y) \leq T \end{matrix} \tag{2.5}$$

where g(x,y) is the new pixel values of the segmented image; f(x,y) is the gray level of the pixel located on (x,y); T is the threshold value determined by image processing software or manually. Figure 2.13 shows a grayscale image which consists of bright coins with dark background and binary version of it. Since there are two possible pixel values, this image format is very efficient in terms of storage and processing. An example binary image together with the pixel values is shown in Figure 2.14.

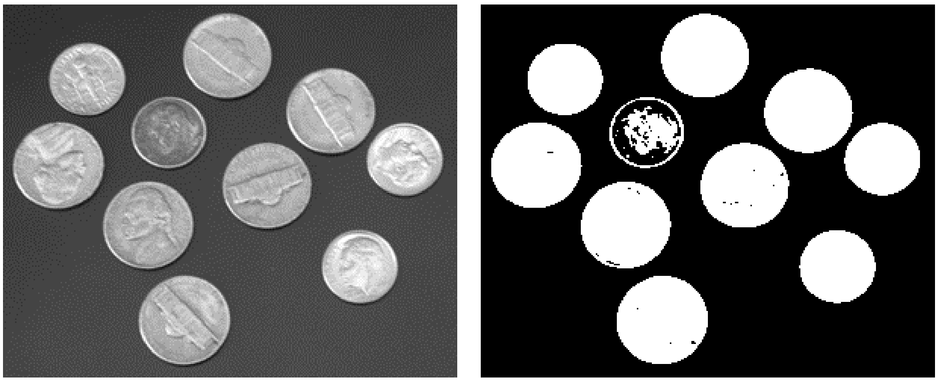

Figure 2.13. Grayscale and binary images (MATLAB, 2015)

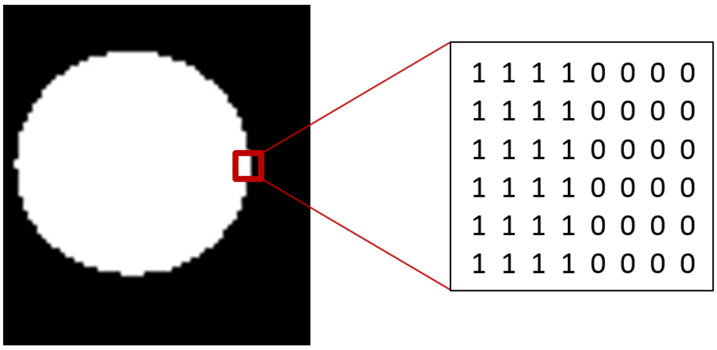

Figure 2.14. A binary image

2.8.4.2. Filling Holes

When some pixels are outside the desirable brightness range due to the color variations or noise, holes in the particles can be observed. These holes are filled with eight connectivity or four connectivity pixels by implementing suitable morphological procedures. By conducting this operation, miscalculation of the particle shape parameters such as area, perimeter, major axis, etc. is prevented. Figure 2.15 shows the coins with binary format before and after the image filling operation.

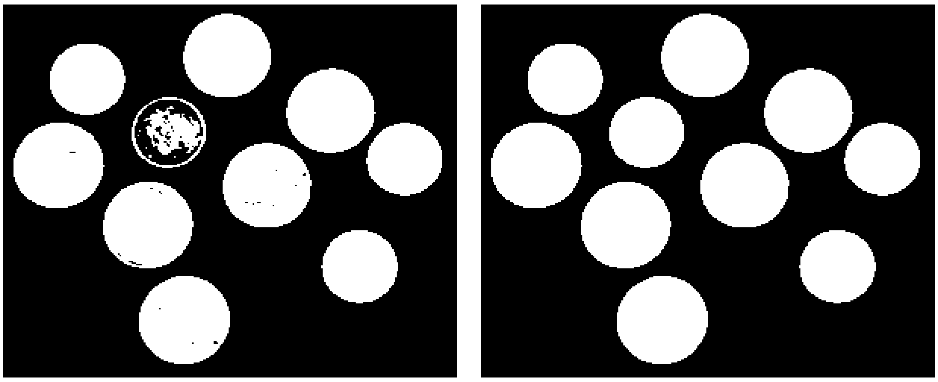

Figure 2.15. Image filling operation to coins (MATLAB, 2015)

2.8.4.3. Separation

In the binary image, some particles may touch each other and thus the adjacent particles should be separated to prevent unrealistic results. The separation is conducted by the help of morphological operations such as erosion and watershed segmentation. If two adjacent particles touch each other, image analysis program treats these particles as one particle, therefore, producing erroneous results. In order to prevent this problem, particles must be separated using an intelligent algorithm without deteriorating the original particle geometry.

2.8.5. Representation and Description

After the segmentation step, an image with row pixel data is obtained and the row data are used to obtain the characteristic features of the image in the representation and description step. The boundary or the complete region properties of image objects can be obtained in this step. Several important features obtained from a binary image can be counted as; area, centroid, perimeter and orientation. The measured properties of the particles can be summarized as follows (Gonzales et al., 2009):

-Area: It is the number of the pixels in the region of interest.

-Orientation: It is the angle between horizontal axis and the major axis of ellipse with same second moments as the region.

-Centroid: The center of mass of the object.

-Image: The binary image of an object in the bounding box with same size.

-Major axis length: The length of the major axis length of equivalent ellipse.

-Perimeter: The total number of pixels in the object boundary.

In this study, Labview®-Vision Assistant software was used to obtain maximum Feret diameter of the particles. Maximum Feret diameter can be defined as the length of the longest line connecting two border points of the particle.

2.8.6. Recognition and Interpretation

In the recognition step, a label is assigned to an object based on the information provided by the descriptors. Interpretation is implemented to assign meaning to a group of recognized objects.

2.9. Superpave Mix Design

Superpave mix design procedure was developed to achieve a ‘’comprehensive system for the design of asphalt materials’’ as part of Strategic Highway Research Program (SHRP). Asphalt binder grading system was implemented associated with the climate and traffic level. To increase the performance of asphalt pavements, specifications were developed about the quality control of aggregate. In the scope of this procedure, limits for the passing aggregate percentages for specific sieve sizes were determined to control the gradation.

In Superpave design method, aggregate is selected based on availability and the specification criteria such as mechanical and shape properties. The binder is selected according to performance grade (PG) considering temperature limits and traffic volume in the area. The viscosity tests are performed to determine the mixing and compaction temperatures of the mixtures. The number of compaction effort is selected based on the design equivalent single axle loads (ESAL). Superpave gyratory compactor (SGC) is used to compact mixtures and the gyratory compactor simulates the field conditions successfully and it is better than Marshall Compactor in this aspect. Particle orientations after the compaction are also very similar to that obtained from the field (Roberts, 1996). The compaction effort is controlled by three parameters which are gyration angle, vertical pressure and number of gyrations. In the gyratory compactor, gyration angle (1.25 deg), pressure (600kPa) and rate of gyration (30 rev/min) are fixed and specimens with different diameters, 100 mm and 150 mm, can be produced. Aggregate gradation is selected based on the criteria determined according to the samples compacted at initial densification effort (N_{ini}), design densification effort (N_{des}) and maximum densification effort (N_{max}). In addition to estimated asphalt content, the mixtures with three more asphalt contents (estimated±0.5, estimated+1%) are compacted and the optimum binder content is selected according to the volumetric test results. When the mixture is compacted to N_{des} gyration, 4% air void should be achieved at optimum bitumen content. The design mixture should satisfy other volumetric criteria because volumetric properties and binder properties control the performance characteristics. The most important three criteria in Superpave mix design are voids in mineral aggregate (VMA), voids filled with asphalt (VFA) and dust to binder ratio. The design should satisfy all of these specification limits at the same time.

2.9.1. Compaction of Asphalt Mixture

Asphalt mixture compaction is a complex process and it is affected by design, construction and material properties. The main design factors such as binder content, mixing and compaction temperature, aggregate gradation and layer thickness. The compaction method and compaction effort are other important factors affecting the quality of the asphalt concrete.

N_{des} is the number of gyrations which produce a specimen with a density equal to the expected density in the field under the expected traffic loading. N_{ini} is the indicator of mixture compactibility and specimen should have at least 11% air void at N_{ini}. If mixture compacts quickly, it may behave as a tender mix during construction. N_{max} is the number of gyrations to produce a density that should not be exceeded in the field. The minimum air void criteria at N_{max} is 2%. All samples should be aged at compaction temperature in an oven for two hours before the compaction starts to simulate aging during the construction process.

2.10. Mechanical Properties

The selected type of mechanical testing is important to be able to observe the influence of specimen inhomogeneity on performance. If the test is sensitive to aggregate distribution, the mechanical response between homogenous and segregated specimens can be separated easily. However, if the test is insensitive to aggregate distribution, it will not reflect the true behavior of mixture and can only be used to evaluate some general properties.

To investigate if there is a relationship between aggregate distribution characteristics and the mechanical performance of asphalt mixture specimens, a mechanical test should be selected which is sensitive to aggregate distribution in the specimen. The direction of inhomogeneity such as vertical or radial is also an important when monitoring the effect of aggregate distribution on mechanical performance.

There are some requirements for the selected mechanical test to study the effect of aggregate distribution: First, it should measure the resistance of aggregate skeleton rather than binder effect under repetitive load. Second, test configuration should reflect the true aggregate behavior under applied loading; in other words, there should be introduced variation due to test configuration. In this study, compression mode of loading is selected to evaluate effect of inhomogeneity on rutting resistance of asphalt concrete samples.

The behavior of hot mix asphalt in compression is evaluated with simple performance test (Witczak, 2005). The proposed test is used for both characterizing the constitutive behavior of mixture and evaluating the mixture performance under repeated loading.

2.10.1. Rutting in Asphalt Mixture

Rutting, which is the most critical load related distress of flexible pavements, can be defined as the excessive permanent deformation at the wheel path which occurs because of high number of loading cycles. This distress causes an unrecoverable deformation in asphalt concrete pavements. Rutting happens in consequence of different mechanisms such as consolidation, surface wear, plastic flow and mechanical deformation. There are two stages defined in the rutting mechanism. When the road is opened to traffic, permanent deformation occurs along the wheel paths due to the densification process and then the plastic deformation starts. Permanent deformation in asphalt pavements results from aggregate characteristics, gradation, design methodology, binder type and compaction level. Other significant factors that are not related to mix properties are vehicle type, vehicle axle configuration, pavement temperature, traffic level, etc. To decrease rutting damage in asphalt concrete pavements, quality of asphalt mixture should be strictly controlled. Aggregate characteristics and aggregate distribution are considered one of most important parameters for rutting resistance. Rut resistant hot mix asphalt should be placed in such a way as to avoid segregation and excessive compaction that cause damage in mixes (Gul, 2008).

2.10.2. Repeated Creep Test

Repeated creep test, also known as flow number (FN) test, is conducted to measure permanent deformation under the repeated axial loading on asphalt concrete specimens. In NCHRP Report 465 (Witczak et al., 2002), the test procedure is described by applying a loading cycle of 1 Hz comprising 0.1 second loading and 0.9 second rest period. The test is conducted at a single effective temperature and a design stress level. The test conditions are selected considering the service condition of asphalt concrete pavement. The repeated creep test can be run as confined or unconfined test. In Superpave mix design method, binder grading is determined based on the average maximum seven-day temperature and this temperature was used in some studies as a test temperature (Guler, 2003). The test continues until 10000 cycles or until the specimen reaches 5% cumulative permanent strain, whichever comes first. A schematic diagram of the permanent deformation tester is shown in Figure 2.16.

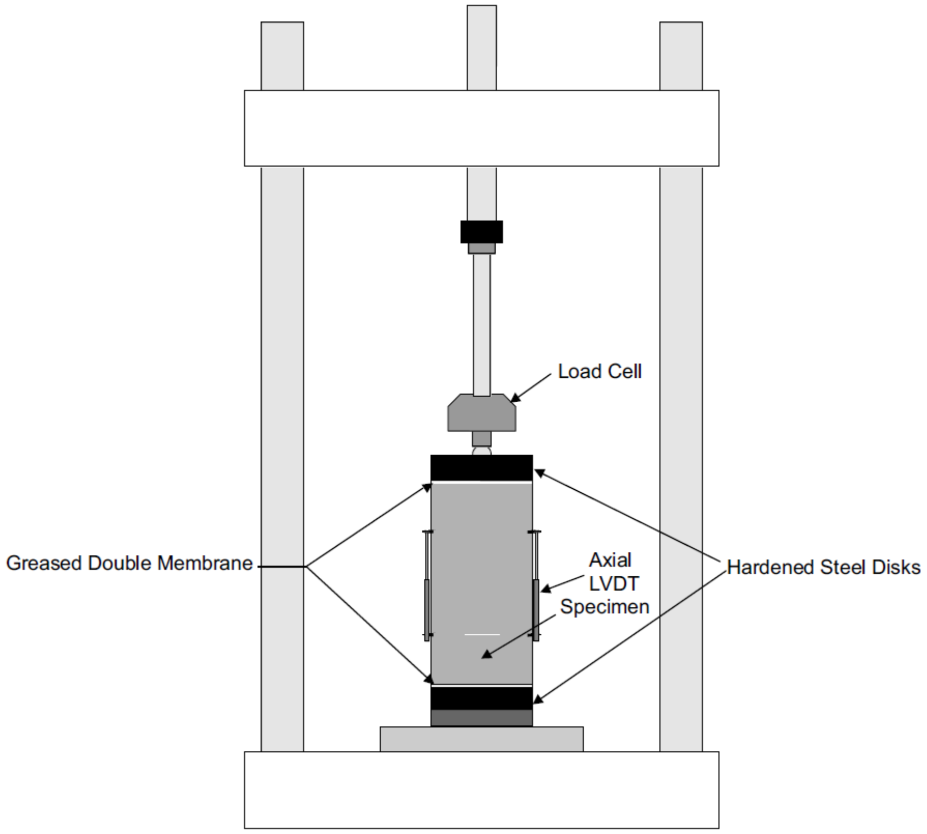

Figure 2.16. Schematic of repeated load permanent deformation test (Witczak et al., 2002)

A minimum of 1.5 aspect ratio requirement must be satisfied as described in the test procedure (Witczak et al., 2002). A cylindrical specimen with 100 mm diameter and 150 mm height is tested under haversine loading and test specimens are cored from the center of gyratory compacted specimens prepared in the laboratory. The ends of the specimens should be smooth and perpendicular to the specimen axis to prevent eccentricity. Rough specimen ends cause friction between the specimen surface and the loading platens causing end effect problem during testing. To obtain specimens with smooth end surfaces, the top and bottom surfaces must be cut using a continuous diamond blade carefully. As part of the end treatment, rubber membranes with silicon grease between specimen ends and loading platens should be used.

Linear variable differential transformers (LVDT) are utilized at two sides of the specimen to measure axial deformations during the test. Circular pads are glued on the side surfaces of the specimen using epoxy before mounting the LVDT holders. Four pads are glued for each specimen using two LVDT holders and then holders are attached to the previously glued pads. The location of the circular pads and the LVDT holders are shown in Figure 2.17.

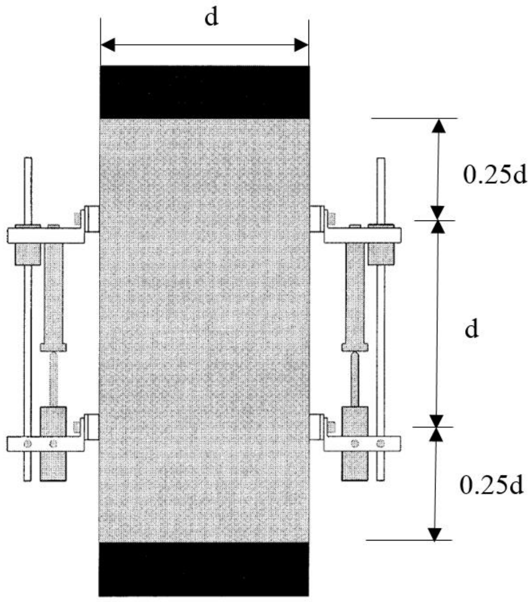

Figure 2.17. Location of LVDT holders (Witczak et al., 2002)

Plastic deformations are measured by the LVDT sensors to determine the flow number and the other test parameters. To obtain the cumulative permanent strain, the average deformation obtained from the sensors is divided by the gage length of the specimen

(100 mm) for each step of loading. The number of cycles versus the cumulative axial permanent strain graph is plotted in a log-log scale to identify the location of flow number and the other test parameters. The flow number is equal to the number of loading cycles corresponding to the minimum rate of strain.

During repeated loading, permanent deformation is developed in three different stages. The densification and the reduction air volume occur rapidly in the first zone named as the primary zone. The rate of permanent deformation becomes nearly constant in the secondary zone. In the final zone, which is also called tertiary zone, the rate of deformation increases with further loading cycles and the plastic flows start under constant volume of test specimen. The flow number can also be referred as the cycle number to start the tertiary zone. Figure 2.18 shows a typical permanent deformation behavior of asphalt concrete sample.

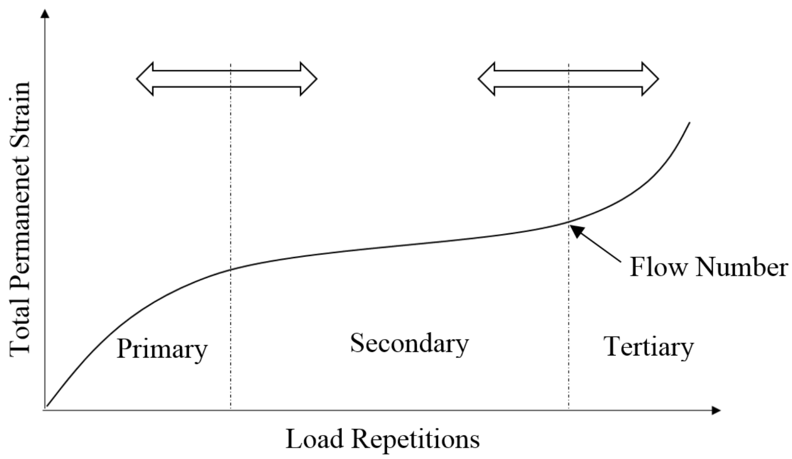

Figure 2.18. Typical permanent deformation graph of asphalt mixture

2.10.3. Calculation of Flow Number

Currently there is no a widely accepted method to calculate the flow number; however, researchers have proposed several successful methods. The most widely used methods are summarized in Table 2.2.

Table 2.2. *Summary of flow number calculation methods*

Model name	Equation	Description
Three-stage model (Zhou, 2004)	Primary stage: $\varepsilon_p = aN^b, N < N_{PS}$ Secondary stage: $\varepsilon_p = \varepsilon_{PS} + C(N - N_{PS}), N_{PS} \le N < N_{ST}$ Tertiary stage: $\varepsilon_p = \varepsilon_{ST} + d\left(e^{f(N-N_{ST})} - 1\right), N \ge N_{ST}$	Using this method, the primary, secondary and tertiary stages can be determined. The maximum number of cycles for the secondary stage gives the flow number.
Francken model (Francken, 1977)	$\varepsilon_p(N) = AN^B + C(e^{DN} - 1)$	The regression constants A, B, C and D are calculated. FN is defined as the cycle number at which the second derivative changes from negative value to a positive value.
Polynomial curve fitting (Witczak, 2002)	$\varepsilon_p(N) = a + bN + cN^2$ $\frac{\delta\varepsilon_p(N)}{\delta N} = b + 2cN$	A polynomial equation is fitted by five points at a cycle N_1 (Two point backward-two point forward). FN is equal to the cycle number at which the rate of change in strain is zero.
Moving average method (Bonaquist et al., 2003)	$\frac{\delta(\varepsilon_p)_i}{\delta N} = \frac{(\varepsilon_{pi+\Delta N} - \varepsilon_{pi-\Delta N})}{2\Delta N}$	Strain rate for all loading cycles is calculated and then strain rates are smoothed by using a five point moving average method. FN is defined as the cycle number at which the minimum strain rate is reached.
Simple stepwise method (Goh & You, 2009)	$Strain\ rate = \frac{\varepsilon_p}{N}$	The strain rate is calculated by dividing the cumulative strain by the number of loading cycles. FN is equal to the loading at which the strain rate is minimum.
Hoerl model (Li et al., 2010)	$\frac{d\varepsilon_p}{dN} = (AxB^N xN^C)$	The regression coefficients are calculated. FN is the cycle number where the derivative of the model altered from a negative to a positive value.

Ameri et al. (2014) conducted a study to evaluate and compare available flow number calculation methods. 12 mixtures were used to evaluate the ability of these methods to determine the flow number. Result showed that the Francken model has the lowest variability and this method is suggested to calculate flow number. There are also other studies which show the ability of the Francken model to fit all three stages of the permanent strain curves (Dongre et al., 2009; Biligiri et al., 2007). Thus, the Francken models was used to fit the repeated creep test data and determine the flow number in this thesis study.

CHAPTER 3

DEVELOPMENT OF INHOMOGENEITY INDEX

3.1. Sample Preparation

To carry out the inhomogeneity analyses, asphalt concrete (AC) samples were fabricated in four different design mixtures by varying aggregate and gradation at two levels. The selected mix design parameters are given in Table 3.1. The test specimens were prepared according to the Superpave mix design procedures and a 150 mm diameter mold was used to compact the specimens.

Table 3.1. *Properties of produces mixtures*

Mix Design	**1**	**2**	**3**	**4**
Gradation	Type-1	Type-2	Type-1	Type-2
Aggregate Type	Basalt	Basalt	Limestone	Limestone

In the study program, two aggregate types, which are basalt and limestone, were used. The maximum nominal aggregate sizes for the coarse and fine gradations are 19 mm and 12.5 mm, respectively. Percent passing corresponding to each size are given for coarse and fine gradations in Table 3.2. The selected gradations can also be seen from Figure 3.1.

Table 3.2. *Gradation of asphalt mixtures*

Sieve Sizes (mm)		**19**	**12.5**	**9.5**	**4.75**	**2**	**0.425**	**0.18**	**0.075**
Percent Passing	Type-1	100	88	72	42	25	10	7	3
	Type-2	100	100	90	72	53	28	16	8

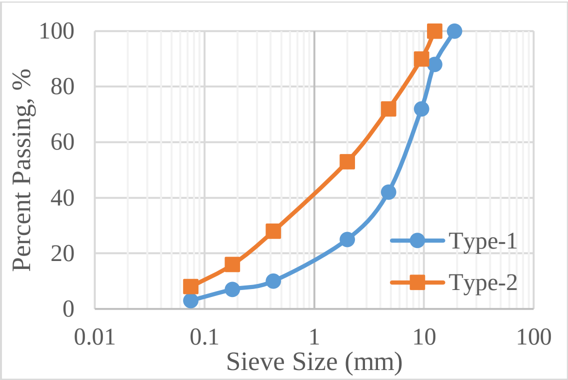

Figure 3.1. Gradations with different maximum aggregate sizes

One specimen for each design was fabricated in the laboratory. The specimens were cut in three sections with one cutting section at the middle of the specimen and 2 cutting sections in the 30 mm apart from the middle section using a diamond saw. After the cutting process, 2-dimensional images were obtained from the cut surfaces of each specimen using a flatbed scanner (Figure 3.2).

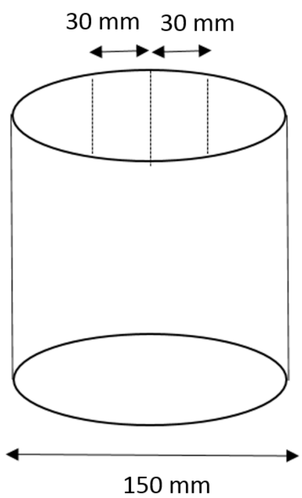

Figure 3.2. Locations of the cut sections

Distance between each cut section was selected according to the maximum nominal aggregate size of mixtures. The maximum nominal aggregate size for the coarse graded mixtures is 19 mm, hence 30 mm spacing is large enough to exceed the nominal maximum size of the mixtures. A total of twelve images were obtained from 4 specimens by capturing three images per specimen for the analyses.

3.2. Image Acquisition and Enhancement

The first step of digital image processing was acquiring the image frames and transferring them to computer memory. Different devices can be used for image acquisition but a 2D flatbed scanner was used in this study (Figure 3.3). Flatbed scanners are one of the best options for practical and low cost image acquisition applications. The resolution of the scanner was set to 600 dpi to capturing the small size particles. At this resolution level, particles larger than 0.425 mm could be successfully detected. After the image acquisition step, image enhancement operations were implemented.

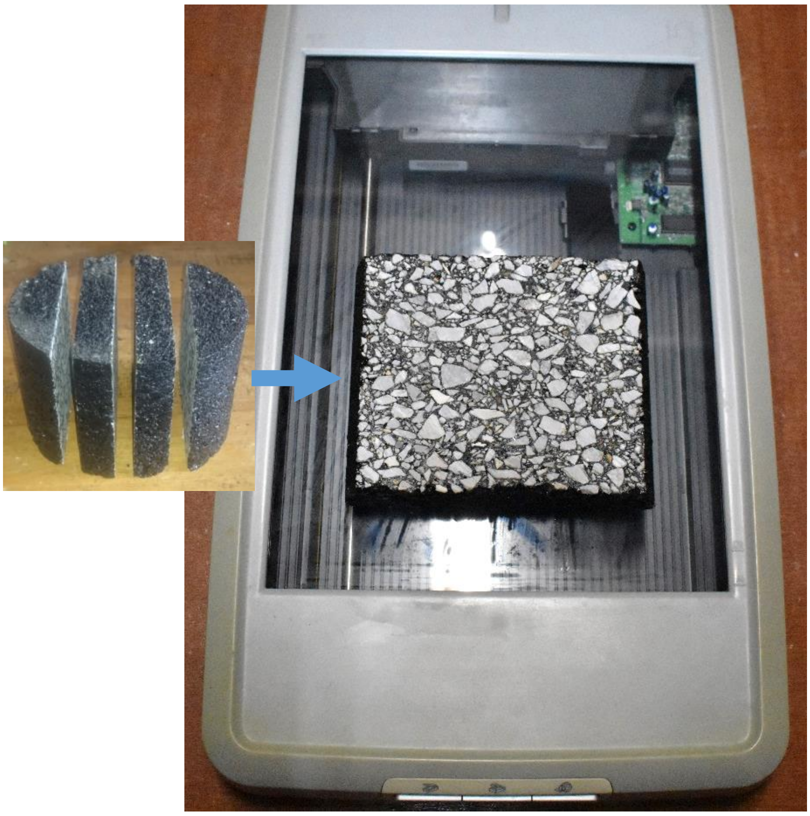

Figure 3.3. Obtaining the images with a flatbed scanner

After scanning the cross sectional images, the output format was a lossless TIFF format image with 24 bit RGB color scale. To conduct further image analysis techniques, the original images had to be converted into binary images by following a series of suitable processing and thresholding methods. To prevent loss of information from the image during the binary conversion step, image enhancement operations should be conducted. Random noises in an image or color variations between aggregates or a single particle surface can cause important problems during the particle recognition. To eliminate these potential problems, image enhancement filters such as smoothing and contrast stretching were used in this study. The smoothing filter was used to remove noises. In this operation each pixel value was replaced with the average of its 3x3 neighborhood. To increase contrast between aggregate and binder phases, contrast stretching (or normalization) operation was implemented. This method stretches the range of intensity values between 0 and 255. After the enhancement operations, the images were converted to binary format by using automatic thresholding method using the ImageJ software. Flowchart of the image acquisition and enhancement operation steps is given in Figure 3.4.

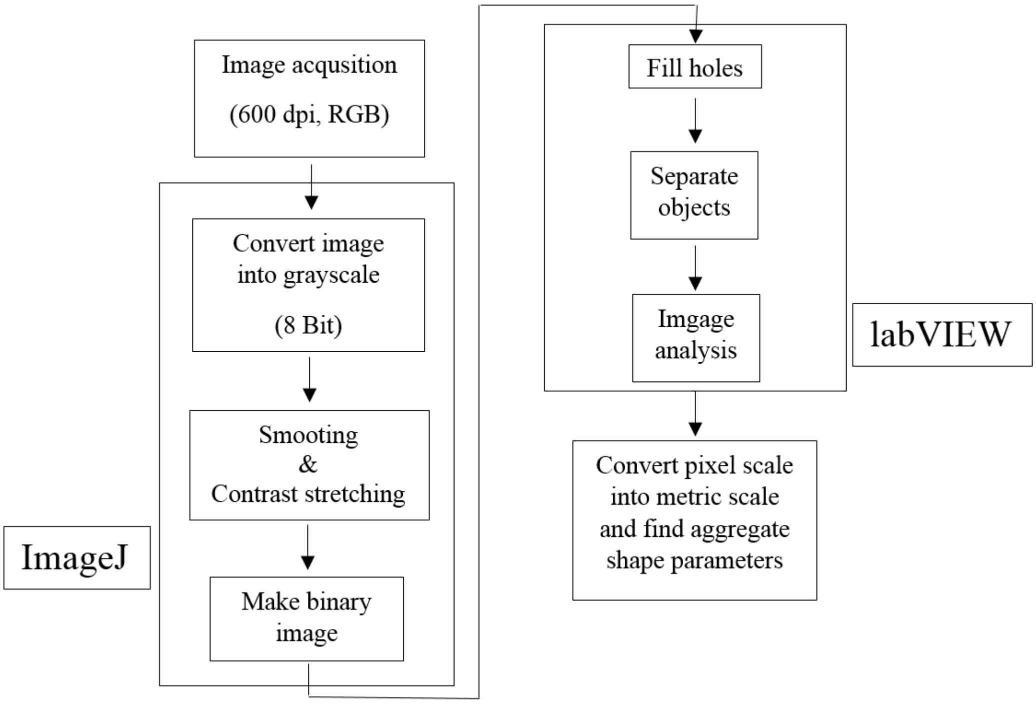

Figure 3.4. Flowchart of the image operations

Figure 3.5 shows an original RGB image and its binary equivalent for a vertical section of an asphalt concrete specimen. To convert the original RGB image into final binary version, the procedure given in the flow chart was followed in a step-by-step process.

(a) (b)

Figure 3.5. Vertical section image of the gyratory compacted specimen; a) Original image, b) Binary image

Holes on the aggregate surfaces caused by noise or color variations were filled with four connectivity elements by the help of the image processing software. One of the most important steps in image processing is the separation of particles. If two aggregate particles touch each other, image analysis program treats these particles as one particle, thus producing erroneous results. In order to prevent this problem, particles must be separated using an intelligent algorithm without deteriorating the original particle geometry. Separation operation of the overlapping aggregate particles was achieved using an algorithm developed in a Labview® program. The algorithm separates particles using various morphological image operations, thus helping author conduct particle analyses accurately for the cross section images. An example of a cross sectional image before and after the separation is shown in Figure 3.6.

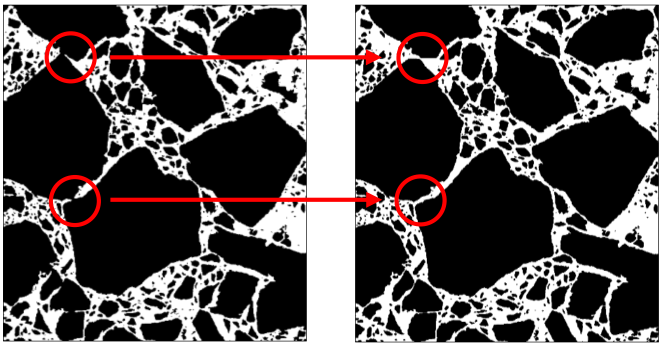

(a) (b)

Figure 3.6. Particle separation; a) Before separation, b) After separation

Example steps of the image processing operations are given in Figure 3.7. A small part of a cross section image is depicted in this example, so that the details can be seen. The diagram starts with converting the original image into 8-bit grayscale format and then smoothing and contrast stretching operations are implemented. After removing noises and increasing the contrast between binder and aggregate phases, the image was ready for binarization. Using the automatic thresholding method, the image was converted to the binary format. Finally, image filling and particle separation operations were implemented. After all these steps, the image is ready for particle analysis.

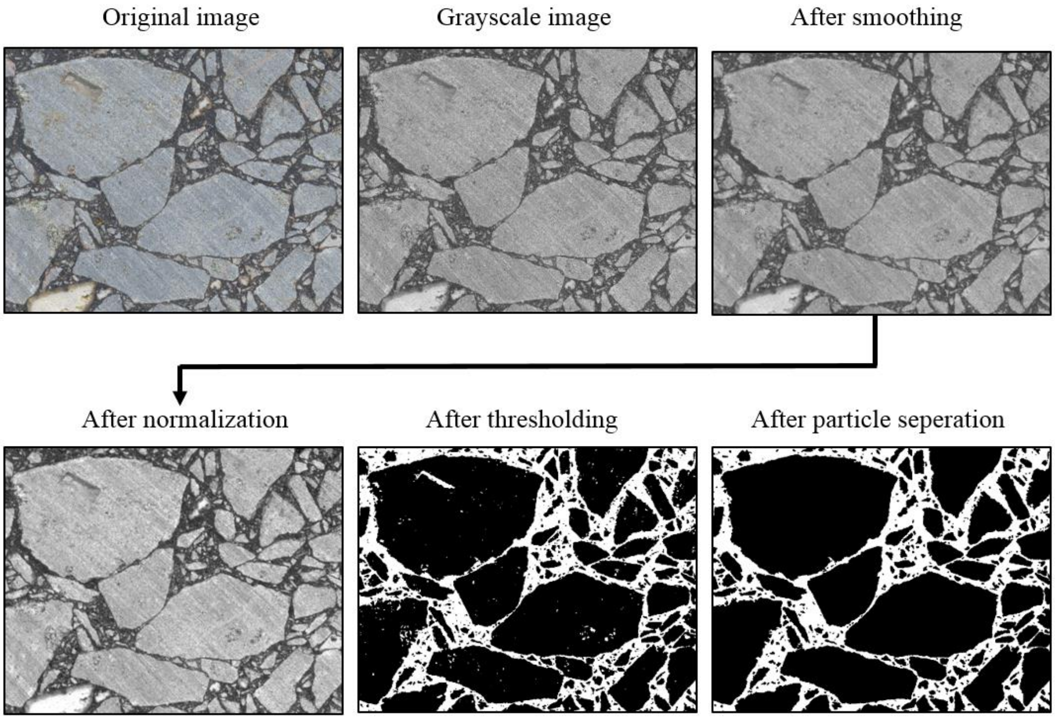

Figure 3.7. Image processing steps

3.3. Aggregate Shape Parameters

Aggregate shape parameters were obtained from the binary images and aggregate size distribution of the specimens were determined based on 2D cross sectional images. The area of particles is computed as the sum of the all pixels contained within an aggregate cross section. The optimal shape parameter to predict the actual aggregate size distribution (gradation) was previously found to be maximum Feret diameter by Ozen and Guler (2014). There are also other shape parameters used for particle shape analysis in the previous studies such as particle area, equivalent circle diameter, equivalent ellipse major axis, polygon diameter, major axis length, minor axis length (Yue & Morin, 1996). In this study, the size distribution of aggregates was predicted by using the maximum Feret diameter of aggregate particles. In the particle shape analysis, maximum Feret diameter is defined as a line segment connecting the two perimeter points with the farthest distance between them (Figure 3.8).

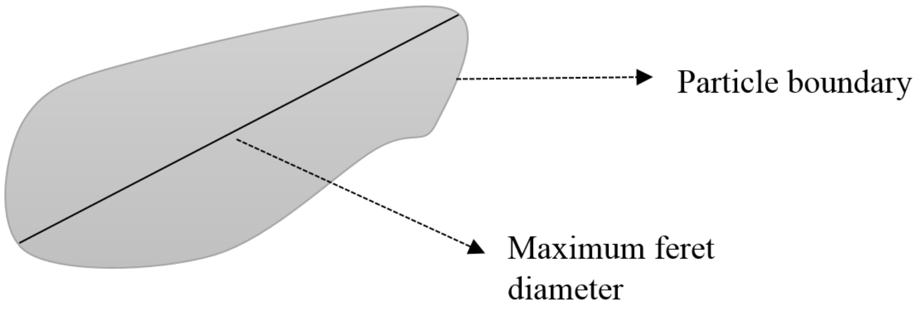

Figure 3.8. Maximum Feret diameter of an aggregate particle

Maximum Feret diameter of the particles was determined using Labview®-Vision Assistant software. In addition, the other parameters such as area, orientation, centroid, perimeter, etc. were determined using regionprops function in Matlab®. Finally, these parameters are combined by the developed algorithm for homogeneity analyses.

3.4. Size Distribution Analysis of Aggregates

Aggregate size distributions of AC specimens were estimated using their 2D vertical cross section images. Slice faces used for gradation analysis were also utilized for the homogeneity evaluation. In mechanical sieving, particle size distribution analysis is conducted using mass of particles; however, particle shape parameters are used in the digital image based particle size distribution estimations. An elongated particle with greater length than the standard (square) sieve size can still pass from the sieve. Therefore, if a particle breath is smaller than the diagonal sieve size, the particle passes from the corresponding sieve. To find the percent retaining on each size fraction, maximum Feret diameters were calculated and compared with the standard diagonal sieve sizes. The view of the sieve openings is given in Figure 3.9.

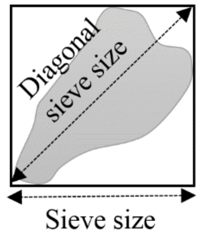

Figure 3.9. The view of the sieve opening

It is generally difficult to detect fine particles in 2D cross sectional images because of the limitation in the resolution of the flatbed scanner used. After some trials conducted using several image resolutions, it is concluded that the detection of particles smaller than 0.425 mm is not practical. Thus, particles smaller than 0.425 mm were excluded from the image analyses. The ratio of particle areas retaining on a specific sieve to the total aggregate area larger than 0.425 mm gives the retaining percentage of the corresponding sieve. Equation 3.1 calculates the normalized percent retaining for each sieve used to eliminate the effect of the excluded small particles.

$$P_e = \frac{(100 - P_f)}{100} P_i \tag{3.1}$$

where P_e=normalized percent retaining; P_f=actual percentage of excluded particles from the image analysis; and P_i=retaining percentage calculated in the image analysis.

The actual gradation and estimated gradation results that are calculated based on the explained procedure are given in Table 3.3. Three cross sectional images for each specimen were used to estimate the aggregate size distributions. The results show both the aggregate size distributions calculated based on each sectional image (S-1, S-2 and S-3) and combination of three section images for the corresponding specimen. In all surfaces, particles in three images were combined and considered together. It can be seen from the results that the proposed method successfully estimates the actual gradation from 2D cross sectional images.

Table 3.3. *Results of the gradation analysis*

Sieve Size (mm)	**Actual Gradation (%)**	**Percent Passed**							
		All Surfaces	**S-1**	**S-2**	**S-3**	**All Surfaces**	**S-1**	**S-2**	**S-3**
		Mix-1				Mix-3			
19	100	100.0	100.0	100.0	100.0	100.0	100.0	100.0	100.0
12.5	88	89.2	88.6	85.2	94.0	93.0	94.9	92.9	91.0
9.5	72	74.1	71.5	72.2	78.6	81.7	87.4	84.2	73.1
4.75	42	44.3	44.6	43.4	45.0	47.5	48.9	52.0	41.6
2	25	23.7	23.5	23.2	24.5	24.2	24.5	25.5	22.5
0.425	10	10.0	10.0	10.0	10.0	10.0	10.0	10.0	10.0
		Mix-2				Mix-4			
12.5	100	100.0	100.0	100.0	100.0	100.0	100.0	100.0	100.0
9.5	90	94.0	94.8	92.1	95.0	95.3	92.6	96.0	97.3
4.75	72	70.6	72.2	68.6	71.0	72.6	73.2	73.1	71.6
2	53	47.2	48.1	46.5	47.0	52.4	52.7	53.0	51.6
0.425	28	28.0	28.0	28.0	28.0	28.0	28.0	28.0	20.0

The graphical comparison of the gradation analyses is given in Figure 3.10 (a-d). While the largest deviation from the actual size fraction occurred around 9.7% for mix-3, it was found only 5.3% for mix-4. For the other size fractions, the total deviations from the actual size fractions are negligible.

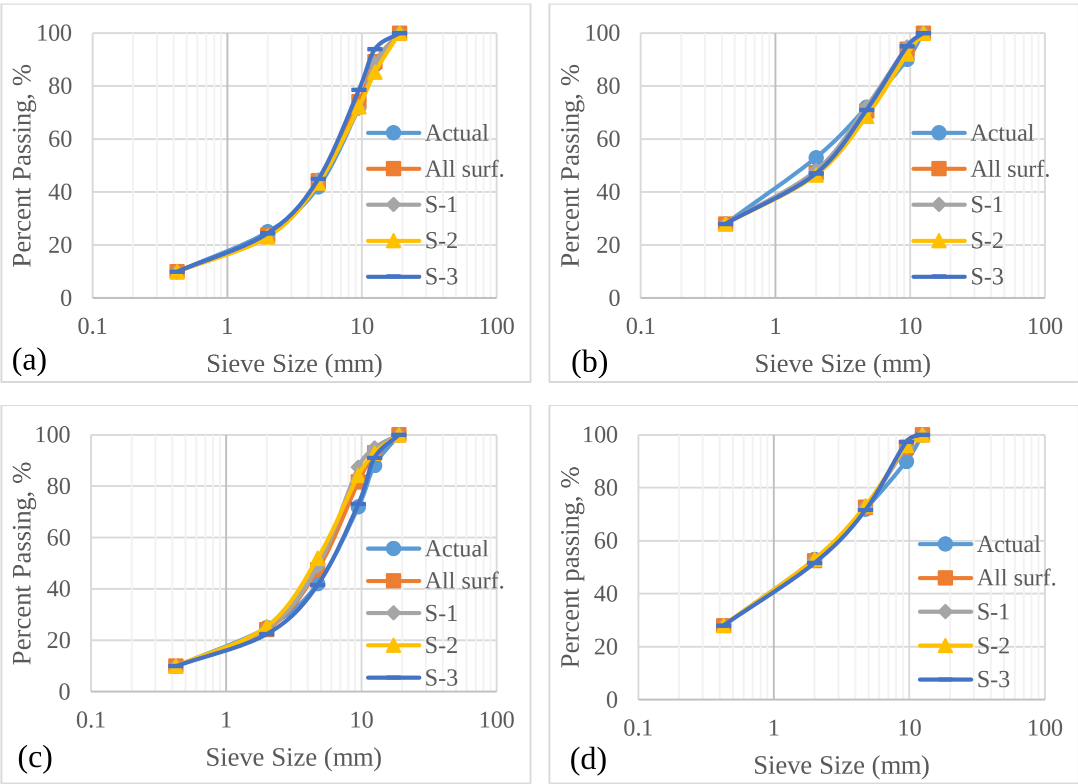

Figure 3.10. Actual and estimated aggregate gradations; a) Mix-1, b) Mix-2, c) Mix-3, d) Mix-4

The results show that gradations of asphalt mixture specimens can be estimated based on 2D cross sectional images. Maximum Feret diameter produces acceptable results as a shape parameter to estimate the size distribution of aggregates. Thus, this parameter is proposed as the best shape parameter to study the size distribution of aggregates from 2D image of AC samples.

3.5. Redistribution of Aggregates

To determine the aggregate distribution characteristics and the range of inhomogeneity indices for the test specimens, a Matlab® algorithm was been developed. The algorithm is able to detect all aggregates in a cross section, and then the particles are spatially redistributed at random locations to obtain synthetic cross sectional images. The center coordinates and the orientation of each particle are randomly determined in the generated synthetic images. In this way, a great number of synthetic images can be generated using the original cross section particles. To eliminate overlapping problem, particles are sorted from large to small sizes according to their maximum Feret diameters and then redistributed into the new image. During this process, if any overlapping is detected, a redistribution is carried out subsequently. An input binary and the generated synthetic image by redistribution algorithm are shown in Figure 3.11.

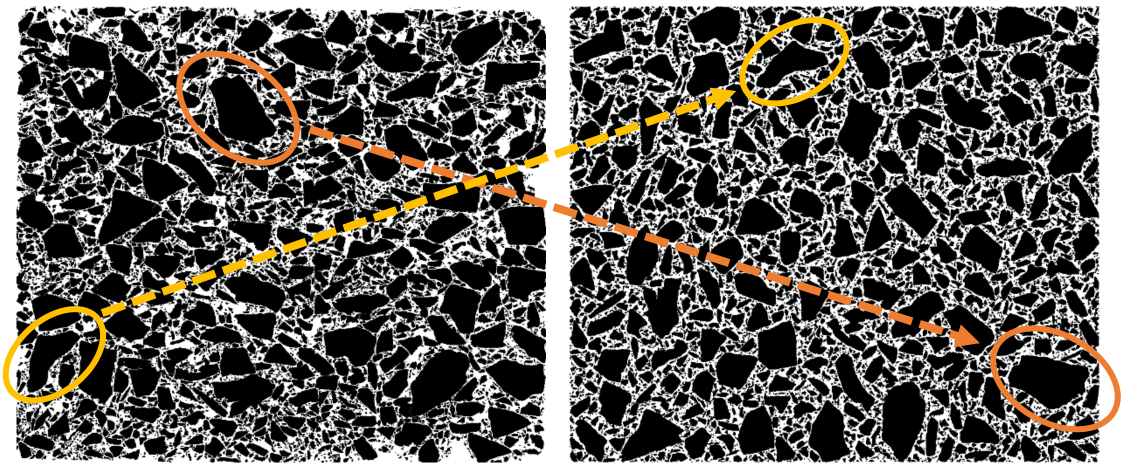

(a) (b)

Figure 3.11. Aggregate redistribution: a) Original image, b) Synthetic redistributed image

The output format is binary image similar to the input image and the output image size also equals to the input image size.

3.5.1. Particle Labeling and Shape Parameters

The developed algorithm calls two input files after running. The first input is the original binary image of asphalt mixture cross section and the other input is the excel file that contains maximum Feret diameters of all particles in the input image. Since Matlab® image processing toolbox does not have a function to find the maximum Feret diameter, this data set is determined using the Vision Assistant software. The first step in the redistribution algorithm is the object labeling. All connected components are detected using bwlabel function. The selection of four or eight connectivity is optional in MATLAB; however, in the case of eight connectivity usage, if corners of the two particles touch each other, they are identified as one particle. Therefore, four connectivity was used for separation of the overlapped particles. In the four connectivity case, pixels are connected if their edges touch each other not just at corners. Two adjoining pixels are accepted as part of the same object, if they are connected along the horizontal or vertical direction as shown in Figure 3.12.

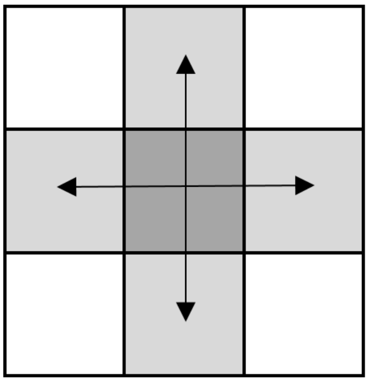

Figure 3.12. Four connected components

After labeling, the image becomes ready for the determination of aggregate shape parameters. As discussed previously, shape parameters are obtained using regionprops function in Matlab®. The maximum Feret diameter values taken from another software are combined with the shape parameters table obtained from regionprops function. The aggregate shape parameters are determined based on the input cross section image. Maximum Feret diameter is used as an optimal shape parameter to calculate the size distribution of aggregate particles as discussed in the previous sections.

3.5.2. Particle Redistribution Algorithm

The first step of the redistribution algorithm is that a blank image section with the same size as the original image is created. Then, x and y coordinates of the particle centroid are assigned randomly by the algorithm. In addition to the centroid coordinates, orientations of the particles are assigned randomly. The rotation of the particle is controlled by imrotate function in Matlab®. The image rotate function rotates a particle by an angle around its centerline. There are three different methods to rotate images in image rotate function. These are nearest-neighbor interpolation, bilinear interpolation and bicubic interpolation. In this study, nearest-neighbor interpolation was used. To minimize particle overlapping problem, redistribution operation starts with the particle which has the largest maximum Feret diameter and continue until the smallest particle is positioned. If any particle overlaps with previously located particles, the location of the particle is determined again by the algorithm until positioning without overlapping. The redistribution operation ends, after all the particles are positioned within image section. The steps of the particle redistribution algorithm are summarized in Figure 3.13. The strategy used in the algorithm is to relocate the coarse particles first within the image and then the smaller particles next, thereby increasing the efficiency of the algorithm and reducing the computation time to complete the redistribution operation.

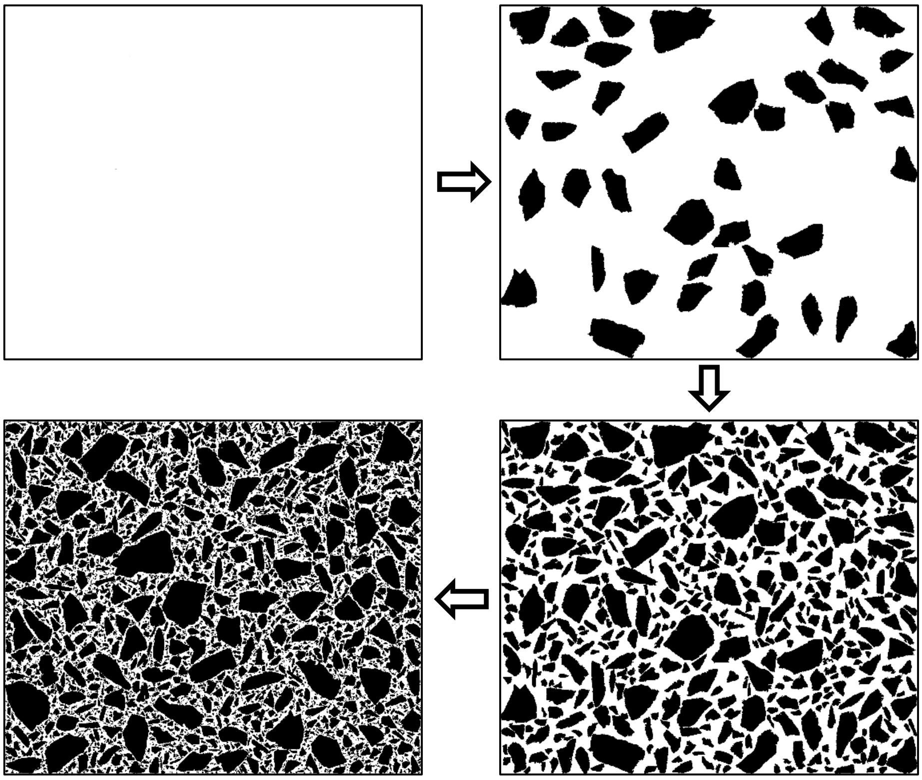

Figure 3.13. Particle positioning

For this example, redistribution application, middle slice face of the Superpave gyratory compacted specimen was used. There were approximately 5000 particles in the given cross section. First image shows blank image and particles from the original cross section are positioned within this image starting from the largest particle first. Second figure shows the synthetic cross section image after the completion of positioning of 40 particles according to the maximum Feret diameter from largest to smallest particles. After positioning 400 particles, the synthetic image becomes as shown in the third figure. The last figure shows the finalized synthetic cross section image. Particles smaller than 0.425 mm are not included in the redistribution process to reduce analysis time.

During the particle redistribution, the centroids of aggregate particles are randomly determined by the algorithm. The lower limits of particle centroid as coordinates are

(1,1) and the upper limits are the image size in both x and y directions. The centroid of a particle is restricted to the given limits which describe the image section; however, some parts of the particle may be outside of the image area. In this case, the particle is moved inside the image section by the algorithm. As shown in Figure 3.14 (a-b), if some parts of the particle exceed the image borders, the particle is moved with one pixel step size to the opposite direction of the exceeding part until it is completely positioned within the image area. If any particle exceeds the image border around the corners as shown in Figure 3.14 (c), the particle is moved diagonally until it is completely positioned within the image. If this operation is not implemented and particles are redistributed again in case of border exceeding, small particles concentrates in the region near the edges and coarse particles concentrate at the center. To prevent unrealistic aggregate distribution, this procedure was developed and implemented in the scope of this study.

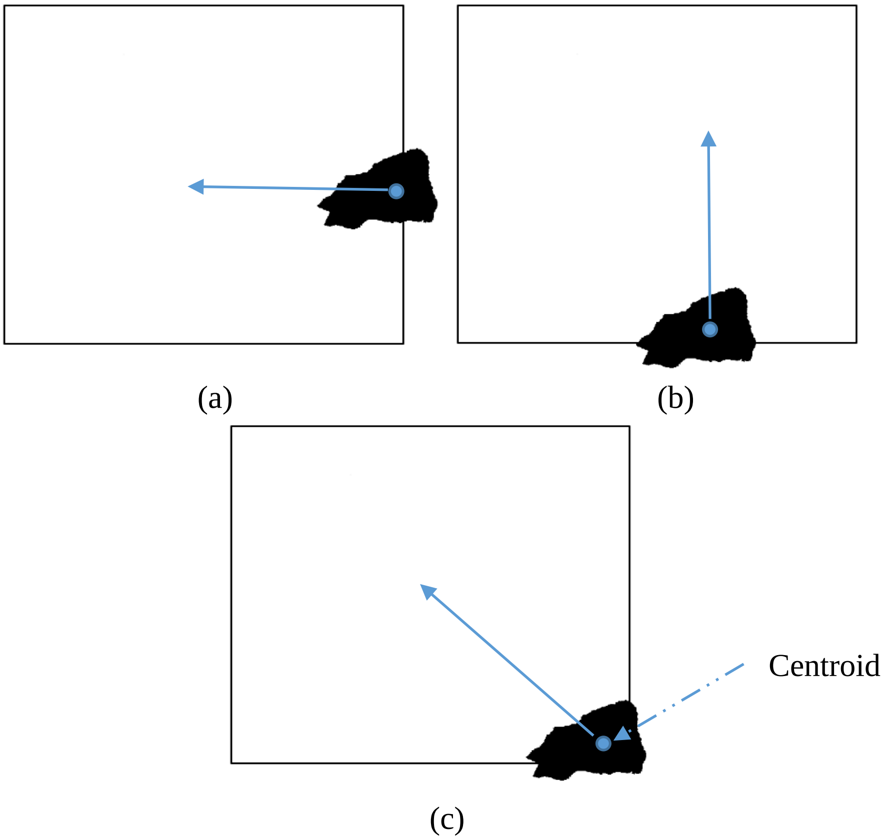

Figure 3.14. Particle positioning

3.5.3. Synthetic Image Outputs

The algorithm records all the information belonging to all particles during the redistribution. The most important parameters can be listed as area, centroid coordinate and maximum Feret diameter. These parameters are used for the microstructural characterization of image cross sections. The algorithm also records the spatial distribution of aggregates in the synthetic images for each size fraction as shown in Figure 3.15. D is the sieve size for the aggregates. This function of the algorithm is very crucial for the homogeneity evaluation.

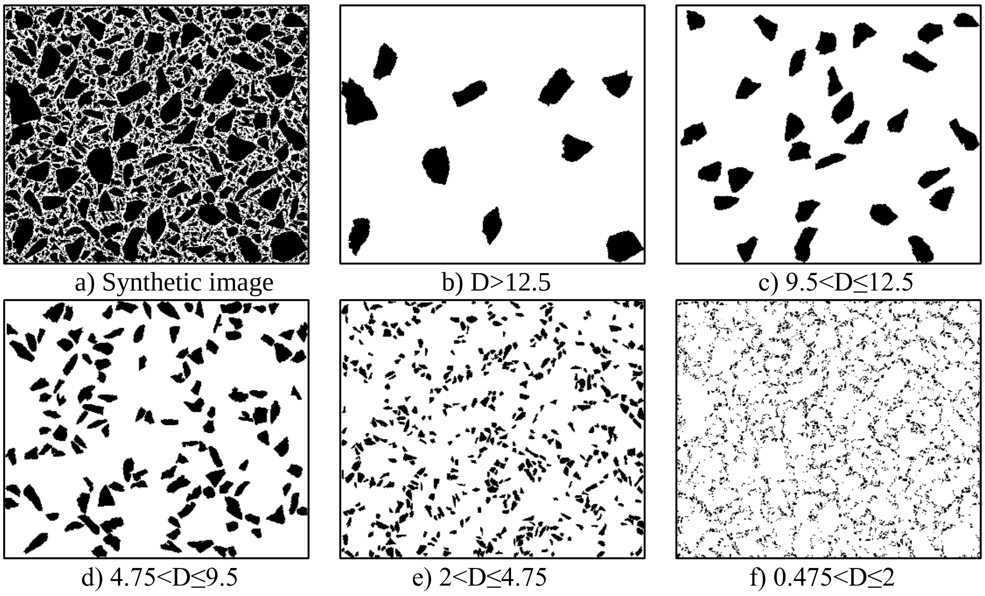

Figure 3.15. Distribution of aggregates from each size fraction

Figure 3.15 (a) shows the synthetic cross section image produced by the algorithm and the other figures show particles retained on sieves 12.5, 9.5, 4.75, 2 and 0.475, respectively. Particles from each size fraction were determined according to their maximum Feret diameters as explained in the previous sections. Because the resolution of images is known, the algorithm can convert pixel data to metric units. The determination of aggregate distribution for each fraction is implemented for both the original image and synthetic images. Therefore, the main advantage of this feature is that a user can observe if there is coarse or fine aggregate pockets in the mixture by examining the results of the original cross section image.

3.6. Evaluation of Mixture Inhomogeneity Using Macro Blocks

The distribution of coarse and fine aggregates is expected to be uniform within a homogenous mixture. The probability of finding particles from a specific size fraction is expected to be equal throughout a homogenous specimen cross section. Macro block is a block of pixels selected in the cross section image and it is a representative sample element of the section images. When any macro block is positioned within a cross section image, the aggregate size distribution of this macro block should be equal or close to the overall size distribution of the mixture. The deviation from the expected size distribution in each macro block positioning controls the level of inhomogeneity.

To measure the correlation of the observed and expected values, there are some widely used statistical methods. These methods are Mean Absolute Error (MAE), Mean Absolute Percentage Error (MAPE) and Root Mean Square Error (RMSE). In this study, MAPE index was used in the analyses to determine degree of deviation. However, standard MAPE expression was modified in order to include effect of area proportion of each size fraction. MAPE actually calculates the arithmetic mean absolute percent error but the equation was modified as weighted average to reflect the importance of each size fraction in proportion to the area. Modified MAPE expression ($MAPE_w$) is given in Equation 3.2.

$$MAPE_w = \sum_{i=1}^{n} w_i \left| \frac{O_i - E_i}{E_i} \right| x100\% \tag{3.2}$$

where E = Expected aggregate area (pixel) retained on *i*th sieve; O = Observed aggregate area (pixel) retained on *i*th sieve; w = The aggregate proportion of *i*th size fraction; n = Number of aggregate size fractions.

The expected aggregate area term (E_i) represents the anticipated aggregate area of *i*th size fraction in any macro block. E_i is calculated based on the actual aggregate proportions and it includes aggregate areas of each size fraction in the case of ideal uniform distribution. The observed aggregate area (O_i) denotes the area of aggregates retained on *i*th sieve for each new position of a macro block. The modified MAPE expression given in Equation (3.2) is only for a single macro block. However, in the proposed test method, a number of macro blocks are used to calculate the MAPE index for each cross section image. The average of the modified MAPE values are then calculated to obtain the inhomogeneity index of the cross section using Equation 3.3.

$$Inhomogeneity\ Index = \frac{1}{k}\sum_{i=1}^{k}(MAPE_w)_i \tag{3.3}$$

where k = the number of macro blocks positioned within specimen section image. As the inhomogeneity index increases, the deviation from the expected size distribution increases. In the case of the ideal uniform aggregate distribution, the inhomogeneity index is expected to be 0.

3.6.1. Macro Block Application Methods

In the scope of this study, three macro block application methods have been discussed. After many trials, the moving macro block method was selected as the most feasible method to calculate the MAPA index for inhomogeneity analysis. The details of the method are given in the below sections.

3.6.1.1. Discrete Level Tiling Method

In discrete level tiling methodology, a section image is divided into equal size of non-overlapping rectangles and analyses are conducted based on the information of aggregate particles available on each rectangular macro block. In this method, the number of macro blocks is very limited. Only 4, 6 or 9 macro blocks could be used in this method because of size limitation of the cross section images. If the number of macro blocks is increased, the size of macro blocks decreases, hence analyses produce biased results. Because of these limitations, this procedure was not preferred in this study. A graphical description of the method is shown in Figure 3.16. The figure shows the whole section image and rectangular macro blocks.

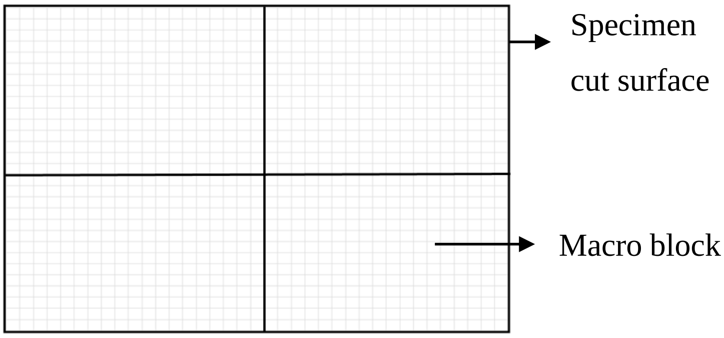

Figure 3.16. Graphical description of the DLT method

3.6.1.2. Randomly Located Macro Blocks

In the randomly located macro block method, the macro blocks are positioned randomly within an image section for the calculation of the inhomogeneity index. At first, the location of first corner of a square macro block (P1) is determined randomly and then the coordinates of the other three corners are calculated by the algorithm using the dimensions of the macro block. Many macro block can be positioned within image section using this method. The process is repeated till so many inhomogeneity indices are calculated to determine the overall sample inhomogeneity. Application of random macro block method is depicted in Figure 3.17. P1, P2, P3 and P4 show the corner points of any macro block.

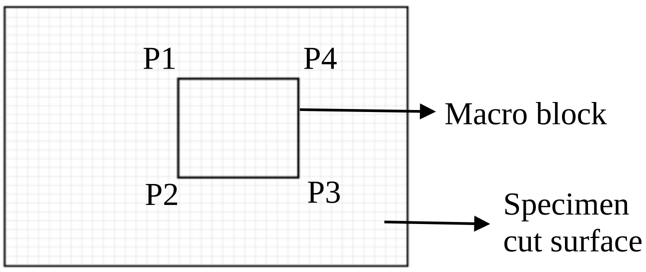

Figure 3.17. Random macro block application in the algorithm

In this method, the macro block positions are selected randomly by the algorithm, as a result all cross sections may not be sampled. Although it is an easy and practical method, it was not used in the study because of the possibility of incomplete sampling of the entire image.

3.6.1.3. Moving Macro Block Method

This method was introduced by Hamad et al. (2007) to measure homogeneity in images of chemical mixtures. The authors used the average intensity values of the included pixels in the macroblocks and several modified versions of this method were used in many fields so far.

In the moving macro block method, an image is scanned starting from the upper left corner of the image using macro blocks and data are recorded in each step. In this method, a macro block is firstly positioned on the upper left hand corner of the image and moves downward with a specific step size until reaching the bottom edge of the image frame. The aggregate areas in the selected macro block are compared with the expected aggregate areas for each size fraction to determine the degree of segregation. Figure 3.18 shows initial position of the macro block.

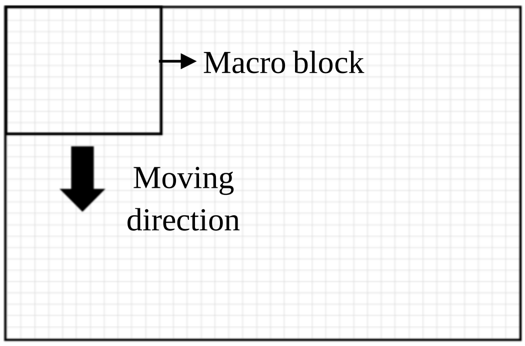

Figure 3.18. Inıtial position of macro block

Figure 3.19 shows first steps of macro block with a constant step size. A macro block continues scanning the image until it reaches the bottom of image.

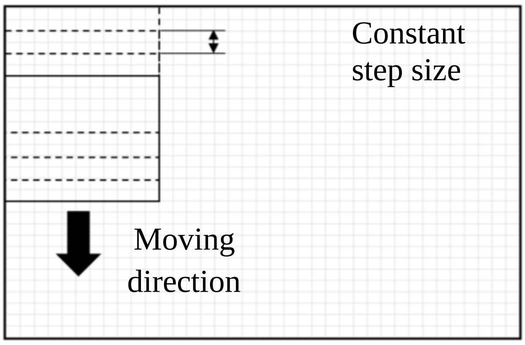

Figure 3.19. Macro block movement at the beginning

After reaching the bottom-left corner of the image, the macro block moves up top of the image and moves right with the same step size and continues scanning until finishing all the image. After the completion of the scanning, index values are determined for each step and the average of the index values is calculated to find an overall index value corresponding to the entire cross section.

There are two possible deficiencies in this method. First one is that if small step sizes like one pixel are used, it results in very long computation time. Second possible problem is that if the step size is increased, some parts of the macro block may be outside the image area during the scanning. The solutions of these two possible problems are discussed in the following sections.

3.6.2. Minimum Representative Macro Block Size Selection Criteria

Side length of a square macro block in pixel unit is named as macro block size. The minimum representative macro block size has to be large enough to represent the actual gradation of the test samples, however, small enough to capture local variations in homogeneity within the specimen cross sections. The representative macroblock size was determined according to the particle size distribution of the mixtures obtained from the section images. It is expected that a representative macro block located on any position in the image should contain at least one particle which retained on the largest sieve available in the mixture. The average area of the aggregates retained on the largest sieve is calculated to find the expected aggregate area of the largest size fraction in the representative macro block. The average area of particles in largest size fraction is used as a reference value during the expected area calculation of other size fractions. The area of the other size fractions which the macro block is expected to contain are calculated considering the retaining area proportions obtained from all sections for a mixture. Area of the aggregates which any macro block is expected to contain is named as representative aggregate area (*r*). To convert the representative aggregate area to macro block size, area fraction which is equal to aggregate area-image area ratio (*p*) is used. The area fraction in a macro block should be equal to total area fraction calculated using all section images used in the analysis. The calculation of the area fraction is given in Equation 3.4.

$$p = \frac{total\ aggregate\ area}{area\ of\ all\ cross\ sectional\ images} \tag{3.4}$$

In this equation, total aggregate area is sum of the aggregate areas larger than minimum considered size available in cross sections. Using the area fraction (*p*) and the representative aggregate area (*r*) information, minimum representative macro block size is calculated as shown in Equation 3.5.

$$representative\ macroblock\ size = \sqrt{\frac{r}{p}} \tag{3.5}$$

If any macro block size larger than the calculated representative size is selected, inhomogeneity cannot be distinguished. Similarly, very small macro blocks may cause unrealistic results because of large aggregate particles in the images. Aggregate size distribution, especially coarse aggregate quantity, and aggregate fraction in the cross sections controls the representative macro block size.

Representative macro block size is determined based on two main criteria. First one is that the macro block size should be large enough to contain particles from each size fraction. Second criteria is that the probability of finding an aggregate of a specific size fraction should be same for both macro block and the cross sections. The probability of finding particles retained on *i*th size fraction in the cross section images is equal to;

$$P(i, total) = \frac{A_{i,total}}{total\ image\ area} \tag{3.6}$$

where $A_{i,total}$ = the area of aggregates retained on *i*th sieve in all section images taken from the specimens; *total image area* = area of all section images; *P(i, total)* = the probability finding aggregates retained on *i*th sieve in all sections.

The probability of finding the aggregates retained on *i*th size fraction in a macro block;

$$P(i, macro\ block) = \frac{\frac{A_{i,total}}{k_{1,total}}}{representative\ macro\ block\ area} = \frac{A_{i,total}}{total\ image\ area} \tag{3.7}$$

These two results (Equations 3.6 and 3.7) proves that;

$$P(i, total) = P(i, macro\ block) \tag{3.8}$$

As shown in the results, probability of finding aggregates retained on *i*th sieve is the same as for the tested image sections and any macro block section located on those cross sections.

3.6.3. Optimum Step Size for the Moving Block Method

Implementing the moving macro block method with one pixel step size results in very high computation time and very big data files. One pixel step size is acceptable for images with low resolution and small size; however, when the image size is large, then a significant amount of time may require to complete the analysis. In order to tackle this problem, increasing the step size can be a feasible solution by selecting a step size that can still produce an acceptable level of accuracy. In order to decide on an optimum step size, different step sizes were tried for different mixture images. Effect of the step size on inhomogeneity index was evaluated with this analysis. For this, the middle slice faces of four asphalt concrete specimens were used to calculate optimum macro block sizes. The step size versus inhomogeneity index results are plotted in Figure 3.20.

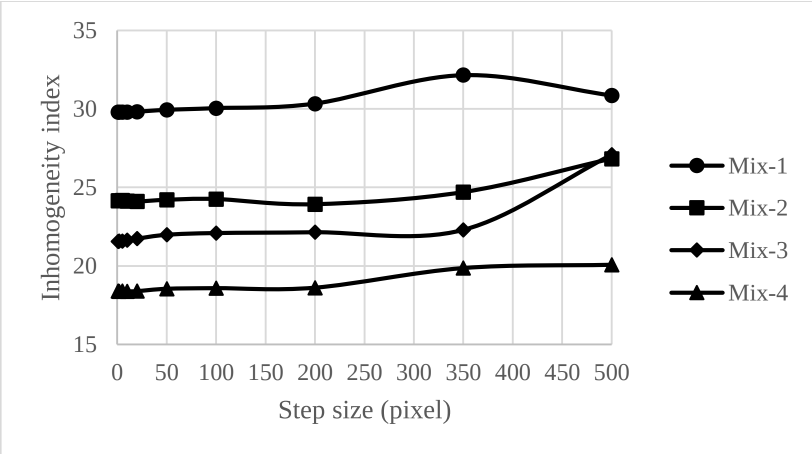

Figure 3.20. Effect of step size on inhomogeneity index

As can be shown in the graph, up to a certain step size the inhomogeneity index is not affected. It was decided to use 50 pixels (approximately 0.2 mm) as a step size for all the images analyzed in this study for an image resolution of 600 dpi.

3.6.4. Image Padding

During moving macro block method application, if some parts of the macro block falls outside of the section image, image padding operation is implemented by the algorithm. In the padding operation, the symmetry of the outer part, which is located inside the image, is used for calculations.

An example image padding is shown in Figure 3.21.

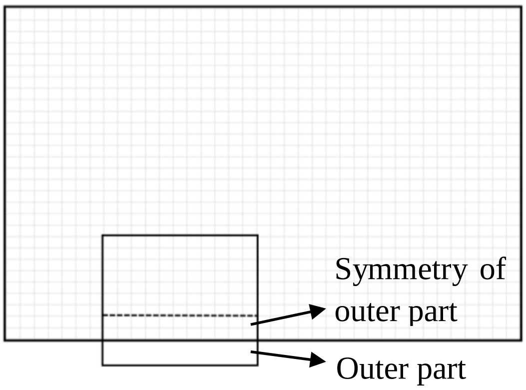

Figure 3.21. Graphical description of image padding

3.6.5. Number of Macro Blocks in Image

In using the moving macro block method, the number of macro blocks positioned within an image section depends on the image size and the selected macro block size. Calculation of the total number of macro blocks is illustrated in Figure 3.22.

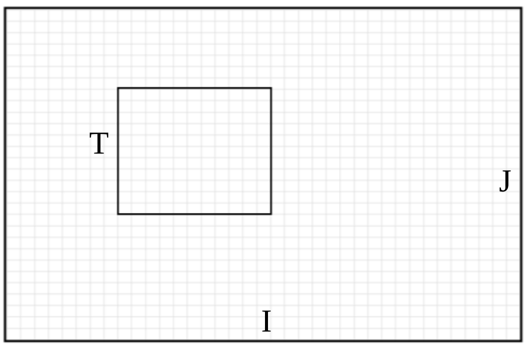

Figure 3.22. Section image and macro block dimensions

where I = Size of long direction of the image; J = Size of short direction of the image; T = Macro block size.

Based on these parameters, the total number of macroblocks can be calculated using Equation 3.9;

$$Number\ of\ Macro\ Blocks = \left[\left(\frac{J-P}{K}\right)+1\right] \times \left[\left(\frac{I-P}{K}\right)+1\right] \tag{3.9}$$

where K = Step size (pixel) for the moving macro block.

3.6.6. Evaluation of Asphalt Mixture Inhomogeneity Level

The calculated inhomogeneity indices cannot be directly used as an indicator of inhomogeneity level because area fraction and aggregate size distributions are different in each cut specimen. Inhomogeneity evaluation of a specimen can be conducted using one or multiple cross sectional images for each specimen according to sensitivity and specimen size. Using a large number of cross sections for each specimen increases the success of the test; however, sometimes small specimen sizes may not allow to use more than one image. To obtain characteristic of aggregate distribution in a cross section and see the change in inhomogeneity index, as many as 1000 synthetic images for each cross section are generated using the redistribution algorithm and the cumulative probability distributions of inhomogeneity indices are determined for all cross sections used in the analysis. The probability level corresponding to the inhomogeneity index of the original cross section gives the inhomogeneity level of the corresponding cross section.

3.7. Implementing the Proposed Test Method

In the analysis of the test samples, macro block sizes were calculated for each mixture separately using the explained methodology. Expected aggregate areas (E_i) within a macro block for each size fraction were calculated based on the actual aggregate proportions within the specimen cross sections. In other words, each size fraction within a macro block was taken proportionally to be equal to the entire aggregate fraction within the specimen cross sections. In this way, the probability of finding aggregates with a specific size fraction is the same for both macro blocks and the cross sections in the expected aggregate distribution condition. The observed area of aggregates (O_i) was determined using the developed algorithm for each new position of the macro blocks. The cumulative distribution functions (CDF) of the inhomogeneity indices for all cross sections of four mixtures were drawn. The CDF plots illustrate the range of inhomogeneity indices under trial combinations of aggregate distributions.

Figure 3.23 shows the cumulative probability distributions of inhomogeneity indices for 4 mixtures obtained from 3 cross sections of each mixture.

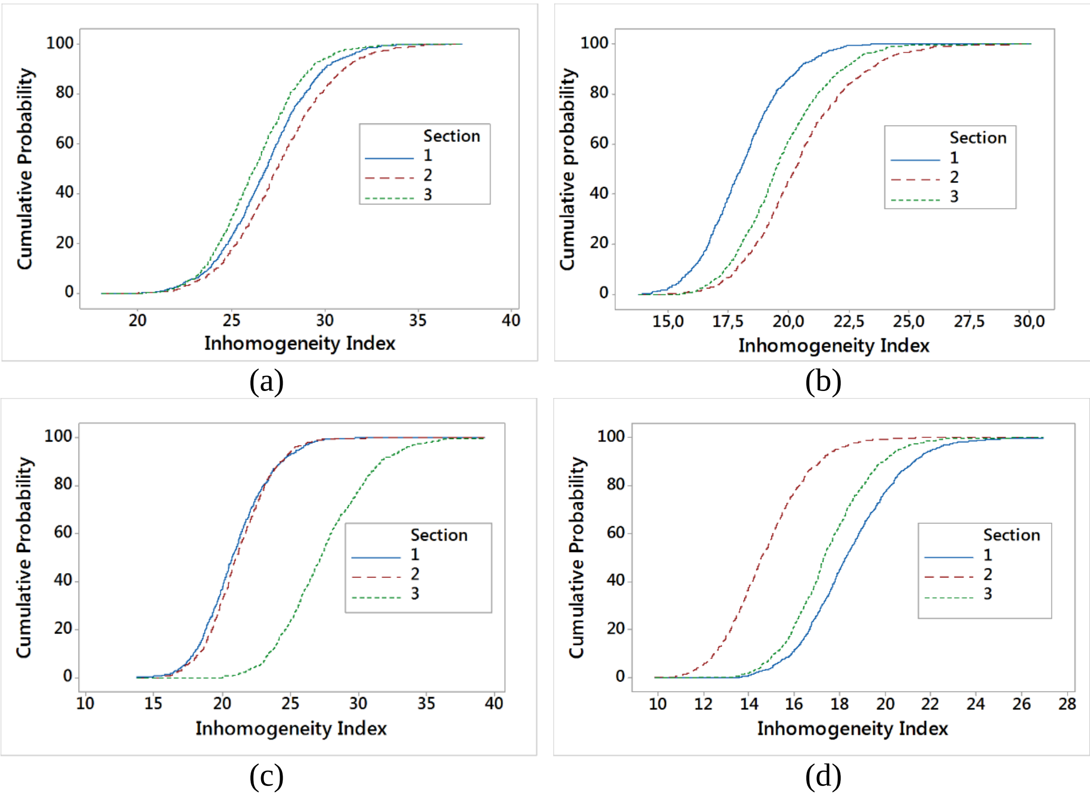

Figure 3.23. Cumulative probability distributions of the cross section indices; a) Mix-1, b) Mix-2, c) Mix-3, d) Mix-4

After analyzing the distributions, it was determined that indices are log-normally distributed. Probability levels corresponding to inhomogeneity indices were determined from empirical cumulative distribution functions for all the cross sections. Probability level means a cumulative probability value corresponding to the inhomogeneity index of the original cross section. Smaller probability levels mean better uniformity of aggregate distribution and greater probability levels shows a more heterogeneous mixture.

Similar to the cross sections, inhomogeneity level of the specimens was determined using all cross section images of the specimen. The sum of three empirical cumulative distribution functions of the cross sections were calculated for each specimen and the distribution functions representing the specimens were obtained. Inhomogeneity index values obtained from three original cross sections were used to find the specimen index by calculating the sum of them. Similar to the cross section homogeneity, probability levels corresponding to the specimen index values were determined. Cumulative probability distributions of the inhomogeneity indices of the four specimens are shown in Figure 3.24. Similar to the cross section indices, specimen indices are log-normally distributed. Inhomogeneity indices and corresponding inhomogeneity levels are given for 4 specimens and their 12 cross sections in Table 3.4.

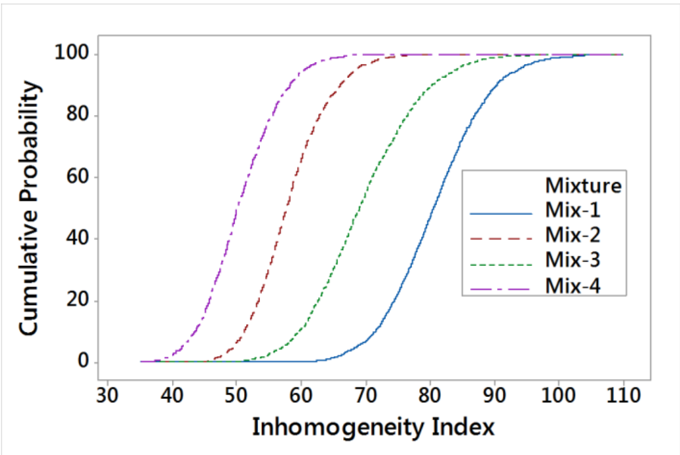

Figure 3.24. Cumulative probability distributions of the specimens

Table 3.4. *Inhomogeneity test results*

Cross Section No.		Image Size (Pixel)	Macro block size (pixel)	Inhomogeneity Index of Cross Section	Inhom. Level of Cross Section	Inhomogeneity Index of Specimen	Inhom. Level of Specimen
Mix-1 (Basalt-Coarse)	1	3504x 2968	1023	29.94	88.5	90.59	89.9
	2	3352x 2976	1023	29.54	77.5		
	3	3324x 3004	1023	31.11	97.4		
Mix-2 (Basalt-Fine)	1	3548x 3028	952	24.21	99.9	66.51	92.0
	2	3160x 3032	952	19.95	43.0		
	3	3184x 3016	952	22.35	91.8		
Mix-3 (Limestone-Coarse)	1	3516x 2721	1225	21.99	67.8	70.13	54.9
	2	3237x 2721	1225	25.16	94.5		
	3	3171x 2724	1225	22.98	7.3		
Mix-4 (Limestone-Fine)	1	3564x 2748	1088	18.54	54.1	56.70	85.5
	2	3184x 2752	1088	16.73	86.9		
	3	3159x 2748	1088	21.43	97.7		

Table 3.4 shows the image size and macro block size values calculated for all cross sections. The macro block sizes were calculated for each mixture separately and all three sections were considered for the calculation. The aggregate surface parameters such as particle areas corresponding to each sieve size and area fraction of the three cross sections were used to calculate macro block size of the specimens. Inhomogeneity indices of all cross sections were determined by implementing the moving macro block method. These inhomogeneity indices do not give any important information about segregation level since the index may change depending on the area fraction and area of particles independent of aggregate spatial distribution. To see aggregate distribution characteristics 1000 synthetic images for each cross section

were created using the redistribution algorithm. The inhomogeneity levels corresponding to inhomogeneity indices of the original cross sections were found. As the inhomogeneity level increases, segregation of the mixture increases. The cumulative probability functions for each specimen were summed up to determine inhomogeneity levels of the specimens. If the number of cross sections is increased for a specimen, it is obvious that the accuracy of the test increases. Inhomogeneity levels for mixtures 1-4 were determined as 89.9, 92, 54.9 and 85.5, respectively. The results show that the most homogenous specimen in this group is mixture-3 and the most segregated specimen is mixture-2.

3.8. Controlled Inhomogeneity in Synthetic Images

Using the aggregate redistribution algorithm, inhomogeneous cross sections can be generated at different levels. By the help of these images, the power of the proposed test index was measured. Figure 3.25 shows example of inhomogeneous section images generated using the center cross section images of the four specimens.

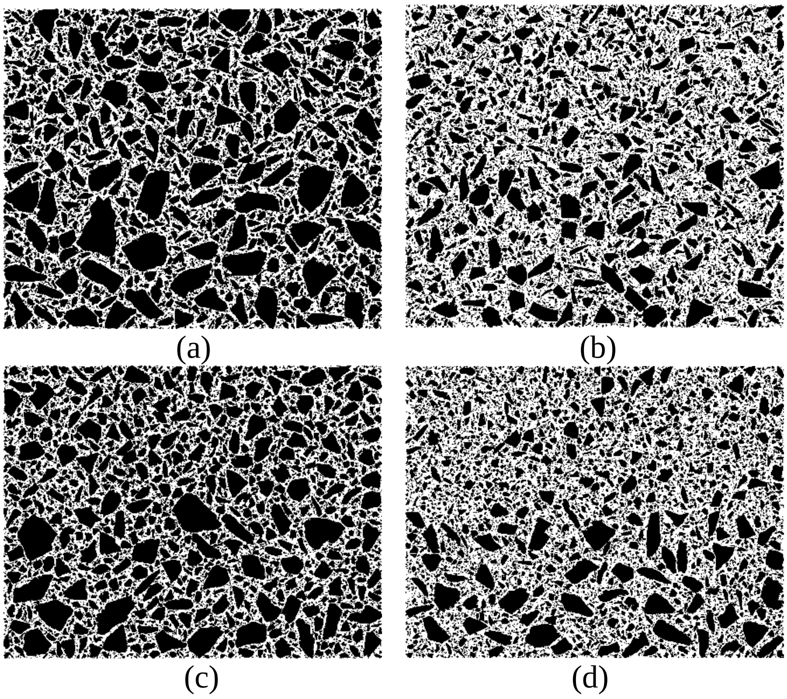

Figure 3.25. Controlled inhomogeneity; a) Mix-1, b) Mix-2, c) Mix-3, d) Mix-4

Controlled inhomogeneous microstructures were produced by restricting the coarser aggregates from upper half part of the images. The size limit for the restricted particles was selected as the sieve size corresponding to 25% retaining for each mixture. The developed controlled inhomogeneity algorithm was applied for 12 cross section images belong to the four mixtures and 1000 synthetic images for each cross section created. Figure 3.26 shows the example microstructures of asphalt mixture cross sections which contain randomly distributed and intentionally segregated aggregates. Synthetic images with all available particles are given on the top, and the distribution of aggregates for all size fractions is also given below. Restriction of coarse aggregates from upper half of the image can be seen obviously in the figures. Since coarser aggregates concentrate on the lower half of image, presence of finer material increases in the upper half section.

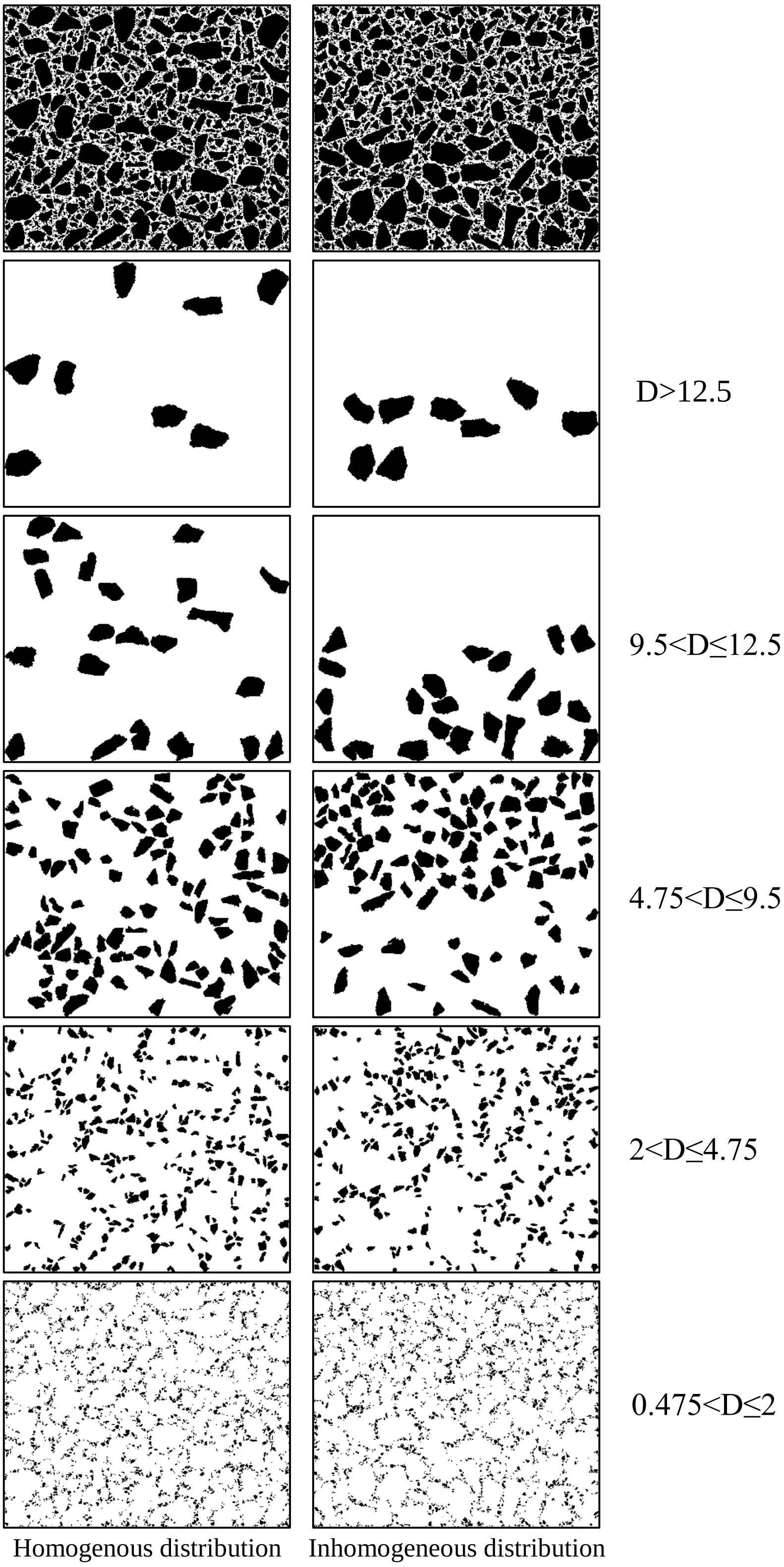

Figure 3.26. Homogenous and inhomogeneous distribution of aggregates

The index of randomly distributed and segregated synthetic cross sections were compared for the power of the test. Minimum coincidence of the probability distributions of random and restricted aggregate distributions is expected for the higher power of the proposed test method (Figure 3.27).

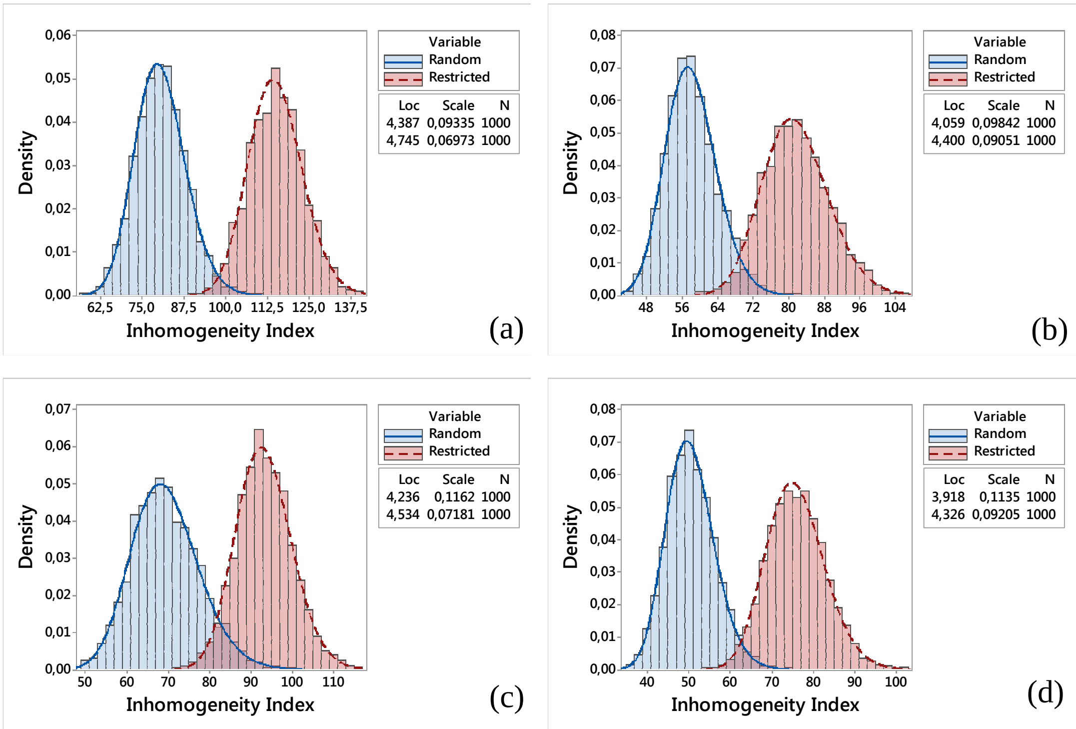

Figure 3.27. Probability distributions of homogenous and inhomogeneous cases; a) Mix-1, b) Mix-2, c) Mix-3, d) Mix-4

Figure 3.27 shows the distribution of the test indices of the four mixtures for the random and restricted distribution of aggregates. Graphs show that the coincidences of the probability distributions are very small for all cases, hence it can be inferred that the power of the proposed test is strong. To determine the power of the proposed test, the distributions of the index under both random and restricted distribution conditions were compared. Critical statistics were determined using the distribution of inhomogeneity in the case of random distribution of the aggregates. In this study, three significance levels, also known as type I error (α), were considered, which are 10%, 5% and 1%. The critical statistics were determined using the cumulative distribution functions corresponding to values of 90%, 95% and 99%, respectively. The critical statistics of available indices were generally calculated for 5% significance level in previous studies. The calculated critical values were used to compute the probabilities of type II error (β). The power of the test is equal to 1- β. If it is close to 1, it means high power. High power of the test means that the method can evaluate inhomogeneity level of the asphalt mixture samples successfully.

Table 3.5 shows the critical values for 10%, 5% and 1% significance levels, probabilities of type two errors (β) and corresponding statistical power of the test.

Table 3.5. *Critical values and power of the test*

Mix	**Critical Values**			**Prob. of Type II Error, β**			**Power of the Test**		
	α=0.10	α=0.05	α=0.01	α=0.10	α=0.05	α=0.01	α=0.10	α=0.05	α=0.01
Mix-1	90.62	93.75	99.90	0.000	0.002	0.022	1.000	0.998	0.978
Mix-2	65.70	68.09	72.82	0.009	0.024	0.108	0.991	0.976	0.892
Mix-3	90.23	83.69	90.59	0.019	0.068	0.350	0.981	0.932	0.650
Mix-4	58.15	60.60	65.47	0.002	0.008	0.058	0.998	0.992	0.942

The data in Table 3.5 show that the power of the test for 5% and 10% significance levels is higher than 0.90 (90%) for all mixtures. The test power for 1% significance level is larger than 90% for all mixtures except for mix-2 and mix-3. Test powers for 5% significance level (95% confidence interval) were determined as 0.998, 0.976, 0.932 and 0.992, respectively. Studies conducted for four different design mixtures indicates that the power of the test is considerable high for all cases. It is concluded that the proposed test method can be used to evaluate the inhomogeneity level of asphalt concrete mixtures.

CHAPTER 4

MECHANICAL TESTING OF ASPHALT MIXTURES

In this chapter, the design and preparation of asphalt mixture specimens and repeated creep test results are discussed. Two groups of specimens were prepared in this thesis study to simulate different field conditions. In the first group, asphalt mixture specimens were compacted under the same compaction effort; however, specimens of second group were compacted at the same density corresponding to 4% air void. Different aggregates and binders were used for two groups. Aggregates of both groups are limestone but they are obtained from different sources. Similarly, both binders were 50/70 penetration grade but they were obtained from different sources. Three sets of specimens were prepared for each group. The only difference between the sets was the segregation levels. To simulate laboratory segregation, biased and unbiased specimens were prepared. The unbiased specimens were prepared as homogenous as possible; however, biased specimens were segregated intentionally using laboratory techniques at medium and high levels. After specimen preparation step, the repeated creep test conditions and the result of the tests for both groups are discussed.

4.1. Asphalt Mixture Design for Specimens Compacted at Same Energy

4.1.1. Aggregate Properties and Selecting Design Gradation

Mixture design was conducted to meet AASHTO Superpave volumetric design standards (AASHTO M 323, 2010; AASHTO R 35, 2010). The mixture design includes one aggregate type, one binder type and one aggregate gradation. Limestone aggregate and 50/70 penetration grade unmodified binder obtained from TGDH (Turkish General Directorate of Highways) were used in this study. The aggregate gradation with a nominal maximum aggregate size of 19 mm was selected considering the Superpave aggregate gradation control points. Control points for the 19 mm nominal maximum aggregate size are shown in Table 4.1.

Table 4.1. *Aggregate gradation control points*

Sieve Size (mm)	Control Points (Percent Passing)	
	Min.	Max.
19	90	100
12.5		90
9.5		
4.75		
2.36	23	49
0.075	2	8

0.45 maximum density line provides a good reference to select the aggregate gradation. This is a straight line connects the origin and the maximum aggregate size. Figure 4.1 shows the control points, 0.45 power line and the design gradation curve that was selected after several trials to meet the specification limits.

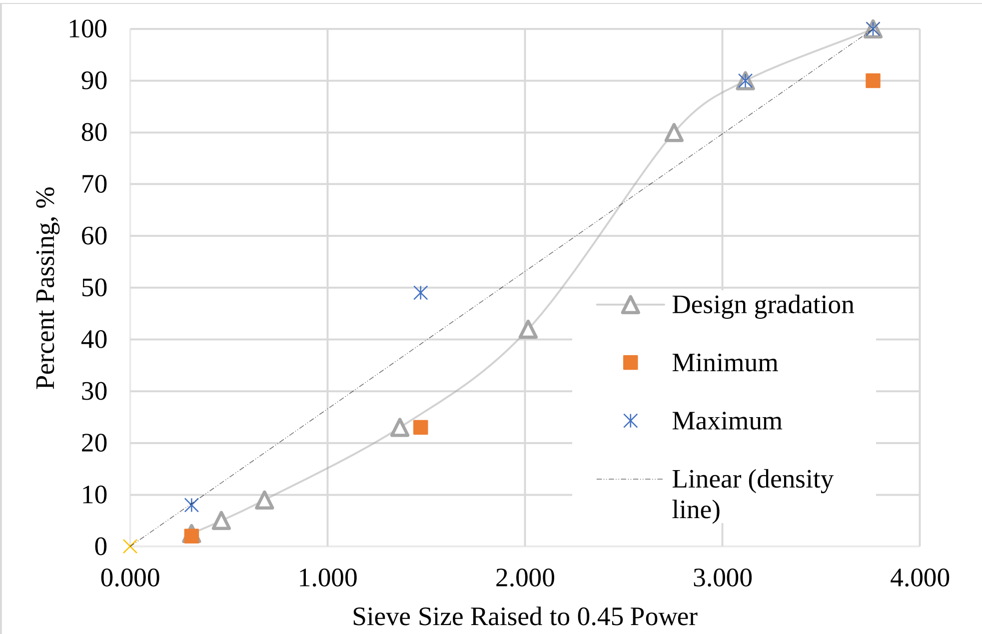

Figure 4.1. Gradation curve

The physical properties of limestone aggregate were determined by conducting necessary experiments. Specific gravity and Los Angeles abrasion test results are given in Table 4.2. Coarse, fine and filler parts of the design gradation were separated and specific gravity tests were conducted for each group separately.

Table 4.2. *Properties of limestone aggregate*

Test	**Result**	**Specification**
Bulk Specific Gravity (Coarse)	2.684	AASHTO T 85 (2010)
Bulk Specific Gravity (Fine)	2.664	AASHTO T 84 (2010)
Apparent Specific Gravity (Filler)	2.704	AASHTO T 100 (2010)
Los Angeles Abrasion (%)	32	AASHTO T 96 (2010)

Using the specific gravity values of coarse aggregate, fine aggregate and filler, bulk specific gravity of the combined aggregate (G_{sb}) is calculated using Equation 4.1.

$$G_{sb} = \frac{P_1 + P_2 + P_3}{\frac{P_1}{G_1} + \frac{P_2}{G_2} + \frac{P_3}{G_3}} \qquad (4.1)$$

where G_{sb} = Bulk specific gravity of the combined aggregate; P_1, P_2, P_3 = Percentages of aggregates; G_1, G_2, G_3 = Bulk specific gravity of aggregates.

The percentages of coarse aggregate, fine aggregate and filler in the blend are 58%, 39% and 3%, respectively. The bulk specific gravity of the combined aggregate (G_{sb}) was obtained as 2.677. This value was used in volumetric calculations.

4.1.2. Mixing and Compaction Temperature

An unmodified binder with a penetration value of 54 was used in the mix design of the asphalt concrete samples. Specific gravity of the binder (G_b) was determined as 1.036. To find the viscosity of asphalt binder at different temperatures, a rotational viscometer was used. The viscosity test was conducted according to AASHTO T 316 (2010) procedure. Starting from 120°C, the viscosity readings were taken at every 10°C temperature intervals until the temperature reaches 180°C. The temperature controller was programmed to reach target temperature within 30 minutes for each increment. The viscosity reading was taken after 10 minutes of equilibrium period at the target temperature. The viscometer speed was set to 20 rpm. The mixing and compaction temperatures of asphalt mixture were selected according to the target viscosity. The target viscosity values for the mixing and compaction temperatures are 0.17 Pa.s±0.02 (170 cP±20) and 0.28 Pa.s±0.03 (280 cP±30), respectively. After the test, the viscosity-temperature chart was obtained according to the procedure explained in the ASTM D2493 (2016). Using this chart, the mixing and compaction temperatures corresponding to the target viscosities were determined (Figure 4.2). According to the viscosity test results, the mixing and compaction temperatures were determined as 152°C and 140°C, respectively.

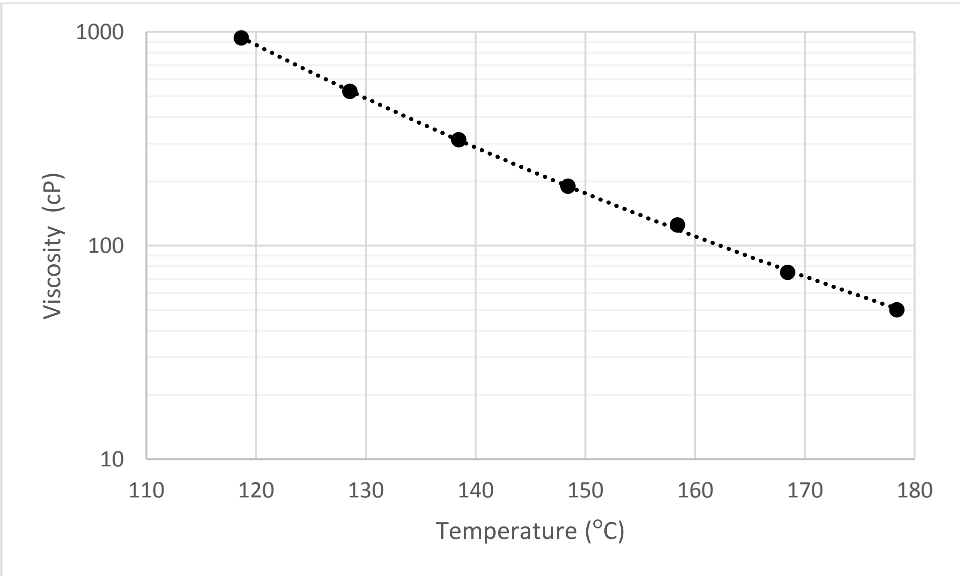

Figure 4.2. Viscosity-temperature chart

4.1.3. Optimum Asphalt Content for the Design Gradation

Trial aggregate gradations were selected and then an initial trial asphalt content was determined for each trial gradation. A design aggregate structure and an estimated design asphalt content were selected based on the volumetric results of trial specimens.

To determine the optimum asphalt content, specimens with four different asphalt contents, i.e., estimated design asphalt content, estimated ± 0.5, estimated +1%) were prepared. In addition to the estimated design asphalt content of 5%, three more asphalt contents, which are 4.5%, 5.5% and 6% were used in the fabrication of specimens. Superpave Gyratory Compactor (SGC) was used for the compaction of mixture samples under 600 kPa (6.6 bar) pressure and 1.25° gyration angle. To fabricate mixture samples, 4900 g aggregate was mixed with asphalt binder at the selected asphalt contents. Table 4.3 shows the Superpave mix design parameters used in this design.

Table 4.3. *Superpave mix design parameters*

Design Parameters	**Selected/Calculated Values**
Number of Gyrations (N_{des})	100
Cumulative Traffic Assumed	3-10 Million
Mixing Temperature	152°C
Compaction Temperature	140°C
Air Void Content Selected for the Design	4%

During the mix design, procedures explained in the literature review part were followed. Filter papers and steel plates were placed on top and bottom of the mixture before the compaction. Mixture samples were conditioned two hours in the oven at the compaction temperature before proceeding to the compaction phase. The compaction was performed using a 150 mm mold that is rotated at 30 rpm while applying 600 kPa of compaction pressure. Compacted specimens were left for cooling before measuring the necessary volumetric properties. To find air void and the other volumetric properties of the specimens, the bulk specific gravity of the specimens (AASHTO T 166, 2010) and the theoretical maximum density of their loose mixtures (AASHTO T 209, 2010) were measured. To determine the theoretical maximum density, 1600 g mixture samples were prepared and then all the aggregate particles were laid on and separated on a clean surface. In addition to air void corresponding to each binder content, voids in mineral aggregates (VMA) and voids filled with asphalt (VFA) were also calculated. The results of these tests are shown in Figure 4.3. The graphs show asphalt contents versus air void, voids in mineral aggregate (VMA), voids filled with asphalt (VFA) and unit weight. All volumetric parameters were calculated according to AASHTO R 35 (2010).

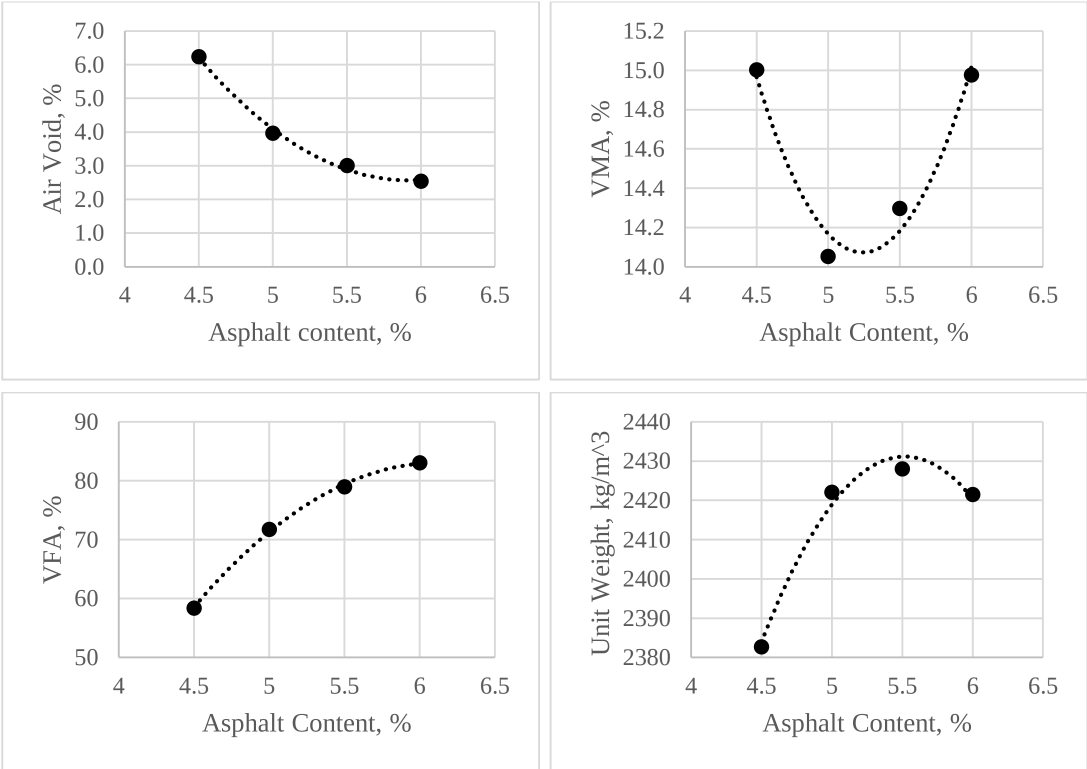

Figure 4.3. Test results

An optimum asphalt content of 5% was determined at 4% air voids. Other volumetric parameters such as voids in mineral aggregates and voids filled with asphalt were determined corresponding to 5% asphalt content to control compliance with the specification requirements. Dust-to-binder ratio was also calculated based on the effective binder content. Results show that all the design mixtures satisfy the Superpave hot mix asphalt design requirements. The necessary design requirements and the volumetric test results at 4% air voids are given in Table 4.4.

Table 4.4. *Results and design requirements*

Parameter	Test results	Design Requirements
Air Void (Va), %	4.000	-
Voids in the Mineral Aggregate (VMA), %	14.1	min. 13
Voids Filled with Asphalt (VFA), %	71.8	65-75
Dust-to-Binder Ratio	0.701	0.6-1.2

4.1.4. Fabrication of Homogenous and Segregated Specimens

Segregation in asphalt mixture can occur as a result of non-uniform distribution of coarse and fine aggregates. Laboratory experiments were carried out to evaluate the effect of segregation at different levels on the rutting resistance of asphalt concrete specimens. To simulate asphalt mixture segregation, special laboratory techniques were used. In addition to homogenous unbiased control asphalt mixture specimens, two sets of artificially segregated mixtures were fabricated to simulate various degrees of segregation. This experimental part included 4 steps: (i) preparing homogenous and segregated asphalt concrete samples; (ii) coring and trimming of the samples to satisfy the size requirements of the rutting tests; (iii) implementing the repeated creep tests to evaluate rutting resistance of the specimens; (iv) cutting the tested specimens vertically from the midpoints and then obtaining digital images of the cut sections to implement inhomogeneity tests in conjunction with the imposed segregation levels.

Six specimens were fabricated for each mixture set and they were labeled as homogenous- unbiased, middle level segregated-biased and high level segregated-biased specimens. The first set was prepared as homogenous as possible. The second and the third sets were intentionally prepared as inhomogeneous mixtures at different levels. To produce the biased specimens, design gradation was batched and mixed as two portions by separating coarser and finer portions, and placed into the mold as two layers. Lower part of the specimens was prepared with coarser gradation than the overall design gradation. The gradation of the upper section was adjusted to a finer gradation than the overall gradation of the sample. However, the overall gradation of the biased specimens was still maintained equal to the design gradation of each mixture sample.

The fine and coarse aggregate percentages in the biased specimens were determined after a number of trials in the laboratory. According to the design gradations, 58% of the aggregates were retained on No. 4 sieve and 42% of the aggregates were passed through No. 4 sieve. To create coarser and finer proportions, coarse and fine aggregates were blended at different percentages. In the medium level segregated-biased case, 68% of the coarse aggregates and 40% of the fine (includes filler) were blended for the coarser portion. The finer portion was prepared by blending 32% of the coarse aggregates and 60% of fine aggregates. In the high level segregated-biased case, 73% of the coarse aggregates and 40% of the fine aggregates were blended for coarser portion. The finer portion was prepared by blending 27% of the coarse aggregates and 60% of fine aggregates. Regardless of the combination of the coarser and finer portions used, the overall gradation of each mixture sample was kept equal to their respective design gradations determined in the first phase phase of the study. Details of the coarser and finer portions used and the actual design gradations are given in Table 4.5.

Table 4.5. *The coarser and the finer portion gradations*

Size Opening (mm)	Design Gradation	Medium Level Segregated-Biased		High Level Segregated-Biased	
		Coarser Portion	**Finer Portion**	**Coarser Portion**	**Finer Portion**
19	100	100.0	100.0	100.0	100.0
12.50	89	86.7	92.0	86.4	92.7
9.5	80	75.8	85.4	75.3	86.8
4.75	42	29.9	57.6	28.4	61.7
2	23	16.4	31.5	15.6	33.8
0.425	8	5.7	11.0	5.4	11.7
0.18	4	2.8	5.5	2.7	5.9
0.075	3	2.1	4.1	2.0	4.4

Graphical representation of the design gradations and the gradations of the coarser and finer portions included in the medium and the high level segregated-biased specimens are shown in Figure 4.4.

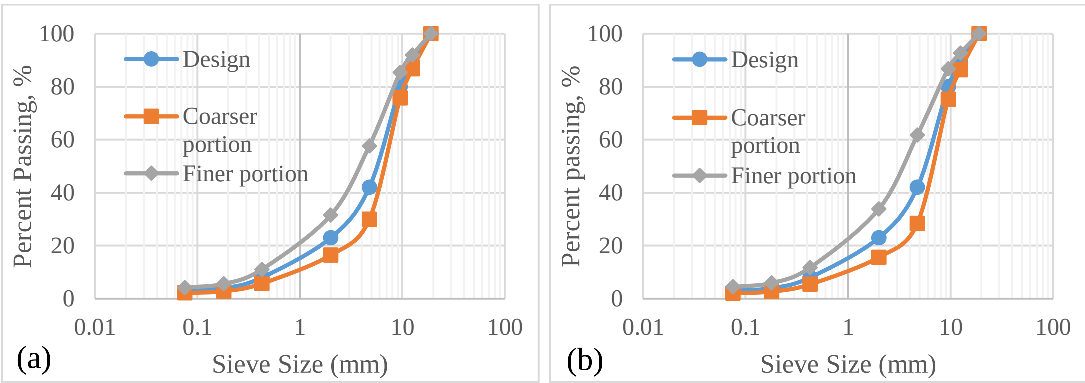

Figure 4.4. Gradations of the coarser and finer portions; a) Medium level segregated-biased, b) High level segregated-biased

Asphalt contents of the coarser and finer portions were calculated based on equal film thickness approach. Overall asphalt content of the inhomogeneous mixtures was equal to the optimum design asphalt content; however, coarser and finer portions had different asphalt contents. Because of the greater aggregate surface area of the finer sections, asphalt contents for these sections were slightly higher than the actual optimum asphalt contents.

4.1.5. Asphalt Film Thickness Calculation

Asphalt film thickness of the mixtures was calculated based on the surface area of aggregates and the asphalt content according to Hveem method (Asphalt Institute, 2014). Surface area of aggregates is equal to the multiplication of the percent passing from the specified sieve size and the corresponding surface area factors. Table 4.6 shows surface area factors for each sieve size and total surface area calculation for the design gradations.

Table 4.6. *Surface area calculation of aggregates*

Sieve Size (mm)	**Passing (%)**	**Surface Area Factor**	**Surface Area, m^2/kg**
19	100	0.41	0.41 x 1 = 0.41
12.5	89	0.41	
9.5	80	0.41	
4.75	42	0.41	0.41 x 0.42 = 0.17
2.36	25.5	0.82	0.82 x 0.255 = 0.21
1.18	15.2	1.64	1.64 x 0.152 = 0.25
0.6	9.7	2.87	2.87 x 0.097 = 0.28
0.3	6	6.14	6.14 x 0.06 = 0.37
0.15	3.7	12.29	12.29 x 0.037 = 0.45
0.075	3	32.77	32.77 x 0.03 = 0.98
			3.12 m^2/kg

Because the sieve openings used in this study and the Hveem's method were different, the percent passing values corresponding to the standard sieve openings were calculated by interpolation. For the design gradations, the total surface area was calculated as 3.12 m^2/kg. The average asphalt film thickness of the design mixtures was calculated using the following formula (Equation 4.2).

$$FT = \frac{W_e AC}{SA \times G_b} \quad (4.2)$$

where where W_eAC = the weight of effective asphalt content, kg/kg of aggregate; SA = surface area, m^2/kg; FT = film thickness, µm; G_b = specific gravity of binder.

Using the above equation, the average film thickness at the optimum asphalt content was calculated as 13.82 µm. Asphalt contents of the coarser and the finer portions of the biased specimens were calculated by considering the equal film thickness of the two parts. Asphalt contents of the design gradation and the biased mixtures are given in Table 4.7.

For the repeated creep tests, the specimens with 100 mm diameter must be cored from the 150 mm diameter compacted samples. To obtain this height requirement, 7000 g of aggregate was used to achieve an overall specimen height of around 165 mm before trimming the specimen ends.

Table 4.7. *Asphalt contents of the finer and coarser portions*

Parameter	**Design Gradation**	**Medium Level Segregated-Biased**		**High Level Segregated-Biased**	
		Finer Portion	**Coarser Portion**	**Finer Portion**	**Coarser Portion**
Surface Area, m^2/kg	3.12	4.13	2.34	4.39	2.25
Asphalt Content, %	5	6.28	3.98	6.61	3.85
Aggregate Weight, g	7000	3063.2	3936.8	2860.2	4139.8
Asphalt Weight	368.5	205.4	163.1	202.6	165.9

During the fabrication of the biased specimens, coarser portion was first blended, mixed and placed into the oven. Next, the finer portion was also prepared by the same procedure and placed in to oven for conditioning. The time gap between placing the coarser and the finer portions into the oven was approximately 10 minutes. Two hours conditioning time was started 5 minutes after putting the coarser portion. After completion of the conditioning time, the coarser portion was initially placed into the mold and the top surface was leveled with a spatula. The finer portion was then placed into the mold. After leveling the top surface and putting filter paper and a steel plate, the compaction was started. For all specimens, 100 compaction cycles were applied using a Superpave gyratory compactor. The same procedure was applied for both the medium and the high level segregated-biased specimens.

4.1.6. Summary of Volumetric Calculations

To conduct repeated creep tests, six specimens for each segregation level were produced in the laboratory. Homogenous unbiased, medium level segregated-biased and high level segregated-biased specimens were fabricated as explained in the previous sections. The same compaction effort,100 gyrations, was applied to all specimens and this group was named as group-1 specimens (G1). After the compaction of the specimens, they were left for cooling at room temperature. AASHTO T 166 (2010) specification procedures (saturated surface dry water displacement method) were used to calculate bulk specific gravity of the compacted specimens. The bulk specific gravity is a key parameter for volumetric calculations and it is used to calculate air voids, VMA and VFA of the test specimens. The height of the specimens is also an important indicator to evaluate the compaction quality of specimens and it was measured and recorded by the gyratory compactor software. Figure 4.5 shows the height of the specimens after the compaction. Unbiased homogenous, medium level segregated-biased and high level segregated-biased were labeled as U1-U6, BM1-BM6 and BH1-BH6, respectively.

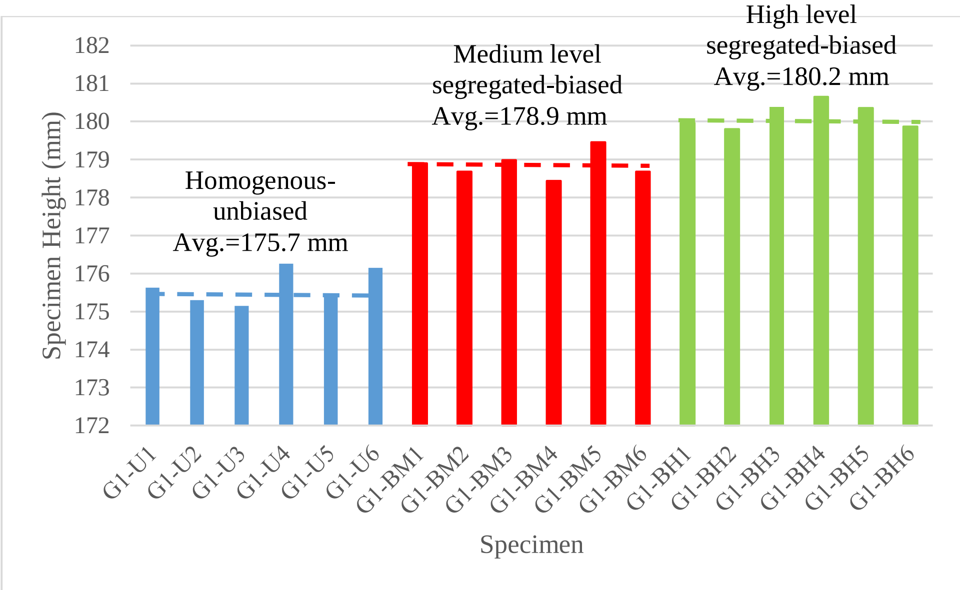

Figure 4.5. Height of specimens

In this graph, the symbols can be summarized; G1: specimens compacted under the same gyration effort (group-1), U: unbiased specimen, BM: medium level segregated-biased, BH: high level segregated-biased. As shown in the figure, same compaction effort results in very different specimen heights for the 3 sets of specimens. The average specimen heights were calculated as 175.7 mm, 178.9 mm and 180.2 mm for homogenous unbiased, medium level segregated-biased and high level segregated-biased specimens, respectively.

Air voids of the specimens were calculated using bulk specific gravity and maximum theoretical specific gravity values. Figure 4.6 shows air voids of 18 specimens.

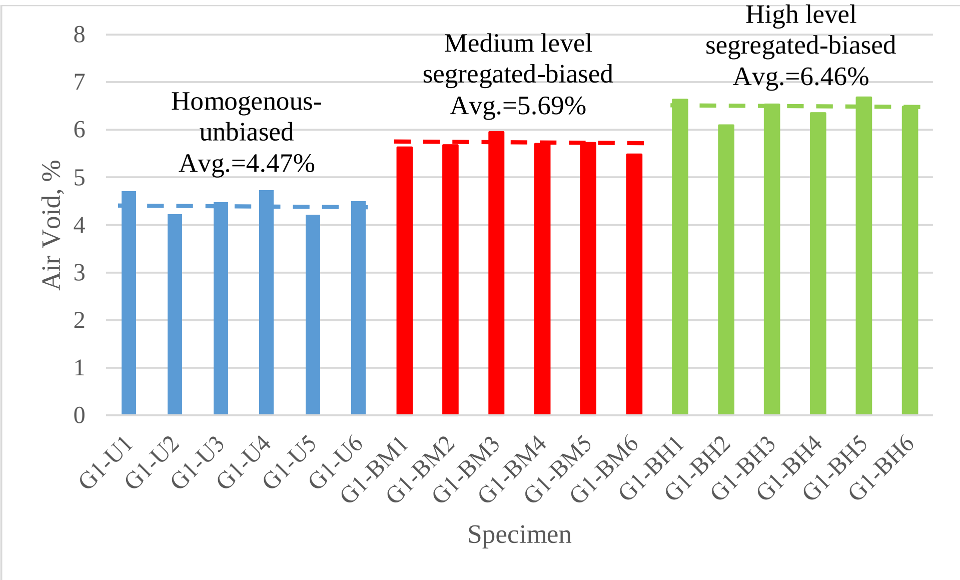

Figure 4.6. Air void of specimens

When the same compaction effort was applied, different air void levels were obtained for each inhomogeneity level. The average air voids were calculated as 4.47%, 5.69% and 6.46% for the homogenous-unbiased, medium level segregated-biased and high level segregated-biased specimens, respectively.

4.2. Asphalt Mixture Design for Specimens Compacted at the Same Density

4.2.1. Aggregate Properties and Selecting Design Gradation

To produce specimens with the same density, another design was done using different aggregate and asphalt sources. The selected aggregate was limestone and it was taken from a different source. A 50/70 penetration grade asphalt provided by TGDH was used for this set of specimens. The same gradation was also chosen for the design of the mixtures. Los Angeles abrasion and specific gravity test results for the limestone aggregate are given in Table 4.8.

Table 4.8. *Properties of limestone aggregate*

Test	Result	Specification
Bulk specific gravity (Coarse)	2.680	AASHTO T 85 (2010)
Bulk specific gravity (Fine)	2.630	AASHTO T 84 (2010)
Apparent specific gravity (Filler)	2.693	AASHTO T 100 (2010)
Los Angeles abrasion (%)	29	AASHTO T 96 (2010)

Percentages of coarse aggregate, fine aggregate and filler in the blends are 58%, 39% and 3%, respectively. The bulk specific gravity of the combined aggregate (G_{sb}) was calculated as 2.661.

4.2.2. Mixing and Compaction Temperature

A 60 penetration grade unmodified binder was selected for this part of the study. Specific gravity of binder (G_b) was determined as 1.033. To find compaction and mixing temperatures, a rotational viscometer was used similar to the previous mixture. After the test, the viscosity-temperature chart was obtained as shown in Figure 4.7.

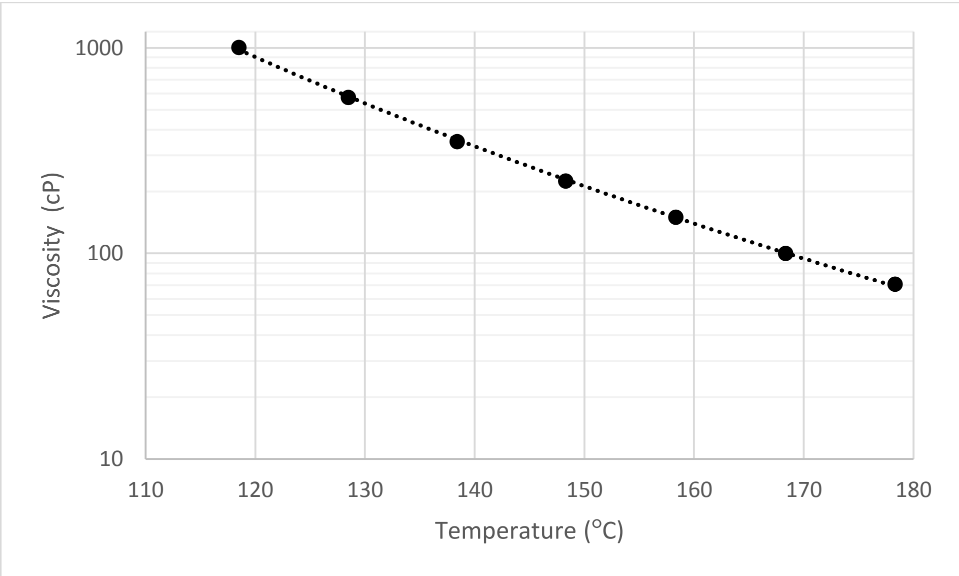

Figure 4.7. Viscosity-temperature chart

According to the chart, mixing and compaction temperatures were determined as 154°C and 143°C, respectively.

4.2.3. Optimum Asphalt Content for the Design Gradation

As previously explained, trial aggregate gradations were selected and then an initial trial asphalt content was determined for each trial gradation. A design aggregate structure and an estimated design asphalt content were selected based on the volumetric results of trial specimens. To determine the optimum asphalt content, specimens with four different asphalt contents (estimated design asphalt content, estimated±0.5, estimated+1%) were prepared. The estimated design asphalt content was found to be 4.5% and three more asphalt contents were selected as 4%, 5% and 5.5% to fabricate the specimens. Table 4.9 shows the Superpave mix design parameters used in this design.

Table 4.9. *Superpave mix design parameters*

Design Parameters	**Selected/Calculated Values**
Number of Gyrations (N_{des})	100
Cumulative Traffic Assumed	3-10 Million
Mixing Temperature	154°C
Compaction Temperature	143°C
Air Void Content Selected for the Design	4%

To find air voids and the other volumetric properties of the asphalt concrete specimens, the bulk specific gravity of specimens (AASHTO T 166, 2010) and the theoretical maximum density of loose mixtures (AASHTO T 209, 2010) were measured. In addition to air voids, corresponding asphalt contents, voids in mineral aggregates (VMA) and voids filled with asphalt (VFA) were calculated. Test results are shown in Figure 4.8. The graphs show the asphalt content versus air void, voids in mineral aggregate (VMA), voids filled with asphalt (VFA) and unit weight. All volumetric parameters were calculated according to AASHTO R 35 (2010).

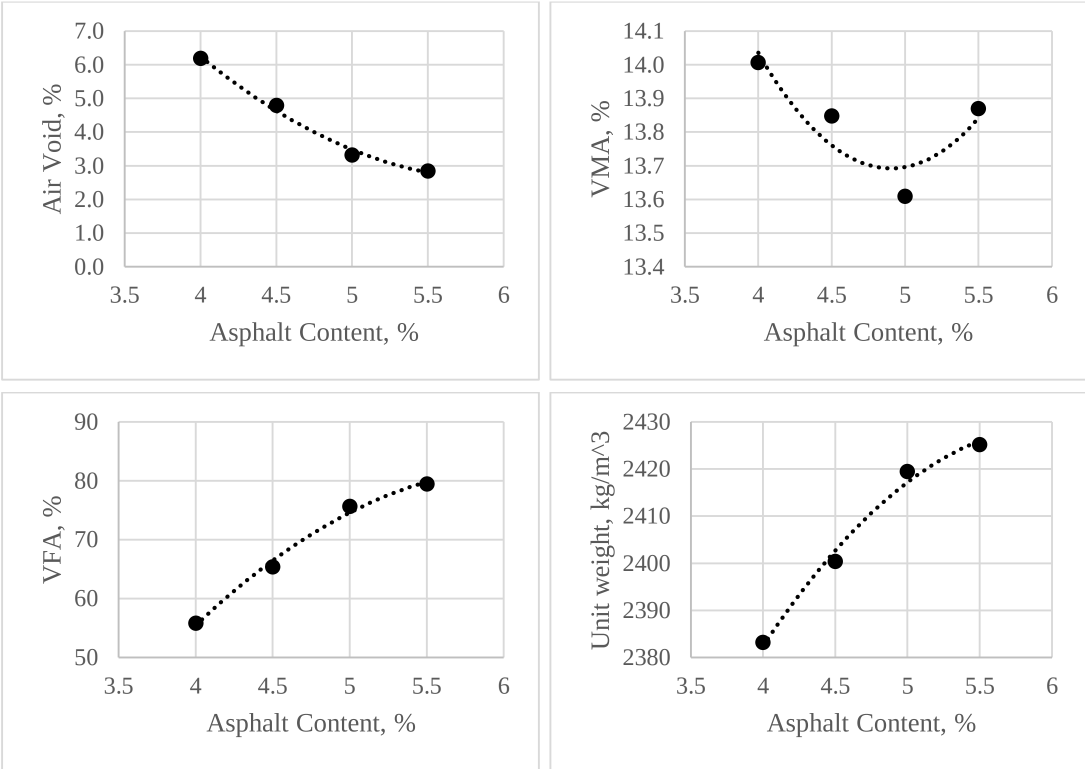

Figure 4.8. Test results

An optimum asphalt content of 4.75% was determined at 4% air voids. The other volumetric parameters corresponding to 4.75% asphalt content were read from the graphs to control compliance with the specification. Design requirements and the volumetric test results at 4% air void are given in Table 4.10.

Table 4.10. *Results and design requirements*

Parameter	Test Results	Design Requirements
Air Void (Va), %	4.000	-
Voids in the Mineral Aggregate (VMA), %	13.7	min. 13
Voids Filled with Asphalt (VFA), %	70.7	65-75
Dust-to-Binder Ratio	0.729	0.6-1.2

4.2.4. Fabrication of Homogenous and Segregated Specimens

Using the given equation in the previous section, the film thickness at optimum asphalt content was calculated as 13.31 μm. Asphalt contents of the coarser and the finer portions of the biased specimens were calculated by considering equal film thickness of the two parts. Asphalt contents of the design gradation and the biased mixtures are given in Table 4.11. For the repeated creep tests, specimens with 100 mm diameter and 150 mm height were used. Therefore, specimen heights should be larger than 150 mm before trimming thin layers from the ends. To obtain this height, aggregate weight was determined as 7000 g by preparing several trial specimens. In the preparation these specimens, the same procedure as used for group-1 was followed.

Table 4.11. *Asphalt contents of the design, coarser and finer gradations*

Parameter	Design Gradation	Medium Level Segregated-Biased		High Level Segregated-Biased	
		Finer Portion	Coarser Portion	Finer Portion	Coarser Portion
Surface Area, m^2/kg	3.12	4.13	2.34	4.39	2.25
Asphalt Content, %	4.75	5.99	3.76	6.31	3.64
Aggregate Weight, g	7000	3063.2	3936.8	2860.2	4139.8
Asphalt Weight	349.1	195.2	153.9	192.6	156.5

4.2.5. Specimen Preparation with Same Density

As discussed in the previous sections, when specimens with different level of segregation are compacted under the same compaction effort, a very wide range of bulk densities are obtained in connection with the aggregate distribution. To achieve the target bulk density for the specimens, software of the Superpave gyratory compactor was utilized. The software measures and records the specimen height corresponding to the number of gyration cycles at specific intervals. The sample weight is entered to the software as an input before the test. Because the mold diameter is known, which is 150 mm, volume of the specimen is calculated by the software. Using the volume and weight of specimen, the estimated bulk density is also calculated by the software. The estimated bulk density is a little incorrect because of surface voids of the specimen. Specimens with different segregation levels (homogenous-unbiased, medium level segregated-biased and high level segregated-biased) were compacted to the target density to achieve 4% air voids for all specimens. The actual bulk density corresponding to 4% air voids was already known from the mix design. The estimated density corresponding to this actual density was determined by producing trial specimens for each inhomogeneity level. To go beyond the target density and to determine the estimated density corresponding to the target actual density, trial homogenous-unbiased, medium level segregated-biased and high level segregated-biased specimens were compacted at 160, 300 and 400 gyrations, respectively. The estimated densities were given by the software with specific gyration intervals. After the compaction operations were completed, the actual densities of the specimens were determined experimentally and the estimated densities were corrected at initially given data points. Figure 4.9 shows the estimated and the actual densities of three specimens.

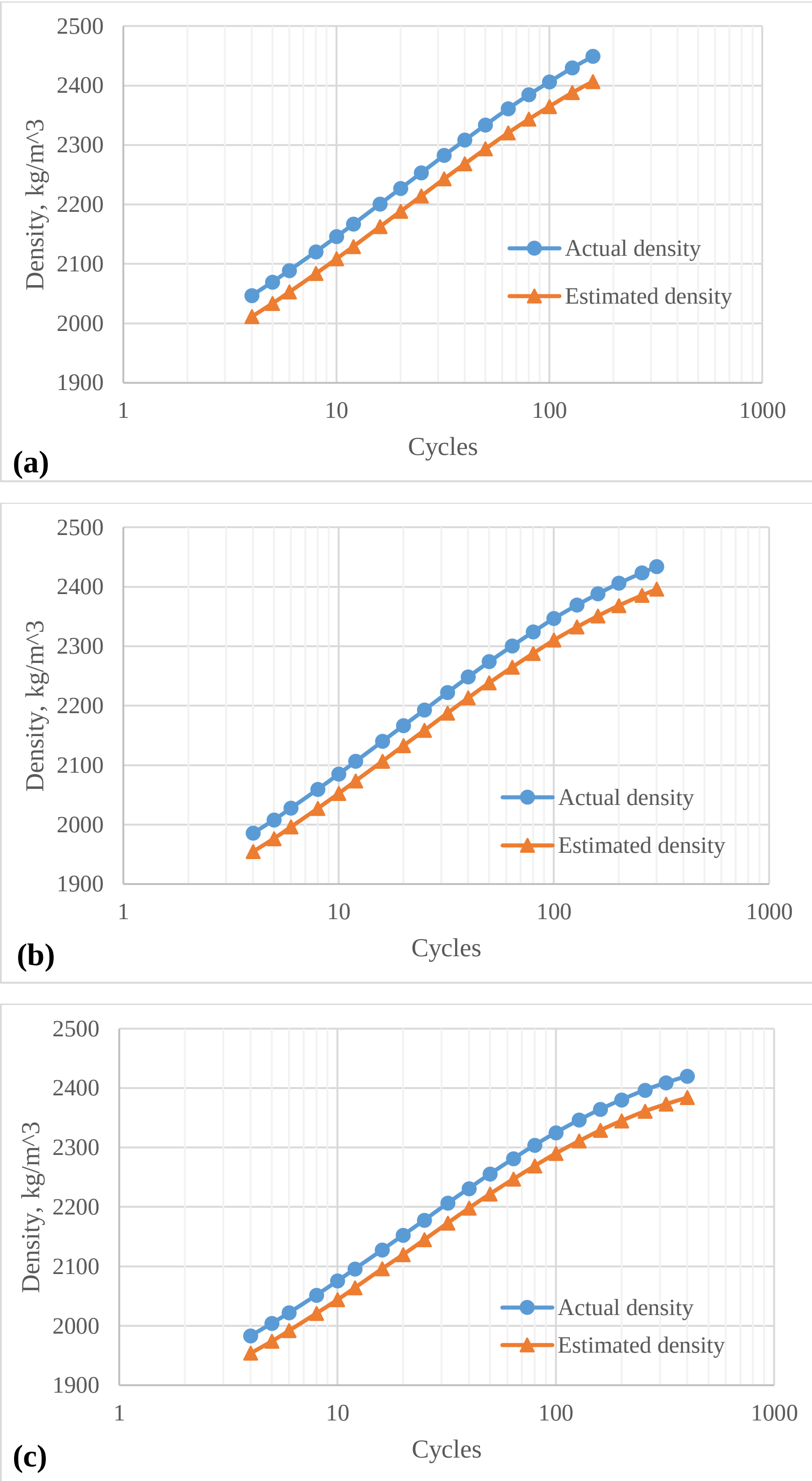

Figure 4.9. Actual and estimated densities; a) Homogenous specimen, b) Medium level segregated-biased specimen, c) High level segregated-biased specimen

Since only estimated densities can be controlled by the software, the estimated density corresponding to the target bulk density were determined from the graphs. For the target air void (4%), the bulk density was calculated as 2411 kg/m^3 during the mix design. Using the number of gyrations versus density graphs, the average estimated density for the three specimens was found as 2372 kg/m^3. Before starting compaction process, the weight of the samples with the other design parameters were entered to the software. The estimated density limit for all the specimens was entered as 2372 kg/m^3. The software stops the compaction when the estimated density of the specimen reaches the limit value. Using this procedure, the specimens of the 3 level of segregations were compacted to the target air void (4%).

Compaction efforts to achieve the target density were different for each level of inhomogeneity. The average number of gyrations was determined as 122, 238 and 315 for unbiased, medium level segregated-biased and high level segregated-biased specimens, respectively. The average compaction effort increases as the segregation level increases.

4.2.6. Summary of Volumetric Calculations

To produce specimens with the same density, all specimens were compacted until they reach the target density. Specimens U1-U6, BM1-BM6 and BH1-BH6 are classified as unbiased homogenous, medium level segregated-biased and high level segregated-biased, respectively. More compaction effort was needed to reach the target density for the segregated specimens as shown in Figure 4.10. The average gyration efforts were determined as 122, 238 and 315 for unbiased homogenous, medium level segregated-biased and high level segregated-biased, respectively. Specimens were also tested to determine the volumetric properties. Air voids were determined as 4±0.2% for all the specimens. The average height of 18 specimens were measured as 174.5 mm.

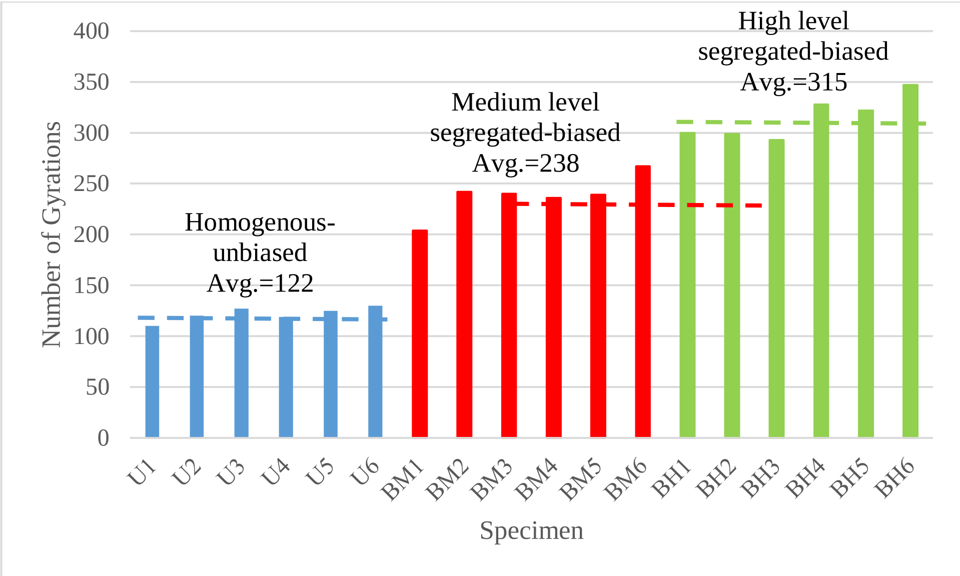

Figure 4.10. Number of gyrations required for the same density level

4.3. Repeated Creep Test

4.3.1. Specimen Coring

NCHPR Report 425 requires specimens with 100 mm diameter and 150 mm height. The specimens were compacted with the Superpave gyratory compactor using 150 mm diameter mold. According to the size requirements mentioned in the specifications, cylindrical specimens were cored from the 150 mm diameter compacted specimens using a circular diamond saw. Wet cutting process was carried out to minimize specimen disturbance and prevent overheating. In order to prevent interruption in the cutting process, the cutting operation was conducted slowly. The circular cutter was arranged in a way that it was aligned perpendicular to the specimen's axis. A thin rubber was placed at the bottom of the specimen to prevent its rotation during the cutting process and to avoid base plate damage. The specimen location was arranged between two rounded steel supports manually in order to bring to its center. One part of the supports was fixed to the base; however, the other part was free to move horizontally. After centering the specimen, the free part was positioned using a circular clamp as seen in Figure 4.11. Rubber membranes were used to increase friction and prevent rotation during cutting between specimens and the supports. A picture of cored specimens can be seen in Figure 4.12.

Figure 4.11. Coring operation

Figure 4.12. Specimen after coring operation

4.3.2. End Treatment

Decreasing friction between specimen ends and loading platens is important part of the repeated creep tests since end effects interfere with the test results. To prevent this problem caused by the interface friction, end treatments are necessary. Specimens were produced with an approximately 170 mm height, so that a thin layer from both ends were cut to obtain smooth end surfaces that are suitable for the test requirements. A diamond saw blade was used for cutting using water to prevent excessive heating and any damage to test specimens as shown in Figure 4.13.

Figure 4.13. Cutting the specimens ends

To prevent non-uniform air void distribution within the specimens, an equal amount of sections was trimmed from the specimen ends. During the end surface cutting, special attention was spent to obtain as smooth surfaces as possible and at the same time perpendicular to the specimen axis. Specimen ends were inspected by measuring at least 3 locations to ensure that they are parallel to each other. If the ends are not parallel, the top platen may slide over the specimen and results in eccentric loading to the test specimen. End treatments also consist of applying silicon grease oil with a viscosity of 12500 cSt at 25 ^{o}C using two latex rubber membranes between the loading platens and the specimen to reduce friction. A correct end treatment procedure should normally lead to uniform radial deformations in the test specimens. However, if the end surface frictions are high, the radial deformations at the top and bottom of the specimen will be smaller relative to the mid-section radial deformations.

4.3.3. Mounting LVDT Holders

The final step of specimen preparation is to install the LVDT holders. Firstly, circular pads are glued onto the specimen side surfaces using an epoxy resin. Two pads are glued onto the test specimen at 180^o radial distances at a gage length of 100 mm using a reference steel plate as shown in Figure 4.14.

Figure 4.14. Gluing LVDT holder pads

Pads locations are arranged so that gluing surfaces can overlap with aggregates rather than binder to achieve better bounding. A 5-minutes quick-setting epoxy was used to glue the pads onto the test specimens. After finishing the curing period of the epoxy, the LVDT holders were subsequently screwed to the pads as shown in Figure 4.15.

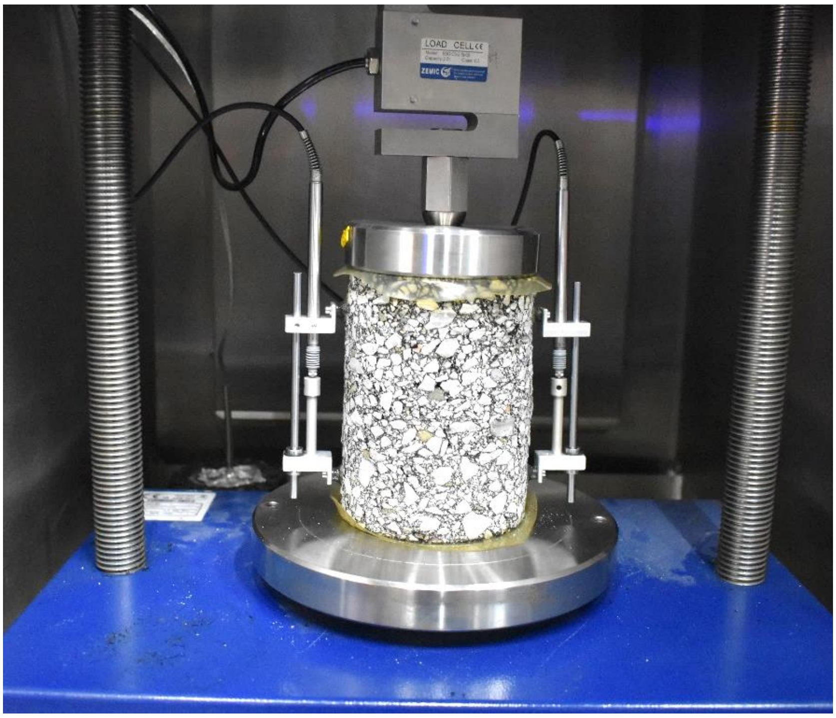

Figure 4.15. LVDT mounting for axial deformation measurement

4.3.4. Test Procedure

As stated in the previous sections, the repeated creep tests were carried out according to the procedures as described in NCHRP Report 465 . The test methodology and the selected test parameters, i.e. deviatoric stress, test temperature, loading frequency, are discussed in the report. In this study, unconfined repeated test mode was selected because it better correlates the field performance of asphalt concrete based on a number research outcomes. To control the test temperature, an environmental chamber that can maintain the test temperature to an accuracy of ±0.5 °C was used. A 16 kN pneumatic universal testing machine capable of applying haversine loading up to 30 Hz was used as shown in Figure 4.16. A minimum of 3 hours conditioning time was applied before starting the load applications. Specimen’s temperature was also checked using a dummy specimen core temperature placed into the was used to measure core temperature inside the chamber. After the temperature equilibrium, silicone grease was applied to the specimen’s ends and LVTDs were attached to the LVDT holders. The specimen and the platens was centered with loading piston to prevent eccentric loading. Subsequently, a cyclic deviatoric loading of 300 kPa was applied at 1 Hz frequency and the selected test temperature of 42 ^{o}C.

Figure 4.16. Testing machine

4.3.5. Stress Level

In NCHRP Report 465, the applied stress level is suggested between 69 and 207 kPa for the unconfined tests. After a number of trials, it was seen that specimens do not pass on the third stage, i.e., tertiary flow, within this loading range. In order to get the specimens to reach to the tertiary stage, the deviatoric stress level was selected as 300 kPa after a number of trial testing. To maintain a positive contact between the loading platens and the specimen, a contact load equal to 5 percent of the cyclic load, 15 kPa, was also applied to the specimen.

4.3.6. Effective Test Temperature for Repeated Creep Test

Effective test temperature (T_{eff}) is a single test temperature and it should be calculated for each geographical location specifically considering all seasons of the year (Witczak et al., 2002). Because the effective temperature is unique for each distress type, an effective temperature for the repeated creep tests was calculated in this study (NCHRP Report 704, 2011). There are several methodologies proposed by the past researchers to determine the effective test temperature for the repeated creep testing. In this study, a method proposed in SHRP A-407 report was used in this study. The effective temperature equation for rutting at 25 mm below the pavement surface is given in Equation 4.3 (Cominsky et al., 1994).

$$T_{eff} = 30.8 - 0.12Z_{cr} + 0.92MAAT_{design} \tag{4.3}$$

where T_{eff} = effective rutting temperature (°C); Z_{cr} = critical depth from the pavement surface (mm).

The equation for $MAAT_{design}$ is:

$$MAAT_{design} = MAAT_{average} + K_{\alpha}\sigma_{MAAT} \tag{4.4}$$

where $MAAT_{design}$ = mean annual air temperature from historical data (°C); σ_{MAAT} = Standard deviation of the distribution of MAAT for the location (°C); and K_{α} = value calculated from normal probability tables at an appropriate reliability level (R).

This equation is based on the mean annual air temperature and the critical depth for which the temperature is calculated. Using historical data, which was obtained from the Turkish State Meteorological Service for Ankara, the mean annual air temperature was computed as 12.6 °C (Cebeci et al., 2013). σ_{MAAT} was calculated according to historical $MAAT_{average}$ data. The critical depth, Z_{cr} , was selected as 25 mm according to the proposed procedure used for surface course layers. Reliability level was selected as 95% because of high variations in climatic data. The corresponding K_{α}value for 95% reliability was determined as 1.645 from the normal probability tables. Using all these parameters, the effective temperature, T_{eff}, was calculated as 42 °C for the repeated creep tests.

4.3.7. Flow Number Calculation

The permanent strain at each cycle was continuously recorded by the software and flow number was determined by calculating the minimum point on the strain rate versus number of cycles graph. A loading cycle takes 1 second which consists of 0.1 second haversine loading and 0.9 second rest period. The test automatically terminates after reaching 10,000 loading cycles or 50,000 μE (5%) total cumulative permanent strain. During the experiments, some parameters such as permanent strain, creep modulus and core temperature were measured and recorded by the software. The repeated creep test results are presented in terms of cumulative permanent strain (ε_p) versus the number of loading cycles (N). An example relationship is given in Figure 4.17. A typical failure condition representing the 5% cumulative permanent strain reached is shown in Figure 4.18.

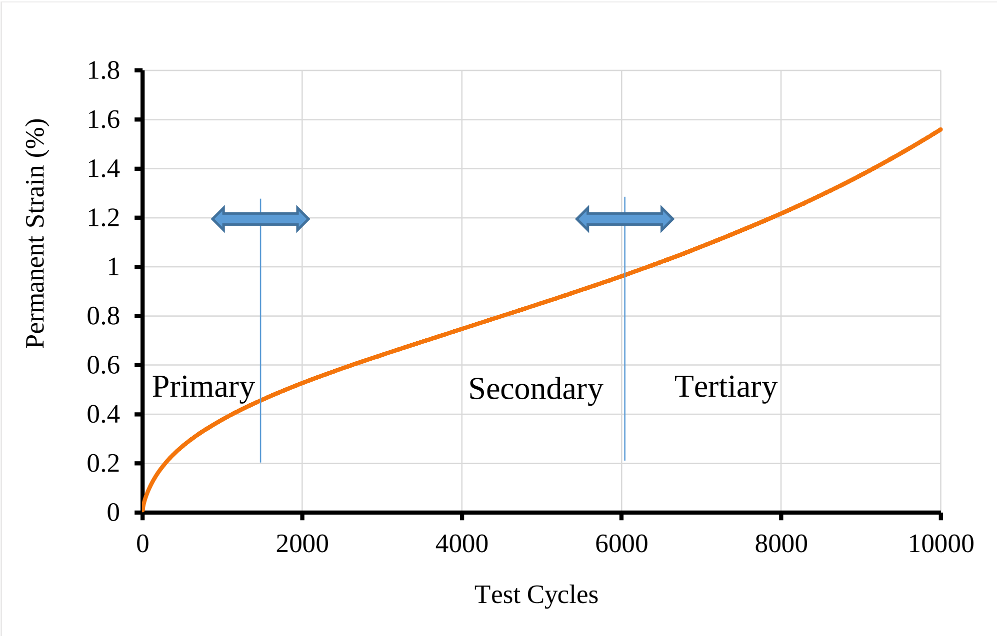

Figure 4.17. Typical relationship between cumulative permanent strain and test cycles

Figure 4.18. The typical failure of a specimen (before and after the test)

The flow number is reported as the minimum point in the permanent strain rate curve. The strain rate was calculated using the cumulative permanent strain data. The strain rate for the current load cycle (N_i) is calculated as the difference between the permanent strain for the neighboring cycles (N_{i+1} and N_{i-1}, respectively), and then divided by two times the cycle interval (ΔN) (Equation 4.5).

$$\frac{\delta(\varepsilon_p)_i}{\delta N} = \frac{(\varepsilon_{pN_{i+1}} - \varepsilon_{pN_{i-1}})}{2\Delta N} \tag{4.5}$$

After the strain rate is calculated for each cycle, the strain rate values are smoothed by the help of a moving averaging method to clarify the graph. The formulation for a moving averaging method is given in Equation 4.6.

$$\frac{\delta(\varepsilon_p)_i}{\delta N} = \frac{(\varepsilon_{pN_{i+10}} - \varepsilon_{pN_{i-10}})}{2\Delta N} \tag{4.6}$$

where $\delta(\varepsilon_p)_i/\delta N$ = strain rate at cycle i; ε_{pNi-10} = permanent strain at i-10 cycles; ε_{pNi+10} = permanent strain at i+10 cycles; and ΔN=number of cycles between calculated points=10.

This smoothing operation is conducted to remove the noise in the plot. In high level noise, the moving average method can be inadequate. In the NCHRP Report 513, a 40 cycle time span was used for better smoothing (Bonaquist et al., 2003). This strategy was also used for the analysis of test data by using 40 cycle smoothing interval, as defined in Equation 4.7.

$$\frac{\delta(\varepsilon_p)_i}{\delta N} = \frac{1}{5}\left(\frac{\delta(\varepsilon_p)_{i-20}}{\delta N} + \frac{\delta(\varepsilon_p)_{i-10}}{\delta N} + \frac{\delta(\varepsilon_p)_i}{\delta N} + \frac{\delta(\varepsilon_p)_{i+10}}{\delta N} + \frac{\delta(\varepsilon_p)_{i+20}}{\delta N}\right) \tag{4.7}$$

where $\delta(\varepsilon_p)_i/\delta N$ = smoothed strain rate at cycle I; $\delta(\varepsilon_p)_{i-20}/\delta N$ = smoothed strain rate at cycle i-20; $\delta(\varepsilon_p)_{i-10}/\delta N$ = smoothed strain rate at cycle i-10; $\delta(\varepsilon_p)_i/\delta N$ = smoothed strain rate at cycle i; $\delta(\varepsilon_p)_{i+10}/\delta N$ = smoothed strain rate at cycle i+10; $\delta(\varepsilon_p)_{i+20}/\delta N$ = smoothed strain rate at cycle i+20.

To calculate the flow number, strain rate-number of loading cycles relationship is plotted on a logarithmic scale. Low flow number is an indicator of better rutting resistance and vice versa. The loading cycle corresponding to the minimum strain rate represents the flow number as shown in Figure 4.19.

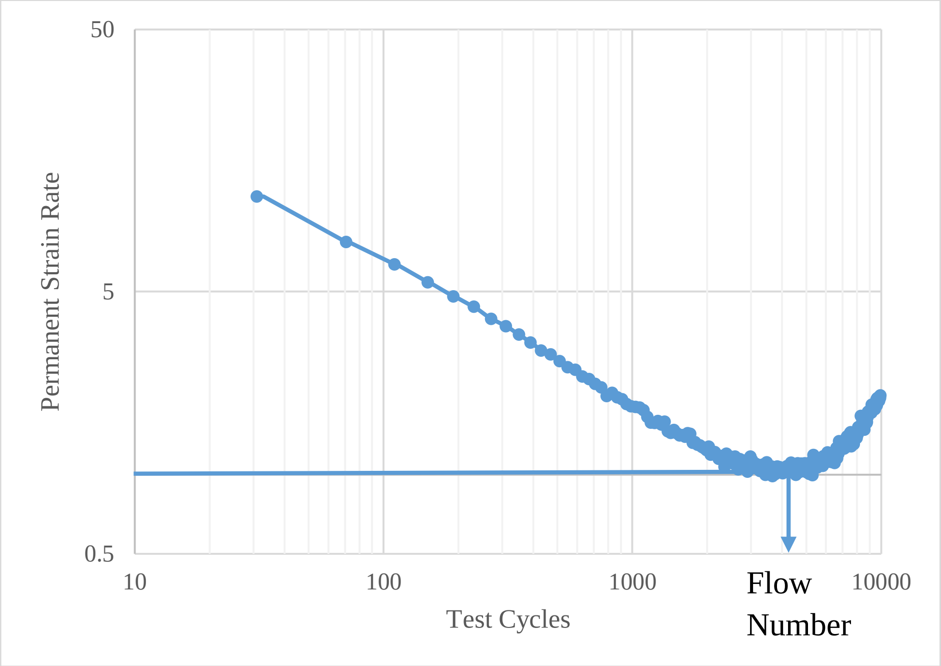

Figure 4.19. Strain rate versus loading cycles plot

4.3.7.1. Power Model

As discussed in the previous section, the cumulative permanent strain curve can be divided into three zones as primary, secondary and tertiary flow. Flow number is referred as the loading cycle at which the tertiary flow stars. The determine the flow number, first permanent strain versus number of loading cycles are plotted on a log-log scale as shown in Figure 4.20. A best fitting straight line is calculated using non-linear regression methods for the second zone while achieving the highest R^2 value. To conduct this analysis, a special algorithm searching the best fitting line to this region was used based on calculating the R^2 values.

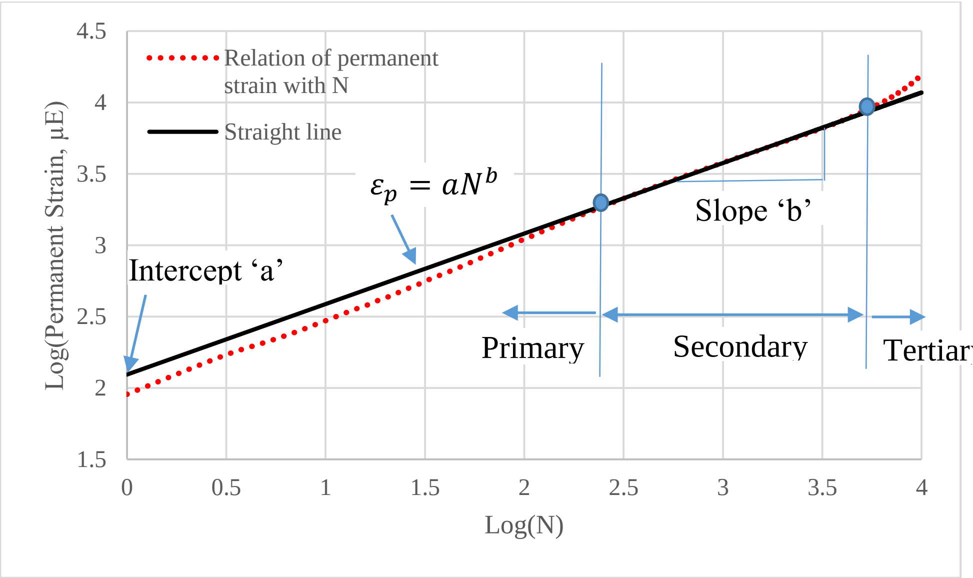

Figure 4.20. Regression constants a and b

Slope (b) of this line denotes the rate of change in permanent strain as a function of loading cycles. The intercept (a) means the offset permanent strain at cycle N=1. These two parameters are determined using the best fitted straight line using a power model. Mathematical representation of this model is given in Equation 4.8.

$$\varepsilon_p = aN^b \tag{4.8}$$

In this equation, N is the number of loading cycles, a and b are the regression constants. It should be noticed that this model ignores the tertiary zone considers only the second zone of the plastic deformations. For a tested specimen, a higher slope (b) means higher potential to develop rutting. Analysis of test data, however, indicates that the intercept constants does not show a significant correlation with the permanent strain parameters according to NCHRP Report 465.

4.3.7.2. Francken Model

To calculate the flow number more precisely, the Francken model, which is the best comprehensive model to fit test data, was used (Ameri et al., 2013). This model was proposed by Biligri et al. (2007) and it is widely used to determine the flow number. The Francken model is described in Equation 4.9 as:

$$\varepsilon_p(N) = AN^B + C(e^{DN} - 1) \tag{4.9}$$

where ε_p(N)=permanent strain; N=number of loading cycles; and A, B, C and D=regression coefficients.

This method consists of a power part and an exponential component. In this equation, C represents the plastic failure. All three stages of permanent deformation test which are primary, secondary and tertiary can be represented using this model. Using a statistical analysis software, the model coefficients (A, B, C and D) were estimated using nonlinear regression methods. The first derivative with respect to number of cycles, N, gives strain rate as shown in Equation 4.10.

$$\frac{d\varepsilon_p}{dN} = \left(A * B * N^{(B-1)}\right) + (C * D * e^{D*N}) \tag{4.10}$$

The second derivative produces the gradient of the slope, i.e., strain rate. The second derivative of the model is used to determine the flow number and it is given in Equation 4.11.

$$\frac{\delta^2\varepsilon(p)}{\delta N^2} = A * B * (B - 1) * N^{B-2} + (C * D^2 * e^{D*N}) \tag{4.11}$$

The cycle number corresponding to the second derivative of the model changes from a negative to a positive value giving the flow number.

The the analysis of test data, the Francken model was used to fit the experimental data and a typical result of the model fitting is shown in Figure 4.21. In general, the model shows an excellent fit to the experimental data. The model was applied for all the test specimens to calculate the permanent deformation constants.

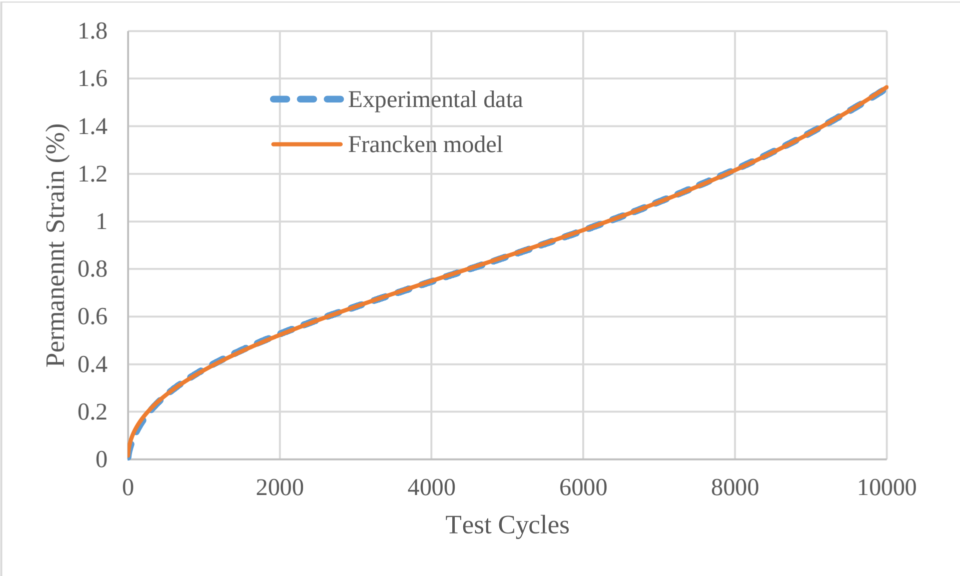

Figure 4.21. Repeated creep test data fitting with Francken model

A typical permanent strain and permanent strain rate response for a repeated creep test are shown in Figure 4.22, in which the strains were estimated by the Francken model.

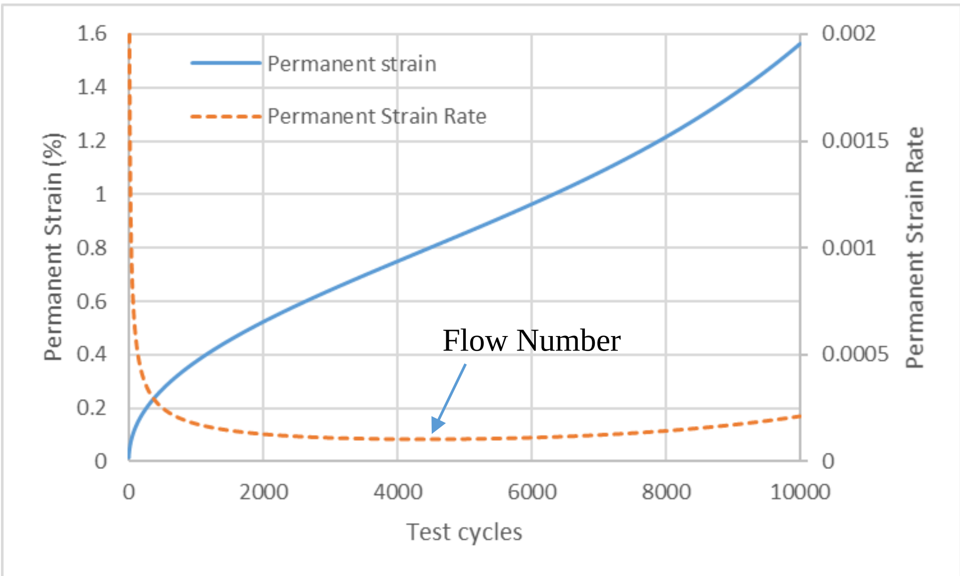

Figure 4.22. Example repeated creep test data

Because the outputs of the Francken model and the averaging method for permanent strain rate fit perfectly, the Francken model was selected for data analysis due to its simplicity to calculate the model constants.

4.4. Result and Discussion of Rutting Tests

4.4.1. Flow Number and Repeated Creep Test Parameters

In this section, results of the repeated creep test are discussed and important test parameters such as flow number, intercept (a) and slope (b) are presented. In addition to these parameters, permanent strain values at specific loading cycles were given to compare specimens in terms of rutting resistance. The repeated creep test parameters indicate the rutting performance of asphalt mixtures in the field. The flow number is the one of the most important parameters describing the rutting performance of asphalt concrete in the field. A higher flow number indicates better rutting resistance and a lower flow number otherwise. Another important rutting test parameter is the slope constant (b), which is a power model coefficient and it refers the rate of change in the permanent strain with respect to loading cycles. It is well known fact that the slope value correlates with the field rut depth. The higher the slope constant, the lower the resistance of asphalt concrete to rutting. Intercept value (a) is also a power model constant and represents the permanent strain at the initial cycle; however, past studies did not show a strong correlation of this parameter with rutting performance of asphalt concrete. The permanent strains at 1000 and 2500 loading cycles for group-1 specimens, i.e., compacted under the same gyration effort (group-1), and at 1000, 2500 and 5000 cycles for group-2 specimens, i.e., compacted at the same density, were also monitored to rate the rutting resistance of the design mixtures. The permanent strain at 2500 loading cycles were selected for both groups since this loading cycle was reached for all the tested specimens. The important rutting test parameters and their impact on the asphalt concrete specimens are summarized in Table 4.12.

Table 4.12. *Important rutting test parameters*

Parameters	Definition	Effect on Rutting Behavior of Asphalt Mix	
		High Value	**Low Value**
Flow Number	Cycle number at which tertiary flow starts	Low rutting	High rutting
Slope (b)	Rate of change in the permanent strain depending on loading cycles	High rutting	Low rutting
Intercept (a)	Permanent strain at cycle 1	High rutting	Low rutting
Permanent Strain @2500 Cycles	Cumulative permanent deformation at 2500 loading cycles	High rutting	Low rutting

4.4.1.1. Specimens Compacted with Same Gyration Effort

Results of repeated creep test for the specimens compacted under the same gyration effort (group-1) are presented in this section. As explained previously, all specimens with three segregation levels, named as homogenous-unbiased, medium level segregated-biased, high level segregated-biased, were compacted under 100 gyration cycles using the Superpave gyratory compactor.

The repeated creep tests were implemented according to the previously explained test conditions. The testing software records the permanent deformation and permanent strain values corresponding to each loading cycle. Figure 4.23 shows the loading cycles versus permanent strain plots for 18 specimens. Specimen test results were labeled according to their preparation method.

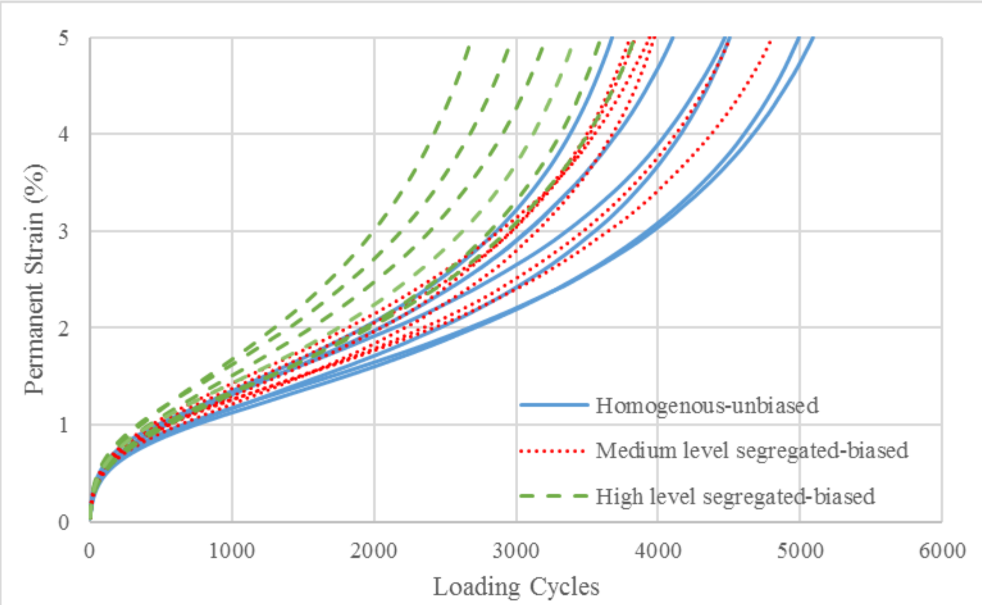

Figure 4.23. Permanent strain-loading cycles graph for group-1 specimens

After obtaining the permanent strain data, the Francken method was utilized to acquire composite models of the all test data. Model coefficients (A, B, C and D) were determined by implementing nonlinear regression methods. The first derivative of the model gives the permanent strain rate depending on loading cycles. Figure 4.24 shows the permanent strain rate versus loading cycles graph plotted according to the first derivative of the Franken model.

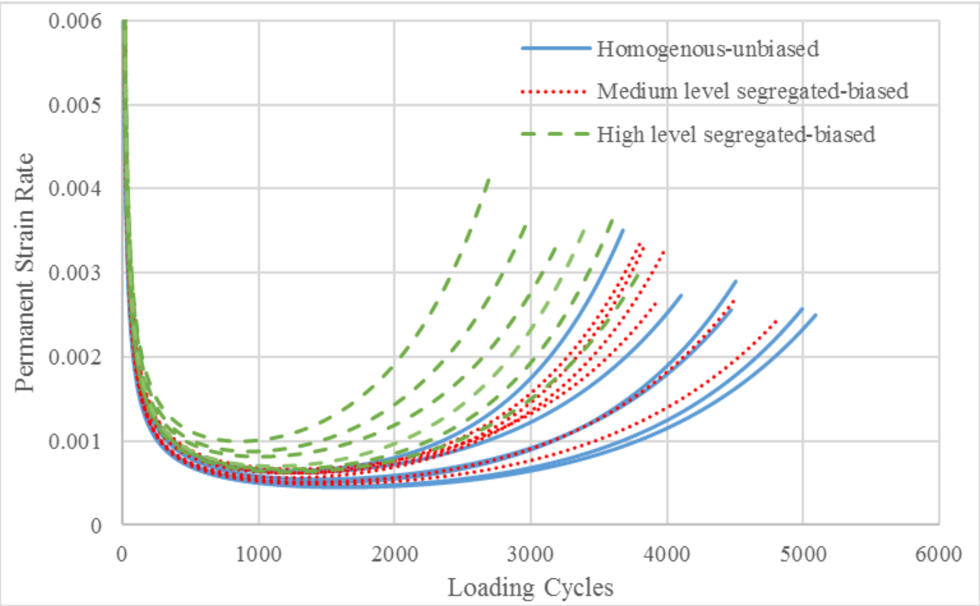

Figure 4.24. Permanent strain-loading cycles graph for group-1 specimens

The flow number is the cycle number corresponding to the minimum point (zero slope) on the permanent strain rate versus loading cycles graph. The minimum point on this line was found by using second derivative of the composite model. The cycle number corresponding to the second derivative of the model changed from a negative value to a positive value gives the flow number.

The test parameters collected from all specimens are summarized in Table 4.13. Slope (b) and intercept (a) values were obtained using the power models for all specimens. The results for the homogenous-biased, medium level segregated-unbiased and high level segregated-unbiased specimens were given separately. G1 means group-1 (specimens compacted with the same compaction effort). U, BM and BH stand for homogenous-unbiased, medium level segregated-biased and high level segregated-biased, respectively. In this table, the average values of the test parameters for each segregation type were also given.

Table 4.13. *Results for the repeated creep test for group-1 specimens*

Specimen		Flow Number	Intercept (a)	Slope (b)	Permanent Strain @1000 Cycles (%)	Permanent Strain @2500 Cycles (%)
Homogenous-Unbiased	G1-U1	1243	2.91	0.41	1.35	2.55
	G1-U2	1447	3.09	0.34	1.33	2.25
	G1-U3	1587	2.92	0.38	1.13	1.88
	G1-U4	1268	2.93	0.39	1.31	2.38
	G1-U5	1439	3.16	0.34	1.17	2.03
	G1-U6	1628	3.00	0.35	1.18	1.90
	Average	1435	3.00	0.37	1.24	2.16
Medium Level Segregated-Biased	G1-BM1	1403	3.02	0.36	1.26	2.11
	G1-BM2	1333	3.02	0.37	1.38	2.48
	G1-BM3	1221	2.92	0.39	1.30	2.42
	G1-BM4	1291	3.03	0.37	1.43	2.59
	G1-BM5	1475	3.04	0.35	1.26	2.05
	G1-BM6	1222	3.00	0.36	1.22	2.26
	Average	1324	3.00	0.37	1.31	2.32
High Level Segregated-Biased	G1-BH1	1014	2.99	0.38	1.51	3.18
	G1-BH2	1195	2.84	0.43	1.32	2.57
	G1-BH3	1226	2.97	0.38	1.34	2.47
	G1-BH4	940	3.04	0.38	1.62	3.59
	G1-BH5	867	2.93	0.42	1.68	4.26
	G1-BH6	1112	3.01	0.38	1.43	2.82
	Average	1059	2.96	0.39	1.48	3.15

The results show that unbiased specimens are more rutting resistant than medium and high level segregated-biased specimens. The most important rutting test parameters are flow number and slope (b) constant. High flow number and low slope (b) are indicator of better rutting resistance. The average flow number for homogenous-unbiased, medium level segregated-biased and high level segregated-biased specimens were found as 1435, 1324 and 1059, respectively. These results indicate that flow numbers for the homogenous-unbiased and medium level segregated-biased specimens are very close each other. However, the average flow number of the high level segregated-biased specimens is much lower than other two sets. There is a variation in each group, but the average slope (b) values are almost same for all three sets. The average slope constant is a bit higher in high level segregated-biased set

(0.39); however, average of other two sets are the same (0.37). Intercept (a) value does not give important information about rutting performance of a mixture, so this parameter was not discussed. Similar trend between specimen sets was observed in the permanent strain at 2500 cycles results. The average permanent strain values of homogenous-unbiased at that cycles, medium level segregated-biased and high level segregated-biased specimens were measured as 2.16%, 2.32% and 3.15%, respectively. As shown in the results, homogenous-unbiased specimens were more resistant under same cyclic loading.

4.4.1.2. Specimens Compacted at Same Density

In this section, repeated creep test results for the specimens compacted at the same density corresponding to 4% air void (group-2) are presented. The segregation types were named as homogenous-unbiased, medium level segregated-biased and high level segregated-biased. Six specimens for each set were tested.

The repeated creep test was implemented according to previously explained test conditions. The testing software records the permanent deformation and permanent strain values corresponding to each loading cycle. Figure 4.25 shows the loading cycle versus permanent strain values for 18 specimens. The specimen test results were labeled according to their preparation methods.

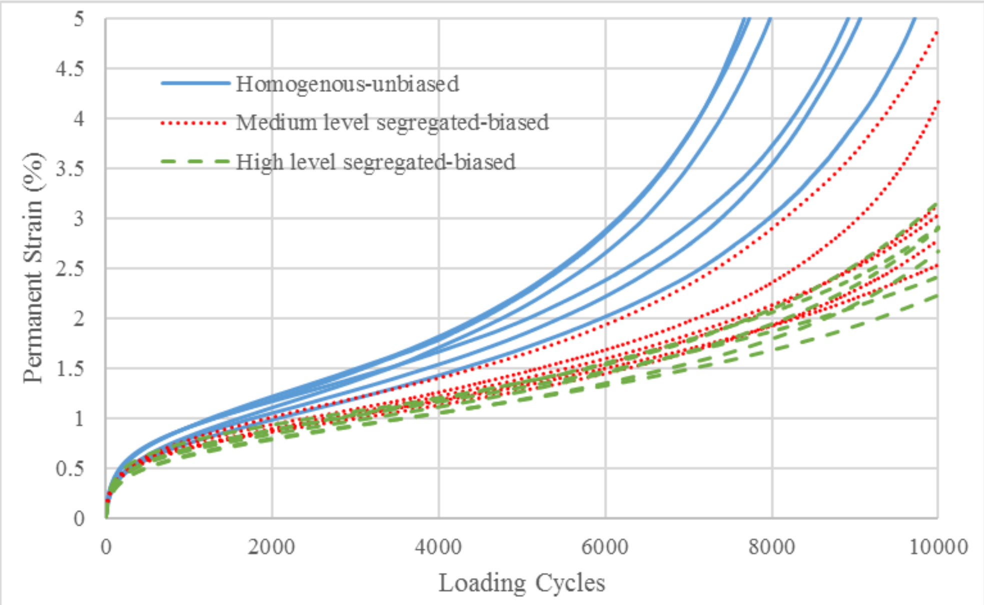

Figure 4.25. Permanent strain-loading cycles graph for group-2 specimens

The Francken model coefficients were determined for all specimens. The first derivative of the model gives the permanent strain rate. Figure 4.26 shows the permanent strain rate versus loading cycles graph.

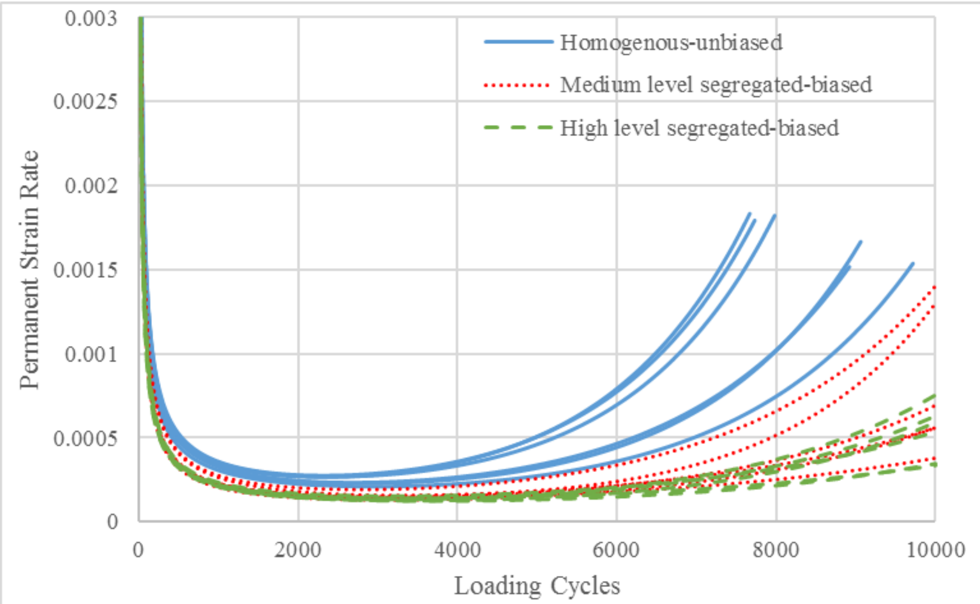

Figure 4.26. Permanent strain-loading cycles graph for group-2 specimens

The test parameters obtained from all specimens are summarized in Table 4.14. The flow number, slope and intercept values obtained from the Francken and classical power models are given. The results for the homogenous-unbiased, medium level segregated-biased and high level segregated-biased specimens are listed separately. G2 means group-2 (specimens compacted at the same density). U, BM and BH stand for homogenous-unbiased, medium level segregated-biased and high level segregated-biased, respectively. In this table, the average values of test parameters for each segregation type were also given.

Table 4.14. *Results for the repeated creep test for group-2 specimens*

Specimen		Flow Number	Intercept (a)	Slope (b)	Permanent Strain @1000 Cycles	Permanent Strain @2500 Cycles (%)	Permanent Strain @5000 Cycles (%)
Homogenous-Unbiased	G2-U1	2423	2.72	0.40	0.82	1.24	2.11
	G2-U2	2319	2.83	0.38	0.91	1.35	2.26
	G2-U3	2937	2.78	0.37	0.75	1.09	1.69
	G2-U4	2801	2.76	0.38	0.80	1.17	1.84
	G2-U5	2685	2.94	0.34	0.91	1.29	1.97
	G2-U6	2301	2.90	0.35	0.91	1.32	2.23
	Average	2578	2.82	0.37	0.85	1.24	2.02
Medium Level Segregated-Biased	G2-BM1	2783	2.86	0.35	0.79	1.11	1.64
	G2-BM2	3025	2.98	0.29	0.71	0.98	1.40
	G2-BM3	3163	2.90	0.31	0.70	0.96	1.35
	G2-BM4	3331	2.91	0.31	0.71	0.96	1.32
	G2-BM5	3145	2.99	0.29	0.71	0.93	1.28
	G2-BM6	3377	2.93	0.31	0.75	1.02	1.46
	Average	3137	2.93	0.31	0.73	0.99	1.41
High Level Segregated-Biased	G2-BH1	3461	2.82	0.32	0.62	0.86	1.19
	G2-BH2	3685	2.81	0.33	0.64	0.87	1.18
	G2-BH3	3229	2.84	0.33	0.70	0.96	1.36
	G2-BH4	3523	2.89	0.32	0.70	0.95	1.31
	G2-BH5	3167	3.03	0.29	0.77	1.00	1.36
	G2-BH6	3179	2.93	0.30	0.68	0.91	1.27
	Average	3374	2.89	0.32	0.68	0.93	1.28

The results show that the flow numbers of medium and high level segregated specimens are much higher than homogenous-biased specimens. The average flow number for each set was calculated as 2578, 3237 and 3374, respectively. The average flow numbers of biased sets were very close to each other but flow numbers of unbiased specimens were lower than other sets. In this group, specimens were compacted at the same density, so number of gyrations were very high in biased specimens than unbiased specimens. Because of the excessive compaction, the flow number results of biased specimens were much higher. There is a similar trend in slope (b) results. Average slope constants of homogenous-unbiased, medium level segregated-biased and high level segregated-biased sets were measured as 0.37, 0.31 and 0.32. The average slope of the unbiased specimens was higher than the biased specimens. Permanent strain at 2500 cycle was also other important parameter to compare specimens. The average values for sets were measured as 1.24%, 0.99% and 0.93%. As can be seen from the results, homogenous-unbiased specimens were less rutting resistant, on the contrary other sets were more resistant due to excessive compaction.

4.4.2. Volumetric Results

Volumetric changes in the specimens during the repeated creep tests were also analyzed by measuring the diameter and height of the specimens before and after testing. The diameters of the specimens were measured at four positions at equal intervals. These four positions are at bottom, middle-bottom, middle-top and top as shown in Figure 4.27. The measurements taken before and after the testing were used to calculate the radial strains and the volumetric strain parameters.

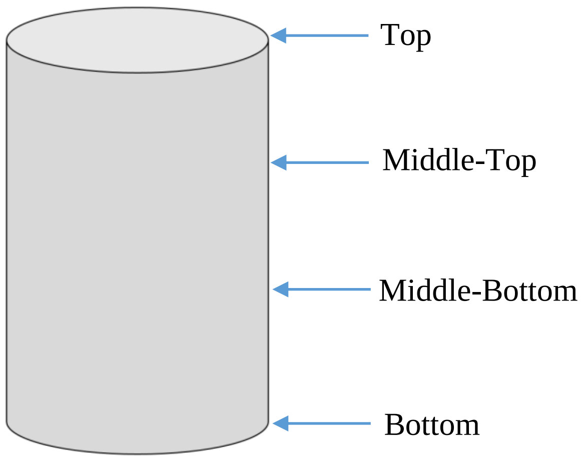

Figure 4.27. Location of the diameter measurements

For each position, three measurements were recorded by rotating the specimen 60° for each reading and then the average of the three readings was used to calculate the diameter at that location. To calculate the volumetric strain, the height of the specimens was also measured before and after testing. Figure 4.28 shows results of radial strains at 4 locations of the specimens for the group-1 specimens. The average radial strain was also calculated for each set.

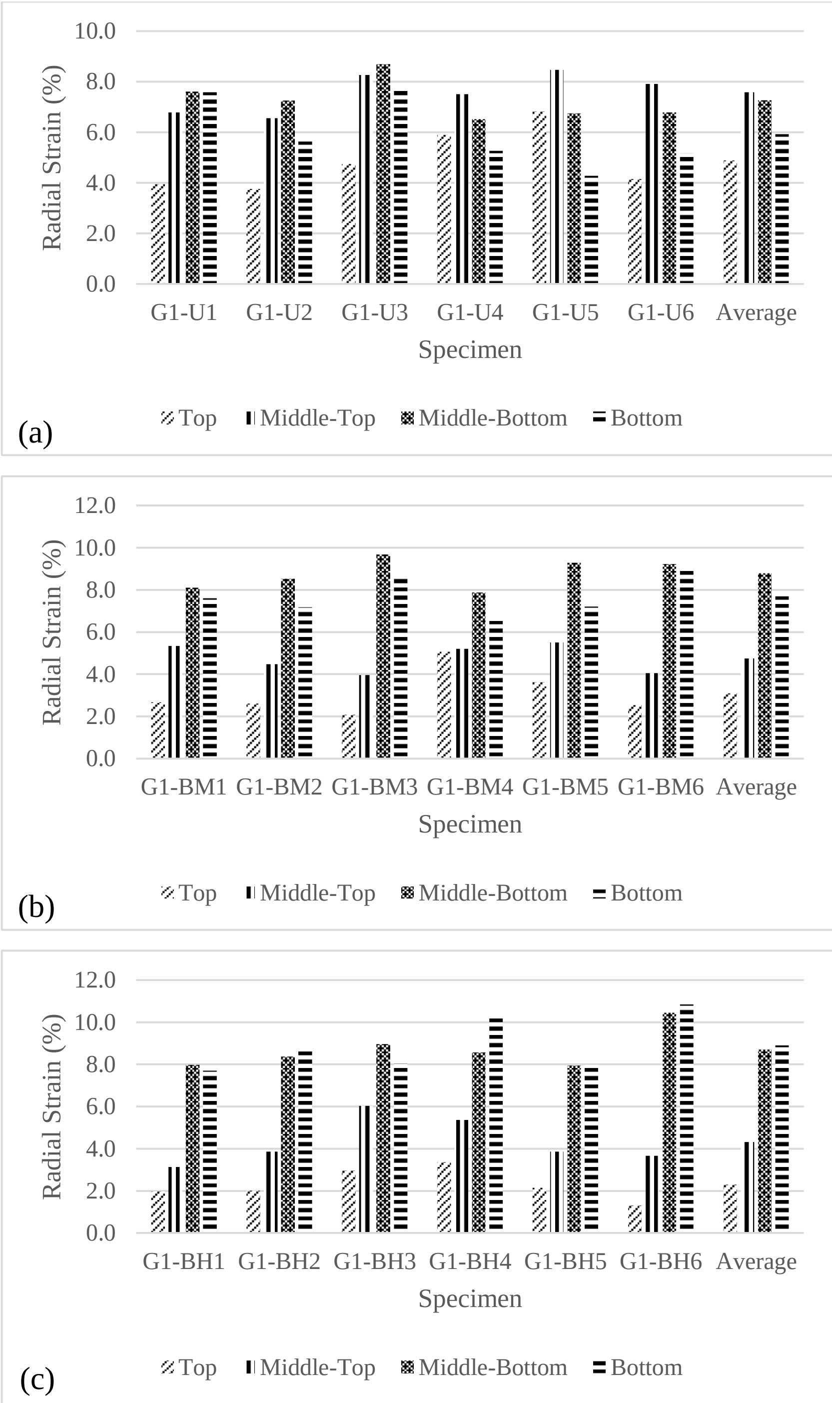

Figure 4.28. Radial strain results; a) Homogenous-unbiased, b) Medium level segregated-biased, c) High level segregated-biased

As shown in the graphs, radial deformations are almost uniform along the specimen height for the homogenous-unbiased specimens. However, it can be noticed that the radial deformations of the upper part are relatively smaller than the bottom part measurements. As indicated in the previous sections, during the mixture preparation stage coarser portion was located in the bottom of the specimens and the finer portion on the top section. Based on this procedure, the finer portions resulted in a stiffer section under loading as compared to the coarser portion, which behaved as a loose mixture. As a result, the radial deformations were measured smaller in the finer portions as compared to the coarser section. Characteristic failures types for these specimens can be observed from Figure 4.29 for homogenous-unbiased, medium level segregated-biased and high level segregated-biased specimens, respectively.

Figure 4.29. Typical specimen failures for group-1

Similar measurement was also carried out for the group-2 specimens, and the results are shown in Figure 4.30.

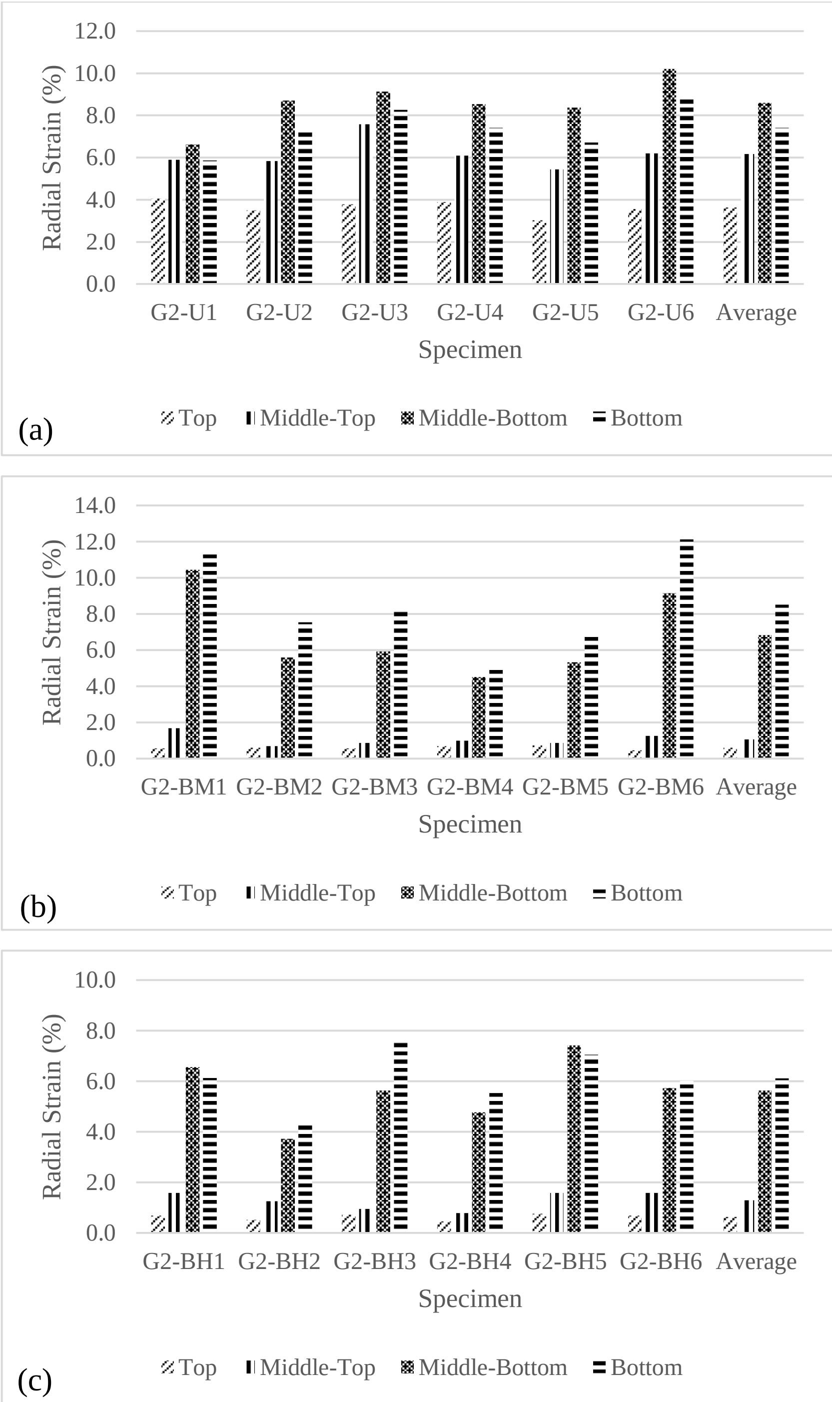

Figure 4.30. Radial strain results; a) Homogenous-unbiased, b) Medium level segregated-biased, c) High level segregated-biased

Similar to the first group, the radial deformations were found to be almost uniform for the homogenous-unbiased specimens. In these specimens, the radial strain values on the top were slightly smaller than on the other 3 locations. This shows that there is a small end effect in the upper part of the test specimens. Similar to the group-1 specimens, the radial deformation in the upper part was less than that in the bottom part for the biased specimens. However, this condition is more severe than for the group-1 specimens because of excessive compaction of the biased specimens. Typical failures for this group can be seen in Figure 4.31 for homogenous-unbiased, medium level segregated-biased and high level segregated-biased specimens, respectively.

Figure 4.31. Typical specimen failures for group-2

Using the initial and the final volume of the specimens, volumetric strains were calculated for all test specimens. Table 4.15 shows the average volumetric strain values for each set. The volumetric strain values were found almost the same for all the segregation levels in group-1. In group-2, the volumetric strain values decrease as the segregation level increases. Since group-2 specimens were compared to the same density, a large amount of compaction effort was needed for medium and high level segregated-biased specimens. It is, therefore, concluded that the volumetric strains of the biased specimens were, in general, smaller due to applied excessive compaction.

Table 4.15. *Volumetric strain results*

Specimen		Volumetric Strain (%)
Group-1	Homogenous-Unbiased	8.7
	Medium Level Segregated-Biased	8.0
	High Level Segregated-Biased	8.1
Group-2	Homogenous-Unbiased	8.7
	Medium Level Segregated-Biased	5.4
	High Level Segregated-Biased	4.4

Volumetric measurements show that radial deformation characteristics are similar for both groups. Radial deformations in the unbiased specimens of both groups were almost uniform along the specimen height. In some specimens, radial deformation on the top was a bit smaller than other locations because of very small end effect. Biased specimens behaved different from unbiased ones, since they composed of two portions which are finer and coarser portions. Radial deformation along the finer portion was smaller than coarser portion, since the finer part behaved more stiff. The difference between radial strains along the height of biased specimens was observed in both groups. Volumetric strain results show that the biased group-2 specimens were extremely stiff because of excessive compaction.

4.4.3. Change in Air Voids Because of Specimen Coring

According to NCHRP Report 425, specimen dimensions should be at least 150 mm in height and 100 mm in diameter. The specimens were compacted with the Superpave gyratory compactor using a mold with 150 mm diameter, and specimen heights as tall as 165 mm was achieved, so that after the end surface trimming at least 150 mm height requirement could be achieved. The laboratory measurements showed that the coring and trimming operations can cause reduction in specimen air voids, since most of the voids are near the side surfaces of the specimens. To determine the amount of air void reduction, the air voids before and after coring were measured and compared to understand the effect of specimen resizing.

Percent reduction in air voids measured for group-1 specimens is depicted in Figure 4.32. Before the cutting and trimming operations, the average air voids for each segregation level were measured as 4.74%, 5.69% and 6.46%, respectively. However, after coring and trimming, the average percent reductions in air voids were measured around 1.26%, 0.92% and 0.62%, and their respective final air voids 3.21%, 4.78% and 5.84% for the homogenous-unbiased (U), medium level segregated-biased (BM) and high level segregated-biased (BH) specimens, respectively.

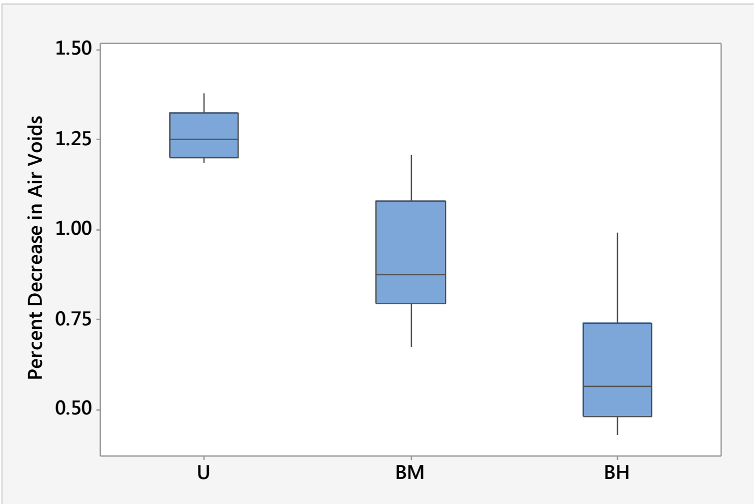

Figure 4.32. Air void reduction in group-1 specimens

The results show that the reduction in air void percentages for homogenous-unbiased specimens is larger than the other levels. In the high level segregated-biased case, the mean percent reduction in air voids is smaller than the other two levels. This can be explained by noting that volume of larger air voids is mainly concentrated in the courser portion of the compacted sample, that was removed after the curing and trimming operations. It can be noticed in Fig. 4.32 that the variability level for the medium level segregated-biased (BM) and high level segregated-biased (BH) specimens are similar while the smallest variation was obtained from the homogenous specimens. For the homogeneous specimens, aggregate structure is better arranged as compared to the segregated specimens, hence resulting in lower variations in air voids.

Reduction in air voids for group-2 specimens is shown in Figure 4.33 as a box plot. Before the coring and trimming operations, the average initial air voids were found 3.94% for all the three inhomogeneity levels. After the cutting and trimming operations, the mean reduction in air voids was measured as 1.38%, 1.29% and 1.29% and the average final air voids 2.56%, 2.65% and 2.66% for the U, BM and BH specimen sets, respectively.

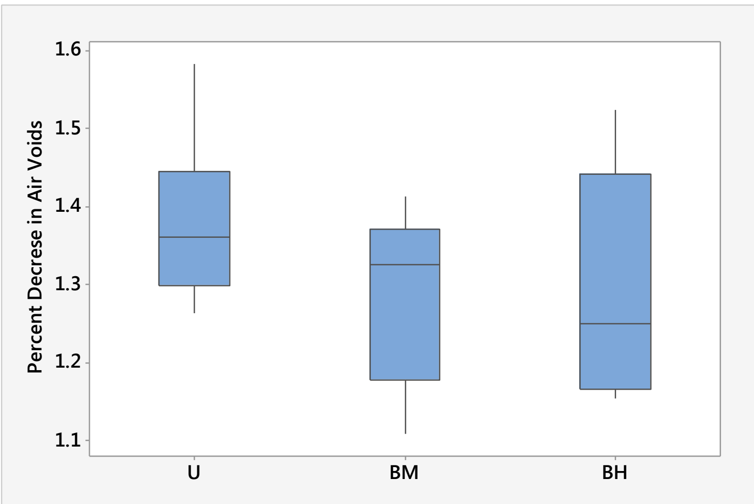

Figure 4.33. Air void reduction in group-2 specimens

The specimens in this group were compacted to the same density, and to compact the heterogeneous specimens, higher compaction efforts were applied. As shown in Fig. 4.33, compacting the unbiased and biased specimens to the same density resulted in similar air void reductions after the cutting and trimming operations. However, even though the average air void reductions are close for each specimen group, the overall variations seem to be quite different between each group. It should be noticed that the largest variation in air void reduction was found for the high level segregated-biased (BH) specimens and the lowest one for the homogenous-unbiased (U) specimens. The largest variation in air voids can be explained for highly segregated aggregate structure of BH specimens due to their poor aggregate orientations leading to non-uniform air void distribution within the specimens. Because the aggregate orientation will be relatively uniform for the homogenous specimens, a lower variation in air voids should be expected for these specimen group.

CHAPTER 5

EVALUATION OF IMAGE ANALYSIS AND RUTTING TEST RESULTS

5.1. Image Analysis of the Test Specimens

To assess the effect of inhomogeneity on rutting performance, all the specimens after the repeated creep tests were cut vertically from the center and cross sectional images were obtained by scanning using a flat bad scanner. The proposed inhomogeneity tests were then applied to the cross sectional images to investigate the relationship between the imposed segregations and the inhomogeneity level. After the completion of the repeated creep tests, all necessary measurements were obtained from the specimens for radial strain and volumetric strain calculations. The outer images of the specimens were taken from four different locations that are 90^{o} apart to record physical behavior of the specimens under repeated loading and then midpoints of the specimens were marked before the vertical cutting operations. Specimens were frozen before the cutting operation to prevent disturbing the internal structure, so the specimens were located on a deep freezer one night before the cutting. This step also helped in achieving smooth cutting surfaces without heating up the specimens. Specimens were centered to the circular cutting blade and fixed by the help of a bolted plate to prevent rotation during cutting. Cutting operation was conducted at very low speed to prevent warming, disturbing and rotation. After cutting, the cut surfaces were washed using tap water to clean dust and mud. 2D sectional images were then obtained from one cutting surface for each specimen using a flatbed scanner after one day drying (Figure 5.1).

Figure 5.1. Vertical sections of a tested specimen

The specimen images were processed following the image processing procedures explained in the previous sections and binary images were obtained. After converting the images into binary format, the next step was to extract image shape parameters. A Matlab® algorithm for particle detection and a Labview® program for particle analysis were used to find aggregate area, Feret diameter, location coordinates and other important shape properties. The estimated size distributions were determined by the developed algorithm using the maximum Feret diameter as an optimal shape parameter for the specimens. This operation was conducted for each group, i.e., specimens compacted using equal compaction energy and equal density separately. Combined size distributions were calculated for each group using the information obtained from the image corss sections. Important aggregate shape parameters such as area and maximum Feret diameter were recorded for the particles larger than 0.425 mm by the algorithm. Figure 5.2 shows percent passing from each sieve size for 18 specimens (with dots) and combined size distribution (connected line) for group-1. Variations in the percent passing from each sieve size can also be observed for all specimens by the help of dots.

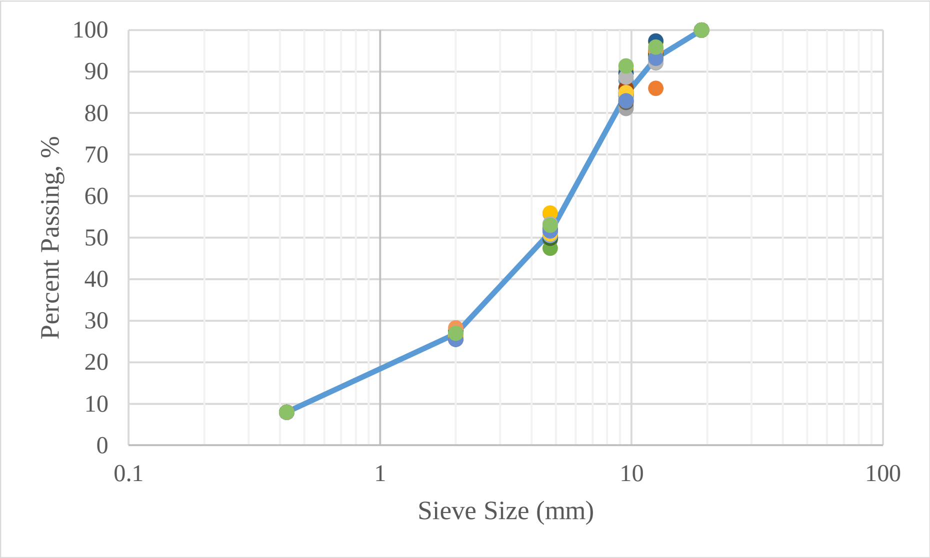

Figure 5.2. Image based size distribution for group-1 specimens

Similar procedures were applied for the group-2 specimens. Figure 5.3 shows the percent passing from each sieve size for 18 specimens (with dots) and combined size distribution (connected line) for group-2.

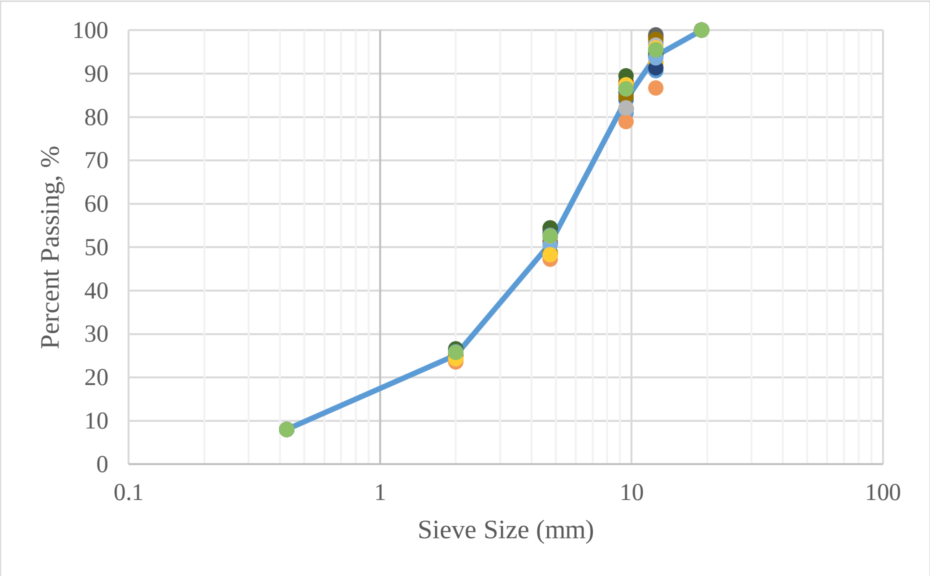

Figure 5.3. Image based size distribution for group-2 specimens

Estimated gradations for group-1 and group-2 specimens obtained from the image analysis and the actual gradation results are given in Table 5.1. The results show that the gradations were successfully estimated with negligible deviations from the actual gradations using 2D cross sectional images.

Table 5.1. *Results of the gradation analysis*

Sieve Size (mm)	**Percent Passed**		
	Actual Gradation (%)	**Group-1**	**Group-2**
19	100	100.0	100.0
12.5	89	93.3	94.1
9.5	80	84.4	84.0
4.75	42	51.3	50.9
2	23	26.9	25.1
0.425	8	8.0	8.0

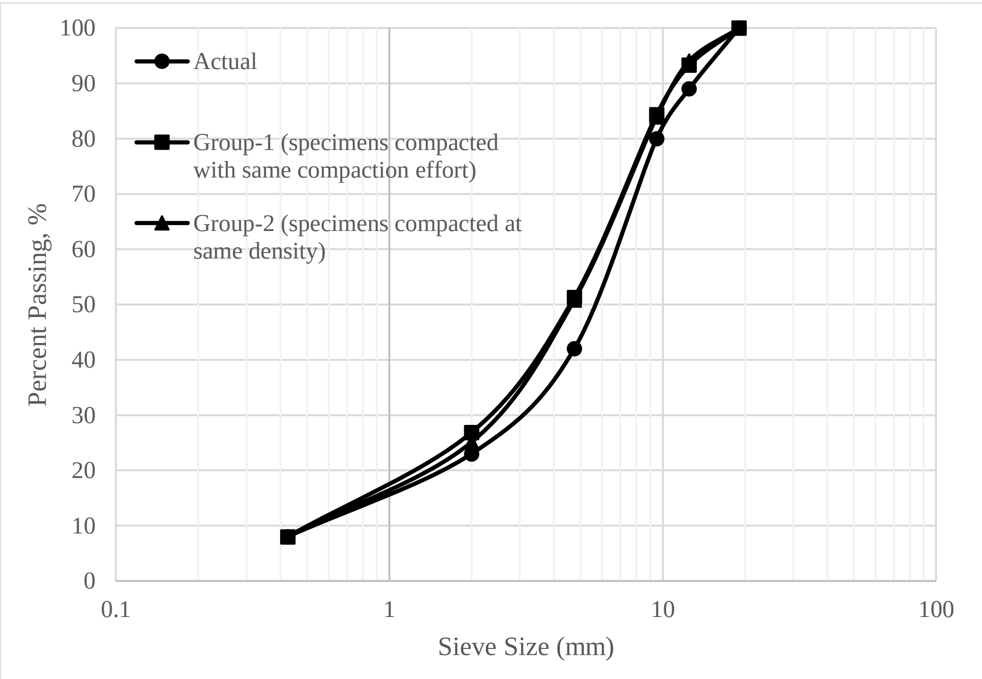

Figure 5.4. Estimated and actual size distributions

The graphical comparison of actual and estimated size distributions is given in Figure 5.4. The largest deviation from the actual size distribution occurred approximately 9% for 4.75 mm for both groups; however, deviations in other size fractions are generally smaller. Better estimations could be done by using more cross sectional images for each specimen but these estimations were considered sufficient to implement the proposed inhomogeneity test.

The next step was the determination of macro block size corresponding to a representative aggregate area for both groups. For the calculation of representative macro block size, combined size distributions involving all size fractions were used for each group. The criteria used in determining the representative macro block size is that (i) it should contain at least one particle retained on the largest sieve, ie., D_{max} and (ii) have equal aggregate/area proportion as the entire image total aggregate/area proportion. Representative aggregate area for a given cross section was calculated according to the aggregate proportions of all size fractions considered in the analyses. Macro block sizes were calculated based on these criteria and the inhomogeneity tests were then conducted for the cross section images. Representative macro block sizes were calculated as 1443 pixels for group-1 and 1476 pixels for group-2 specimens by the algorithm, respectively. As indicated in the previous section, the calculated macro block sizes represent only one side length of a square macro block in unit of pixel. Using the developed redistribution algorithm, cross sectional images of both groups were analyzed. For each cross section, as many as 1000 synthetic images were generated and the aggregate distribution characteristics using the inhomogeneity index were determined using the moving macro block method. Cumulative distribution functions of the synthetic images were obtained and the inhomogeneity levels of the original images were determined by finding the probability level corresponding to the inhomogeneity index of the original image.

Image size for G1-U1 specimen was determined as 2524x3336 pixels. Using the parameters calculated for group-1 specimens such as expected aggregate area (E) for each size fraction and macro block size, the moving macro block method was implemented by using the developed algorithm. Starting from the upper left hand corner, all image was scanned with a square size macro block and aggregate distribution information was gathered. For this section, a total of 897 macro blocks were located to completely scan the cross section image. By taking the average of inhomogeneity indices calculated in each step, a global inhomogeneity index of G1-U1 was found. As many as 1000 synthetic images were generated using the redistribution algorithm and the index values were calculated for each image generated frame by the algorithm. Index values of these synthetic images provide important information to understand the general trend and distribution characteristics of aggregate particles within the mixture section. Cumulative probability plot for the inhomogeneity indices of 1000 synthetic images for G1-U1 specimen is shown Figure 5.5.

In this plot, lognormal distribution function fitted to the calculated cumulative distribution is illustrated. It can be seen that the lognormal distribution perfectly fits to the actual distribution of the specimen's cross section. Inhomogeneity index of the original image was calculated as 27 and the probability level corresponding to this value was determined from the graph as 61.5. This value is considered as the inhomogeneity level of specimen G1-U1.

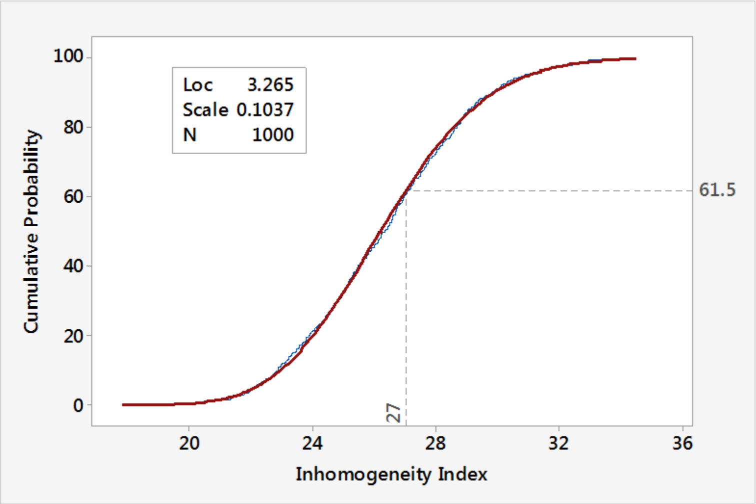

Figure 5.5. Cumulative probability plot for specimen G1-1

Similar to this operation, all inhomogeneity levels of group-1 and group-2 specimens were calculated by using the algorithm. Table 5.2 shows the inhomogeneity indices of all specimens and the corresponding inhomogeneity levels for the first and the second specimen groups.

Table 5.2. *Inhomogeneity level of the specimens*

Specimen	Inhom. Index	Inhom. Level	Specimen	Inhom. Index	Inhom. Level
G1-U1	27.00	61.5	G2-U1	21.64	75.0
G1-U2	30.58	80.1	G2-U2	19.44	36.6
G1-U3	19.41	57.9	G2-U3	17.26	47.7
G1-U4	25.19	85.1	G2-U4	19.36	79.8
G1-U5	21.37	49.2	G2-U5	15.83	20.3
G1-U6	23.96	75.2	G2-U6	15.60	18.2
G1-BM1	28.04	84.9	G2-BM1	19.83	55.0
G1-BM2	28.63	99.2	G2-BM2	36.47	100.0
G1-BM3	26.28	94.6	G2-BM3	32.37	100.0
G1-BM4	22.28	89.4	G2-BM4	34.46	100.0
G1-BM5	28.34	100.0	G2-BM5	28.71	94.5
G1-BM6	23.57	96.4	G2-BM6	25.19	90.0
G1-BH1	31.08	100.0	G2-BH1	27.55	98.5
G1-BH2	26.05	99.4	G2-BH2	30.88	98.5
G1-BH3	29.79	96.7	G2-BH3	32.57	99.5
G1-BH4	23.61	94.5	G2-BH4	32.81	99.1
G1-BH5	23.55	93.1	G2-BH5	32.04	100.0
G1-BH6	32.98	98.3	G2-BH6	31.87	100.0

*Note: G1: specimens group compacted with equal energy; G2: specimens compacted to equal density; U1….U6: homogenous specimens; BM1….BM6: medium segregated biased specimens; BH1….BH6: highly segregated biased specimens.

The inhomogeneity index by itself does not give an idea about specimen inhomogeneity level because each cross section contains particles with very different area fraction and shape properties and these conditions affect general trend of the inhomogeneity indices. Therefore, inhomogeneity level rather than inhomogeneity index should be used to describe the segregation level of asphalt concrete specimens. A higher inhomogeneity level indicates a highly segregated specimen and a lower inhomogeneity level means otherwise.

5.2. Analysis of Rutting Parameters and Inhomogeneity Levels

In this part of the study, the rutting test parameters and inhomogeneity level results were analyzed together to assess the effect of inhomogeneity on rutting resistance of asphalt concrete. The relationship between inhomogeneity level and the rutting test parameters was discussed and specimens were classified according to their inhomogeneity levels. The repeated creep test parameters used for the analyses can be listed as flow number, slope (b), maximum radial strain, volumetric strain, permanent strain at 2500 cycles and loading cycle at 5% permanent deformation. Intercept (a) parameter, which is the intercept of the power model, was not included in the assessment because it did not show a correlation strong enough to consider this parameter as a good indicator of rutting performance of asphalt concrete. Some specimens did not reach 5% permanent strain and the test terminated before 10,000 cycles were reached at a permanent strain smaller than 5%. For these specimens, the Francken model was used to estimate the number of loading cycles corresponding their final permanent strain level. Because the Francken model is able to fit test data for all three phases of permanent deformation, i.e., initial, secondary and tertiary phase, the model estimations can be reliably used to extrapolate for extended number of loading cycles.

5.2.1. Specimens Compacted with Same Compaction Effort

The assessment of inhomogeneity levels and test parameters for group-1 specimens was carried out in this section. In this scope, the inhomogeneity levels of 18 specimens were sorted from largest to smallest and the general trend was observed. The specimens were classified into three groups according to their inhomogeneity levels. Inhomogeneity levels smaller than 80% as homogenous, between 80% and 90% as medium level segregated and larger than 90% high level segregated were classified. After examination of the general trend of the index versus specimen responses, three specimens, G1-U1, G1-BM5 and G1-BH5, were excluded from the analyses because they were outliers. After the classification of the specimens according to their inhomogeneity levels, the number of specimens used in the analyses were 3 for homogenous, 4 for medium level segregated and 8 for high level segregated classes.

To confirm this classification, calculated means of the test parameters for each level were compared statistically by the help of Tukey test. In this statistical test, means were compared to understand whether they are significantly different or not. In this way, the success of inhomogeneity test and classification was evaluated. Inhomogeneity levels of 15 specimens and corresponding repeated creep test parameters are given in Table 5.3. As shown in the table, specimens which were prepared at different segregation levels (U, BM and BH) have inhomogeneity levels that are close to each other.

Table 5.3. *Test results for the group-1 specimens*

Specimen		**Inhom. Level**	**Flow Number**	**Intercept (a)**	**Slope (b)**	**Max. Radial Strain (%)**	**Vol. Strain (%)**	**Per. Strain @2500 Cycles**	**Cycle Number at 5% Perm. Strain**
High Level Segregated	G1-BH1	100.0	1014	3.01	0.38	8.0	6.5	3.18	3212
	G1-BH2	99.4	1195	2.76	0.45	8.6	7.7	2.57	3596
	G1-BM2	99.2	1333	2.91	0.41	8.5	7.5	2.48	3840
	G1-BH6	98.3	1112	3.02	0.37	10.8	8.9	2.82	3412
	G1-BH3	96.7	1226	2.92	0.40	9.0	8.8	2.47	3834
	G1-BM6	96.4	1222	3.00	0.35	9.2	8.2	2.26	3973
	G1-BM3	94.6	1221	2.93	0.39	9.7	8.0	2.42	3803
	G1-BH4	94.5	940	3.05	0.38	10.2	9.3	3.59	2972
Medium Level Segregated	G1-BM4	89.4	1291	3.04	0.36	7.9	7.8	2.59	3939
	G1-U4	85.1	1268	2.86	0.42	7.5	8.3	2.38	4102
	G1-BM1	84.9	1403	3.04	0.35	8.1	7.8	2.11	4509
	G1-U2	80.1	1447	3.12	0.33	7.2	7.7	2.25	4469
Homogenous	G1-U6	75.2	1628	2.99	0.36	7.9	8.0	1.90	5089
	G1-U3	57.9	1587	2.95	0.37	8.7	9.9	1.88	4990
	G1-U5	49.2	1439	3.05	0.33	8.5	8.9	2.03	4503

Tukey test was implemented for the test parameters listed above without the intercept (a) constant. In Tukey tests, 90% confidence level was used and if p-value is smaller than 0.1, it indicates that the means of the parameters are significantly different between the segregation levels. P-values obtained from the Tukey test for the six test parameters are listed in Table 5.4.

Table 5.4. *Tukey test results of group-1 specimens*

Test Parameter	**P-Value**		
	Homogenous-Medium Level Segregated	**Homogenous-High Level Segregated**	**High Level Segregated-Medium Level Segregated**
Flow Number	0.098	0.001	0.042
Slope (b)	0.853	0.189	0.375
Per. Strain @2500 Cycles	0.352	0.019	0.223
Volumetric Strain	0.251	0.326	0.898
Max. Radial Strain	0.481	0.240	0.014
Loading Cycles at 5% Per. Strain	0.078	0.000	0.015

For the flow number parameter, P-values seem smaller than 0.1, therefore, it can be concluded that the means of the flow numbers between each segregation level are significantly different. Difference between the means of the loading cycles at 5% permanent strain parameter was found also significant for the segregation levels. The means of the permanent strain at 2500 cycle parameter were significantly different only between the homogenous and high level segregated specimens, but there was no significant difference between the homogenous-medium level, and high level segregated-medium level segregated cases. The means of the slope (b) values were not significantly different; however, it can be noticed that the slope (b) decreases as the inhomogeneity level decreases. It was, therefore, concluded that the slope (b) constant shows a reasonable behavior with the specimens' inhomogeneity levels. It is believed that this parameter would also indicate a significant difference between the means, were the number of test specimens increased. The other parameters, volumetric strain and maximum radial strain did not show any statistical difference between the imposed segregation levels.

The average of flow numbers and the number of loading cycles at 5% permanent strain parameters were also found to be significantly different. Interval plots for these two parameters are given in Figure 5.6 and Figure 5.7.

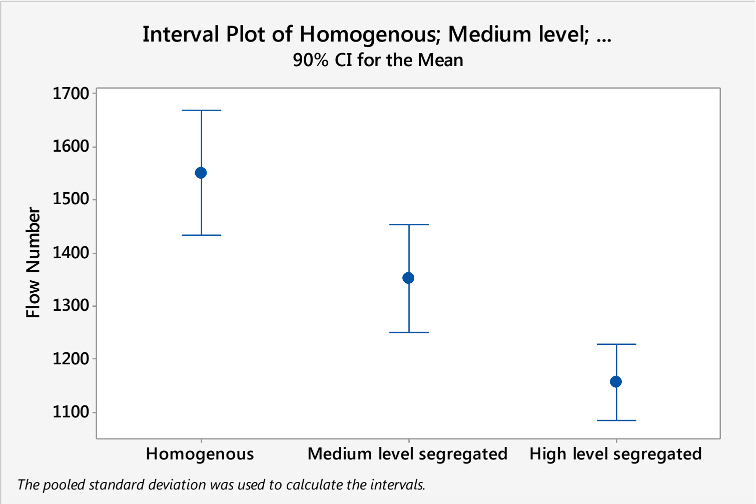

Figure 5.6. Interval plot of flow numbers

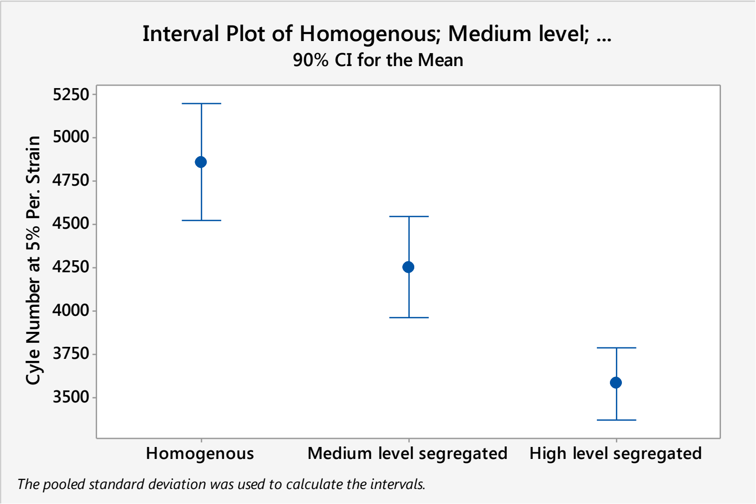

Figure 5.7. Interval plot of cycle number at 5% permanent strain

For the permanent strain at 2500 cycles, the calculated means were significantly different between the homogenous and high level segregated levels; however, they were not significantly different between medium level segregated-high level segregated, and medium level segregated-homogenous levels. Interval plot for this parameter is given in Figure 5.8.

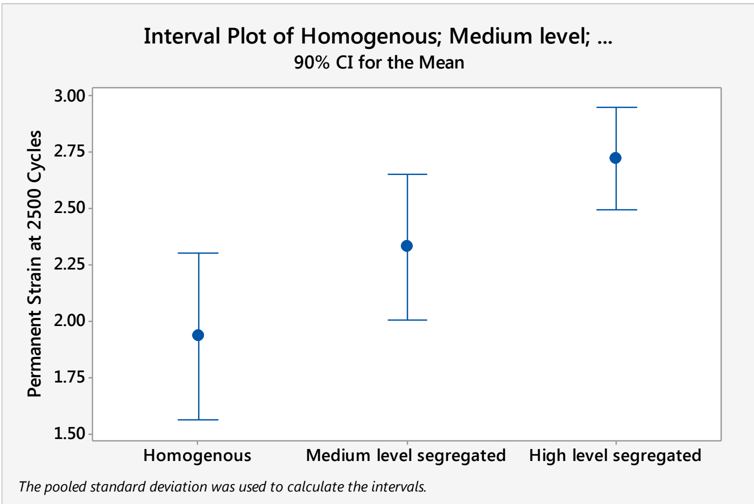

Figure 5.8. Interval plot of permanent strain at 2500 cycles

To discuss the relationship between the inhomogeneity levels and the test parameters in more detail, graphical representation of the results is given here. In this scope, flow number, permanent strain at 2500 cycles and loading cycles at 5% permanent strain parameters were considered. Figure 5.9 shows flow number versus inhomogeneity level plot. The flow number is known as one of the best parameters reflecting the field performance of asphalt concrete. The graph shows the test results of 15 specimens prepared using same gradation, same binder and same compaction level. The only difference between the specimens is the segregation levels. Specimen preparation step was organized to simulate segregation in the mixtures by producing unbiased and biased specimens at different levels. The specimens were previously prepared as three sets which are homogenous-unbiased, medium level segregated-biased and high level segregated-biased; however, after the image analyses, a reclassification was implemented according to the calculated inhomogeneity levels. This new classification consists of three levels which are homogenous, medium level segregated and high level segregated. Some specimens which were prepared at different segregation levels experimentally gave similar flow number and their inhomogeneity levels calculated using the proposed method were almost equal or close to the other segregation levels as shown in the figure. This, in fact, proves the success of the inhomogeneity test to characterize the internal structure of the specimens. The average of flow numbers for homogenous, medium level segregated and high level segregated cases were calculated as 1551, 1352 and 1158, respectively. In medium level segregated and high level segregated cases, the average flow numbers of specimens are 12.83% and 25.34% smaller than homogenous level specimens. A significant decrease in the flow number was observed in the segregated specimens. The coefficient of variation was calculated as 5.07%, 16.36% and 10.36% for homogenous, medium level segregated and high level segregated specimens, respectively. The results show that variation in the flow number results is minimum in the homogenous case.

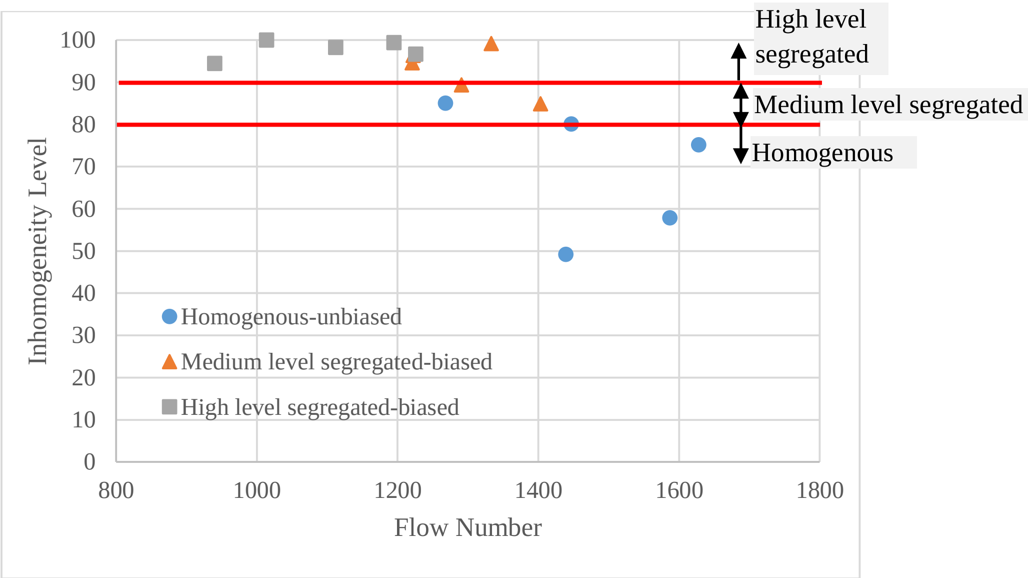

Figure 5.9. Inhomogeneity level versus flow number for group-1 specimens

Figure 5.10 shows inhomogeneity level versus cumulative permanent strain at 2500 loading cycles plot. 2500 cycle was selected as a constant value to compare different specimens. Figure shows that there is a good correlation between inhomogeneity level and the permanent strain at 2500 loading cycles. However, according to the statistical analyses, the means of the test parameters are significantly different between homogenous and high level segregated specimens, but the they seem to be not significantly different between homogenous-medium level segregated and medium level segregated-high level segregated specimens. As stated previously, this may occur due to a limited number of specimens. It is believed that if the number of test specimens are increased, this parameter would most likely show significant difference between the segregation levels.

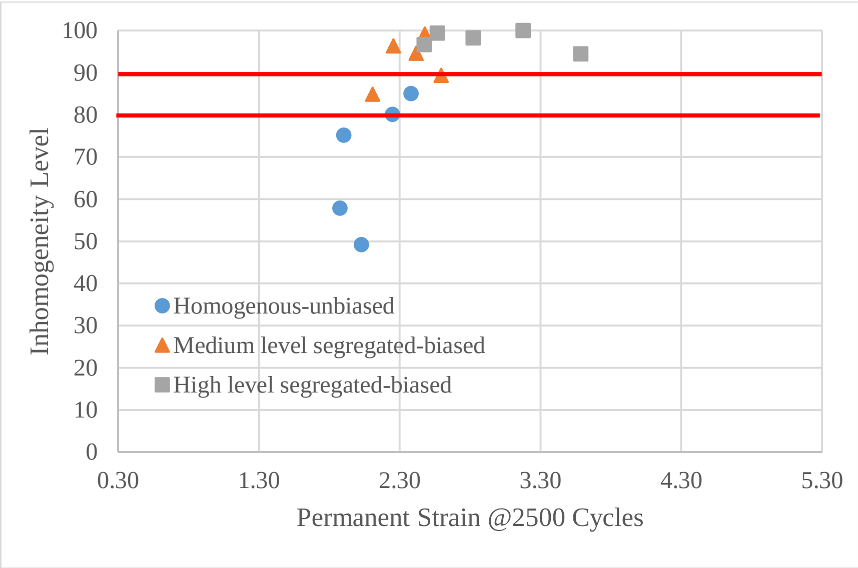

Figure 5.10. Inhomogeneity level versus permanent strain at 2500 cycles for group-1 specimens

Figure 5.11 shows inhomogeneity level versus loading cycles at 5% permanent strain plot. The parameter represents the number of cycles when the cumulative permanent deformation reaches 5%. The average number of cycles were determined as 4861, 4255 and 3580 for homogenous, medium level segregated and high level segregated specimens, respectively. Results show that the homogenous specimens are more rutting resistant and higher loading cycles are necessary to reach 5% permanent deformation as compared to the segregated specimens. The average number of loading cycles to the termination level, i.e., 5%, are 12.47% larger for medium segregated specimens and 26.35% larger for the highly segregated specimens. The coefficient of variation was calculated as 4.61%, 16.81% and 9.21% for homogenous, medium level segregated and high level segregated specimens, respectively. The results indicate that the variations in the results is generally minimum for the homogenous sample group. Similar to the flow number parameter, number of loading cycles to 5% permanent deformation clearly shows the difference between different segregation levels.

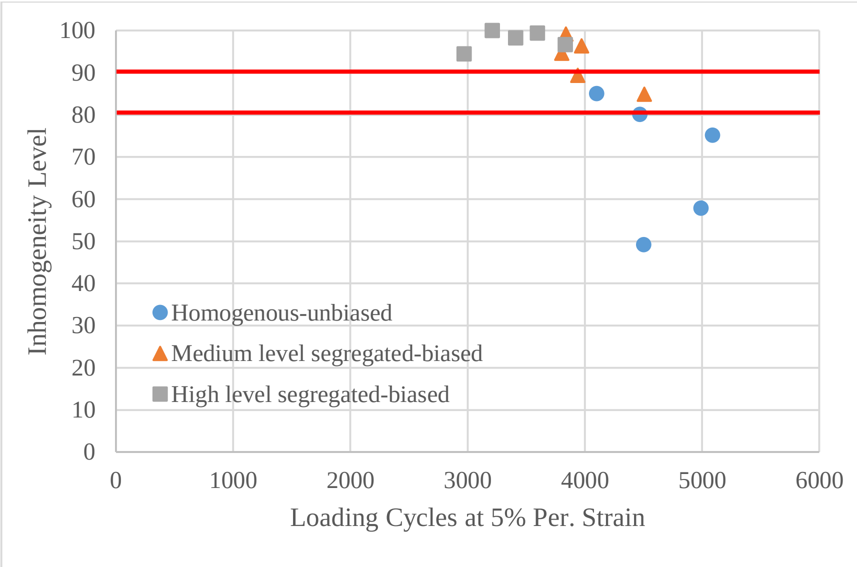

Figure 5.11. Inhomogeneity level versus loading cycles at 5% permanent strain for group-1 specimens

As shown in the given three parameter results, the rutting test parameters are highly correlated with the inhomogeneity levels. These results are indicator of the success of the proposed inhomogeneity test and the significant impact of segregation on rutting resistance. Under the same compaction effort, homogenous specimens are more rutting resistant and the variation in the test results is minimum.

5.2.2. Specimens Compacted at the Same Density

Similar to the first group, rutting test parameters for the second group specimens and their inhomogeneity levels were evaluated together. Specimens were classified according to their inhomogeneity levels calculated from the image analyses. The limits determined previously were also applied for this group. Inhomogeneity levels smaller than 80%, between 80% and 90% and larger than 90% were classified as homogenous, medium level segregated and high level segregated. There were no outliers in this group, so all specimens were considered during analyses. 11 specimens were determined as high level segregated and 7 specimens were determined as homogenous; however, there were no medium level segregated specimen in this group.

Means of the test parameters corresponding to homogenous and high level segregated levels were compared by implementing Tukey test to prove that they are significantly different. The inhomogeneity levels and specimen test parameters are given in Table 5.5.

Table 5.5. *Test results for the group-2 specimens*

Specimen		Inhom. Level	Flow Number	Intercept (a)	Slope (b)	Max. Radial Strain (%)	Vol. Strain (%)	Per. Strain @2500 Cycles	Cycle Number at %5 Perm. Strain
High Level Segregated	G2-BM2	100.0	3025	2.92	0.31	7.5	3.0	0.98	12490
	G2-BM4	100.0	3331	2.95	0.30	5.0	3.7	0.96	13995
	G2-BH4	99.1	3523	2.93	0.30	5.5	3.5	0.95	14545
	G2-BH3	99.5	3229	2.89	0.32	7.6	4.9	0.96	12640
	G2-BM3	100.0	3163	2.93	0.30	8.2	4.7	0.96	11925
	G2-BH5	100.0	3167	3.04	0.28	7.4	4.2	1.00	11730
	G2-BH6	100.0	3179	2.97	0.29	6.0	7.6	0.91	12245
	G2-BH2	98.5	3685	2.83	0.33	4.3	4.3	0.87	14280
	G2-BM5	94.5	3145	3.02	0.27	6.8	5.5	0.93	12580
	G2-BH1	98.5	3461	2.86	0.31	6.6	7.9	0.86	12435
	G2-BM6	90.0	3377	2.97	0.30	12.0	4.4	1.02	10628
Homogenous	G2-U1	75.0	2423	2.77	0.38	6.6	7.1	1.24	7979
	G2-BM1	55.0	2783	2.90	0.33	11.3	5.2	1.11	10106
	G2-U2	36.6	2319	2.75	0.40	8.7	8.4	1.35	7729
	G2-U4	79.8	2801	2.71	0.40	8.5	8.7	1.17	9061
	G2-U3	47.7	2937	2.83	0.35	9.1	9.5	1.09	9715
	G2-U5	20.3	2685	3.00	0.32	8.4	7.9	1.29	4462
	G2-U6	18.2	2301	2.95	0.34	10.2	10.5	1.32	7667

Tukey test was implemented for all test parameters listed above without intercept (a). The means of the test parameters were compared to understand whether they are significantly different between the two levels of segregation. P-values obtained from the Tukey test for these six parameters are given in Table 5.6.

Table 5.6. *Tukey test results for group-2 specimens*

Test Parameter	**P-Value**
	Homogenous-High Level Segregated
Flow Number	0.000
Slope (b)	0.000
Per. Strain @2500 Cycle	0.000
Volumetric Strain	0.001
Max. Radial Strain	0.042
Loading Cycles at 5% Per. Strain	0.000

As shown in the table, all P-values are smaller than 0.1, showing that the means of the test parameters are significantly different at 90% confidence level. Interval plots of the two important rutting test parameters, i.e., flow number and slope, are given in Figure 5.12 and Figure 5.13, respectively. The other parameters also reflect the difference between inhomogeneity levels.

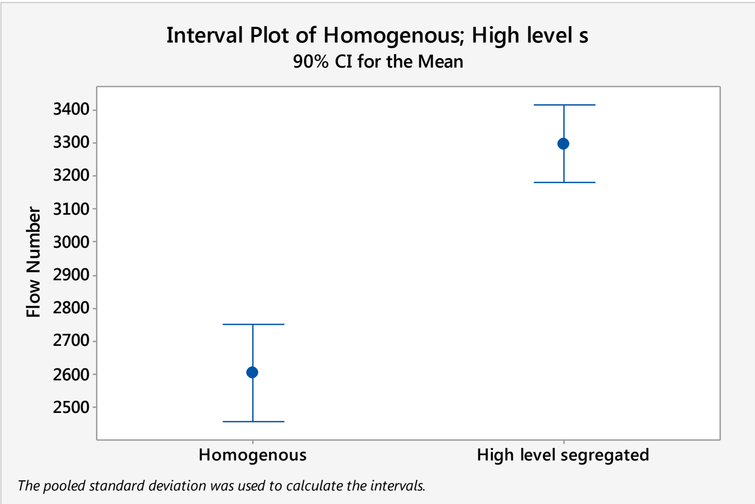

Figure 5.12. Interval plot of flow number

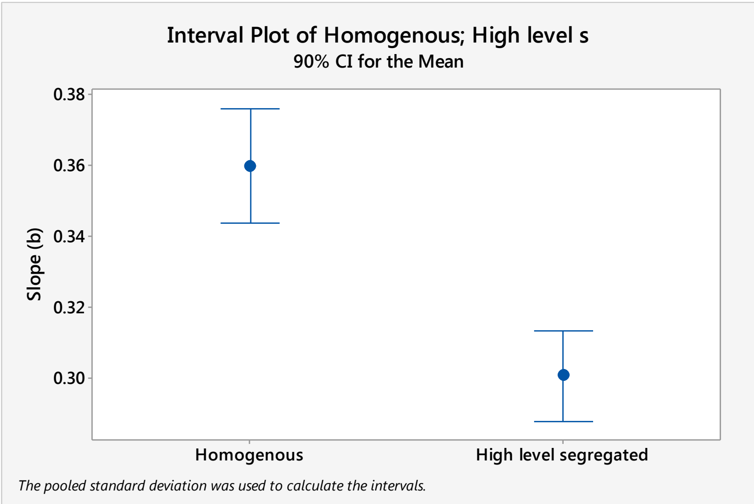

Figure 5.13. Interval plot of slope (b) parameter

To discuss the relationships between inhomogeneity levels and the test parameters in more detail, graphical representation of the results is given here. Figure 5.14 shows inhomogeneity level versus flow number. Specimens with less than 80% inhomogeneity level were classified as homogenous and inhomogeneity level higher than 90% were classified as high level segregated. It should be remembered that the specimens were compacted to the same density in this group. Homogenous specimens were compacted with less gyration effort and vice versa as explained in the previous sections. It is considered that because of excessive compaction for reaching the target air void, the flow numbers of high level segregated specimens are much higher than those of homogenous specimens. The average flow numbers for the homogenous and the high level segregated specimens were calculated as 2607 and 3299, respectively. The average flow number for the homogenous specimens is 20.98% smaller because of less compaction effort needed.

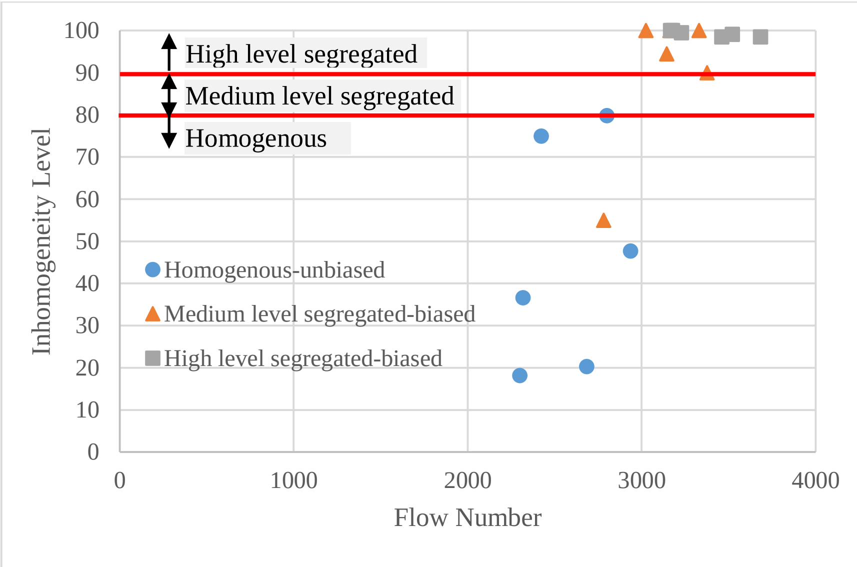

Figure 5.14. Inhomogeneity level versus flow number for group-2 specimens

Relationships between inhomogeneity levels and slope constants are given in Figure 5.15. Similar to the flow number results, the homogenous specimens are more rutting susceptible as their slope constants are higher.

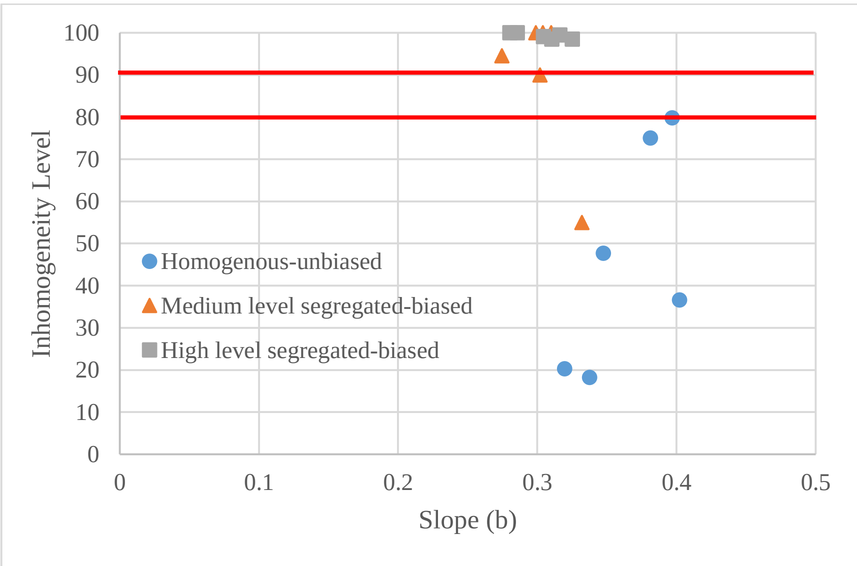

Figure 5.15. Inhomogeneity level versus slope (b) for group-2 specimens

Figure 5.16 shows inhomogeneity level versus permanent strain at 2500 cycles. A correlation between this test parameter and the inhomogeneity level can be seen from the graph.

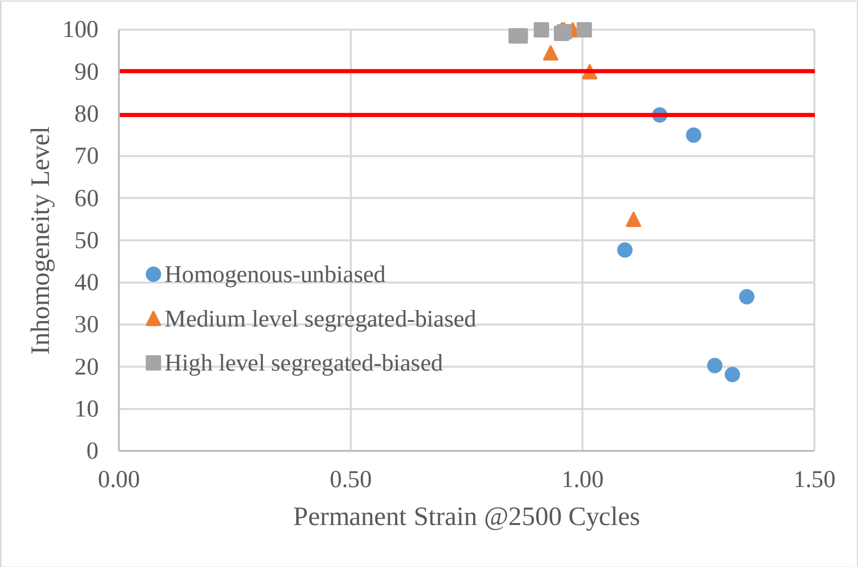

Figure 5.16. Inhomogeneity level versus permanent strain at 2500 cycles for group-2 specimens

In addition, inhomogeneity level versus volumetric strain, maximum radial strain and loading cycles at 5% permanent strain graphs are given in Figure 5.17-19.

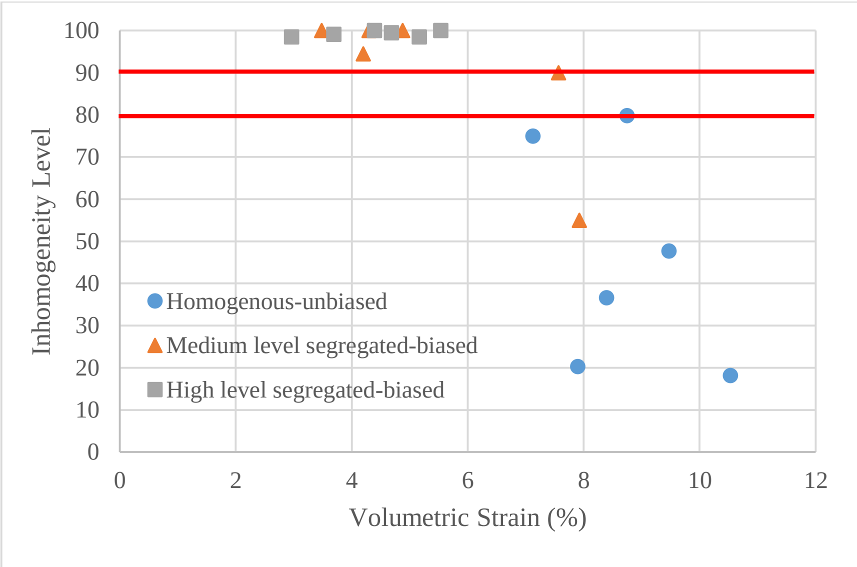

Figure 5.17. Inhomogeneity level versus volumetric strain for group-2 specimens

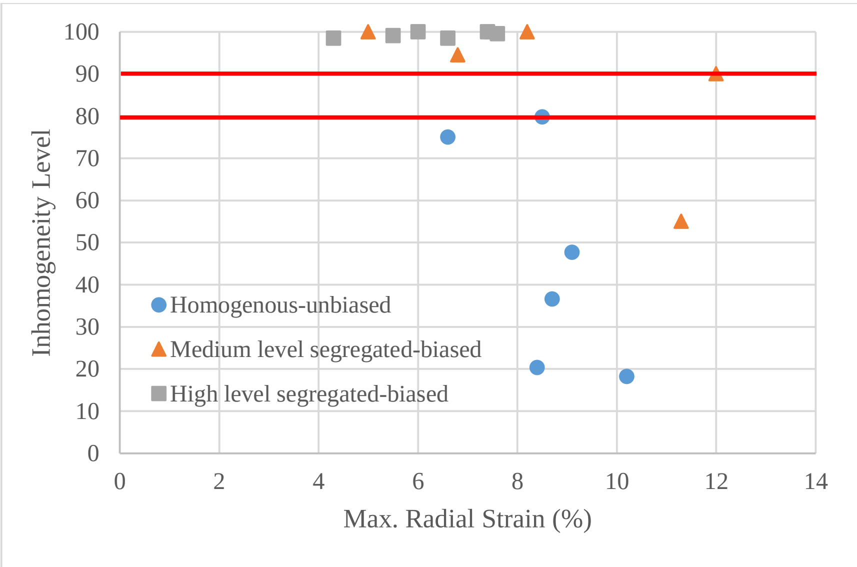

Figure 5.18. Inhomogeneity level versus maximum radial strain for group-2 specimens

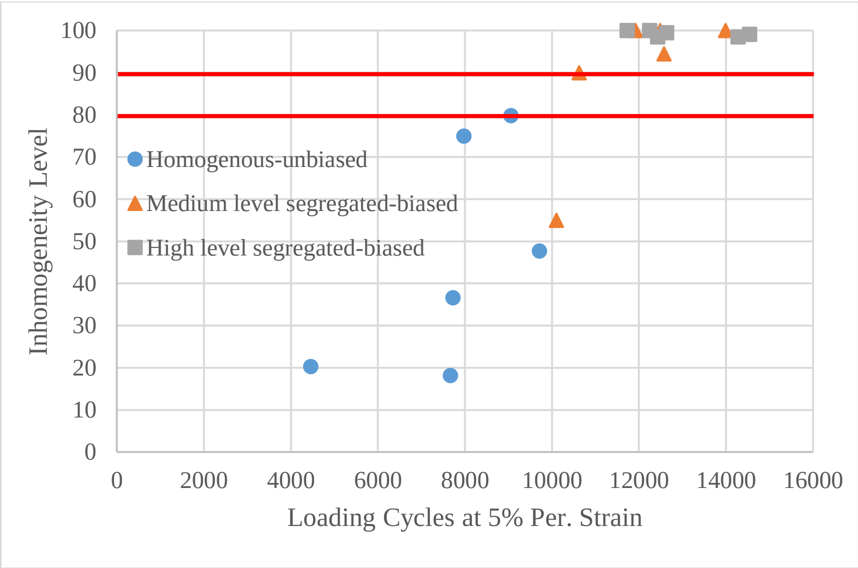

Figure 5.19. Inhomogeneity level versus loading cycles at 5% permanent strain for group-2 specimens

There is a similar trend for all test parameters discussed in this group. High level segregated specimens were more rutting resistant because of the difference between compaction levels. To compact biased specimens, almost three times more compaction effort was applied and this condition resulted in very stiff specimens. Due to increased stiffness, permanent deformation remained very low in high level segregated specimens. Volumetric strain values for high level segregated specimens are also smaller than for homogenous specimens in this group due to the excessive compaction applied. Similar to the first group, the developed method is able to differentiate between homogenous and segregated specimens successfully. Both groups show the importance of segregation on specimen rutting resistance and proves that the inhomogeneity levels from 2D cross section images can be successfully detected.

CHAPTER 6

CONCLUSIONS AND RECOMMENDATIONS

6.1. Conclusions

In this study, the impact of aggregate segregation on rutting resistance of asphalt concrete was investigated. The study focused on two main objectives. In the first phase, an inhomogeneity test method was proposed to evaluate aggregate segregation in asphalt concrete specimens using 2D cross section images. An inhomogeneity index which evaluates aggregate distribution statistically has been developed. The proposed index was applied for different types of mixtures and the power of the proposed test was determined statistically using synthetic images generated via a newly developed redistribution algorithm. In the second phase, the effect of aggregate segregation on rutting resistance of asphalt concrete specimens was assessed. The details of producing unbiased and laboratory segregated specimens were presented and repeated creep tests were conducted to measure rutting resistance of test specimens. Inhomogeneity levels of the test specimens were determined using 2D images obtained from the specimen's vertical cut sections. Finally, the relationships between the inhomogeneity level and the repeated creep test parameters of the specimens were discussed. The findings of this study can be summarized as follows:

1- Image analysis results show that gradation of asphalt mixture specimens can be estimated successfully using their 2D cross sectional images. Maximum feret diameter was selected as a shape parameter and the area of particles was used to calculate percent retaining on each sieve. Success of estimations increases with the number of cross sections used in the analysis. The number of cross sections should be increased for better estimations of the aggregate gradation.

2- Redistribution algorithm developed in this study helps to determine aggregate distribution characteristics and the range of inhomogeneity indices. This algorithm may be used to understand aggregate distribution characteristics of different mixtures and develop a new microstructural characterization index. The algorithm can also be used to determine the power of the available test indices.

3- Power of the proposed inhomogeneity test was determined statistically by creating homogenous and segregated synthetic images of four different mixtures. Results show that the power of the test at %95 confidence interval is higher than at 90% for all the test samples. Thus, the proposed test can be used to evaluate mixture inhomogeneity of laboratory compacted or field cored asphalt concretes.

4- Volumetric calculations carried out for specimens compacted under same gyration effort (group-1) show that the air void level of specimens increases with segregation. Among the three segregation levels, the lowest average air void belongs to unbiased specimens (prepared as homogenous as possible). Air void levels of the biased specimens produced in the laboratory as segregated specimens at two levels of medium and highly segregated were found to be higher.

5- Group-2 specimens were compacted to the same density corresponding to 4% air void. Results indicate that the number of gyrations to reach the same target density increases with increasing segregation level. The average number of gyrations for high level segregated-biased specimens was three times more than the unbiased specimens. Similarly, the average number of gyrations for medium level segregated-biased specimens was found to be more than twice the average of unbiased specimens.

6- Flow number and slope (b) constant parameters show that unbiased group-1 specimens are more rutting resistant than their biased specimens. According to group-2 test results, unbiased specimens are more rutting susceptible than the biased specimens, which results from applying excessive compaction to these biased specimens to reach to the target density.

7- Radial strain were measured almost uniform along with the specimen height in unbiased specimens; however, in biased specimens, measured radial strains in the upper part of the specimens were less than the bottom part. Coarser portion was placed on the bottom and finer portion was located on the upper part. It shows that finer portions of the segregated specimens behave stiffer than the coarser portions which behave more loosely.

8- Volumetric strain results were close for unbiased and biased specimens of group-1 specimens; however, volumetric strain decreases with increasing segregation level in group-2 specimens. This is the result of excessive compaction of the biased specimens in group-2.

9- According to the inhomogeneity test results, group-1 and group-2 specimens were classified as homogenous, medium level segregated and high level segregated. Based on this classification, the relationship between the inhomogeneity levels and the rutting test parameters were investigated and the success of the image analysis based the classification was discussed. The relationship between the repeated creep test parameters and the inhomogeneity levels were assessed based on the Tukey test and the results show that the means of flow numbers and loading cycles to 5% permanent strain are significantly different between the segregation levels (homogenous, medium level segregated and high level segregated) for group-1 specimens. This proves that the proposed inhomogeneity test method can be used to classify specimens according to the results of analyses from cross sectional images. In the second group, specimens were classified at two levels as homogenous and high level segregated. There was no specimen whose inhomogeneity level falls within the limits of medium level segregation. Tukey test conducted for this group shows that the means of all the repeated creep test parameters, flow number, slope (b), permanent strain at 2500 cycles and cycle number at 5% permanent strain are significantly different between homogenous and high level segregated levels.

10- Statistical analyses show that the proposed test method can successfully determine the inhomogeneity level of specimens. According to the rutting tests and inhomogeneity test results, means of the important repeated creep test parameters are significantly different between different segregation levels. These results reveal that aggregate segregation significantly affects the rutting performance of asphalt concrete specimens.

11- Under the same compaction effort (group-1), the average flow numbers of medium level and high level segregated specimens are 12.83% and 25.34% smaller than that of homogenous specimens. The average slope (b) constant of homogenous specimens was 0.35; however, this constant was calculated as 0.39 for high level segregated specimens. There is also a similar trend for the other test parameters, indicating the importance of aggregate segregation on rutting performance of asphalt concrete samples.

12- In group-2 specimens, less compaction effort was applied to homogenous specimens than to high level segregated specimens to reach the target air void. Because of excessive compaction applied, high level segregated specimens behaved more rutting resistant in this group. The average flow numbers for homogenous and high level segregated specimens were calculated as 2607 and 3299, respectively. In other words, the average flow number of the homogenous specimens is 20.98% smaller because of the less compaction effort.

13- Repeated creep test results indicate that the variation in the flow number for homogenous specimens is less than that of medium and high level segregated specimens in group-1. This condition was also observed in other test parameters. This proves a more reliable test results for the homogenous specimens yielding minimum variation under the same compaction effort.

6.2. Recommendations for Future Studies

In the light of the outcomes of this study, following recommendations can be made for future studies:

- To better correlate inhomogeneity level and rutting test parameters, more specimens should be prepared and tested. In this way, relationship between rutting performance and internal structure of specimens can be understood better.

- In this study, only the effect of segregation on rutting performance was investigated. To fully understand the effect of segregation on mechanical performance of asphalt concrete, other performance tests such as indirect tensile and resilient modulus tests can be conducted and the results are correlated with the inhomogeneity levels.

REFERENCES

AASHTO M 323-07. (2010). Superpave Volumetric Mix Design. In *Standard Specifications for Transportation Materials and Methods of Sampling and Testing (Part 1A Specifications)*, Thirtieth Edition. AASHTO, Washington D.C.

AASHTO R 35-09. (2010). Superpave Volumetric Design for Hot Mix Asphalt (HMA). In *Standard Specifications for Transportation Materials and Methods of Sampling and Testing (Part 1A Specifications)*, Thirtieth Edition. AASHTO, Washington D.C.

AASHTO T 84-10. (2010). Specific Gravity and Absorption of Fine Aggregate. In *Standard Specifications for Transportation Materials and Methods of Sampling and Testing (Part 1A Specifications)*, Thirtieth Edition. AASHTO, Washington D.C.

AASHTO T 85-10. (2010). Specific Gravity and Absorption of Coarse Aggregate. In *Standard Specifications for Transportation Materials and Methods of Sampling and Testing (Part 1A Specifications)*, Thirtieth Edition. AASHTO, Washington D.C.

AASHTO T 96-02. (2010). Resistance to Degradation of Small-Size Coarse Aggregate by Abrasion and Impact in the Los Angeles Machine. In *Standard Specifications for Transportation Materials and Methods of Sampling and Testing (Part 1A Specifications)*, Thirtieth Edition. AASHTO, Washington D.C.

AASHTO T 100-06. (2010). Specific Gravity of Soils. In *Standard Specifications for Transportation Materials and Methods of Sampling and Testing (Part 1A Specifications)*, Thirtieth Edition. AASHTO, Washington D.C.

AASHTO T 166-10. (2010). Bulk Specific Gravity of Compacted Hot Mix Asphalt (HMA) Using Saturated Surface-Dry Specimens. In *Standard Specifications for Transportation Materials and Methods of Sampling and Testing (Part 1A Specifications)*, Thirtieth Edition. AASHTO, Washington D.C.

AASHTO T 209-10. (2010). Theoretical Maximum Specific Gravity and Density of Hot Mix Asphalt (HMA). In *Standard Specifications for Transportation Materials and Methods of Sampling and Testing (Part 1A Specifications)*, Thirtieth Edition. AASHTO, Washington D.C.

AASHTO T 316-10. (2010). Viscosity Determination of Asphalt Binder Using Rotational Viscometer. In *Standard Specifications for Transportation Materials and Methods of Sampling and Testing (Part 1A Specifications)*, Thirtieth Edition. AASHTO, Washington D.C.

Adhikari, S., You, Z. P., & Peterson, K. (2013). Multi-phase characterization of asphalt concrete using X-ray microfluorescence. *International Journal of Pavement Research and Technology*, *6*(2), 117-122.

Ameri, M., Sheikhmotevali, A. H., & Fasihpour, A. (2014). Evaluation and comparison of flow number calculation methods. *Road Materials and Pavement Design*, *15*(1), 182-206.

Asphalt Institute. (2014). *Asphalt mix design methods (MS-2)*, 7th edition, 978-1-934154-70-0, USA.

ASTM D2493. (2016). *Standard Practice for Viscosity-Temperature Chart for Asphalt Binders.* ASTM International, West Conshohocken, PA.

Azari, H. (2005). *Effect of aggregate inhomogeneity on mechanical properties of asphalt mixtures* (Doctoral dissertation), University of Maryland at College Park, UMI Number: 3201993, 2005.

Azari, H., McCuen, R., & Stuart, K. (2005). Effect of radial inhomogeneity on shear properties of asphalt mixtures. *Journal of materials in civil engineering*, *17*(1), 80-88.

Biligiri, K., Kaloush, K., Mamlouk, M., & Witczak, M. (2007). Rational modeling of tertiary flow for asphalt mixtures. *Transportation Research Record: Journal of the Transportation Research Board*, (2001), 63-72.

Bonaquist, R. F., Christensen, D. W., & Stump, W. (2003). *Simple performance tester for Superpave mix design: First-article development and evaluation* (NCHRP Report 513). Transportation Research Board.

Bruno, L., Parla, G., & Celauro, C. (2012). Image analysis for detecting aggregate gradation in asphalt mixture from planar images. *Construction and Building Materials*, *28*(1), 21-30.

Castleman, K. R. (1996). *Digital image processing*, Prentice Hall, USA.

Cebeci, İ., Öztürk, F., SARISAMUR, F., & Cebel, H. (2013). Güvenç Havzası Aşındırıcı Güç İndisleri ve Kurak Dönemlerin Belirlenmesi. *Toprak Su Dergisi*, *2*(1), 15-22.

Cominsky, R. J., Huber, G. A., Kennedy, T. W., & Anderson, M. (1994). *The superpave mix design manual for new construction and overlays* (No. SHRP-A-407). Washington, DC: Strategic Highway Research Program.

Cressie, N. (1992). Statistics for spatial data. *Terra Nova*, *4*(5), 613-617.

Cross, S. A., & Brown, E. R. (1993). Effect of segregation on performance of hot-mix asphalt. *Transportation Research Record*, 117-117.

Cross, S. A., Hainin, M. R., & Ado-Osei, A. (1998). *Effects of segregation on mix properties of hot mix asphalt* (No. K-TRAN: KU-96-6,).

Dongre, R., D’Angelo, J., & Copeland, A. (2009). Refinement of flow number as determined by the Asphalt Mixture Performance Tester for use in routine QC/QZ practice. *Transportation Research Board, TRB, Washington DC*.

Francken, L. (1977). Pavement deformation law of bituminous road mixes in repeated load triaxial compression. *Proceedings of the 4th International Conference on the Structural Design of Asphalt Pavements*, Ann Arbor, MI, USA, pp. 483–496, 1977.

Gardiner, M. S., & Brown, E. R. (2000). Segregation in hot-mix asphalt pavements. *National Cooperative Highway Research Program Report*, *441*.

Gonzalez, R. F., & Woods R. E. (2001). *Digital image processing*, Prentice Hall, USA.

Gonzales, R. C., Woods, R. E., & Eddins, S. T. (2009). *Digital image processing using MATLAB*, Gatesmark Publishing.

Goh, S. W., & You, Z. (2009). A simple stepwise method to determine and evaluate the initiation of tertiary flow for asphalt mixtures under dynamic creep test. *Construction and Building Materials*, *23*(11), 3398-3405.

Gul, W. A. (2008). *Effect of recycled cement concrete content on rutting behaviour of asphalt concrete* (Doctoral dissertation, Doctoral Thesis, Middle East Technical University, Ankara).

Guler, M. (2003). *Characterization of hot mixture asphalt shear resistance and correlation with rutting performance*. (Doctoral dissertation, Doctoral Thesis, University of Wisconsin-Madison).

Hunter, A. E., Airey, G. D., & Collop, A. C. (2004). Aggregate orientation and segregation in laboratory-compacted asphalt samples. *Transportation Research Record*, *1891*(1), 8-15.

Hamad, M. L., Ellison, C. D., Khan, M. A., & Lyon, R. C. (2007). Drug product characterization by macropixel analysis of chemical images. *Journal of pharmaceutical sciences*, *96*(12), 3390-3401.

Hu, C., Youtcheff, J., Wang, D., Zhang, X., Kutay, E., & Thyagarajan, S. (2012). Characterization of asphalt mixture homogeneity based on X-ray computed tomography. *Journal of Testing and Evaluation*, *40*(7), 1082-1088.

Khedaywi, T. S., & White, T. D. (1995). Development and analysis of laboratory techniques for simulating segregation. *Transportation Research Record*, (1492), 36-45.

Li, X., Chen, S., Xiong, K., & Liu, X. (2018). Gradation segregation analysis of warm mix asphalt mixture. *Journal of Materials in Civil Engineering*, *30*(4), 04018027.

Li, Q., Lee, H. J., & Hwang, E. Y. (2010). Characterization of permanent deformation of asphalt mixtures based on shear properties. *Transportation Research Record*, *2181*(1), 1-10.

Masad, E., Muhunthan, B., Shashidhar, N., & Harman, T. (1998). Aggregate orientation and segregation in asphalt concrete. In *Application of Geotechnical Principles in Pavement Engineering, Proceedings of Sessions of Geo-Congress 98American Society of Civil Engineers*, *85*, 69-80.

Masad, E., Muhunthan, B., Shashidhar, N., & Harman, T. (1999). Internal structure characterization of asphalt concrete using image analysis. *Journal of computing in civil engineering*, *13*(2), 88-95.

MATLAB. (2015). *Image Processing Toolbox Release 2015a*, The MathWorks, Inc., Natick, Massachusetts, United States.

McAndrew, A. (2004). Introduction to d*igital image processing with MATLAB*, Thomson Course Technology, USA.

McCuen, R. H., & Azari, H. (2001). Assessment of asphalt specimen homogeneity. *Journal of transportation engineering*, *127*(5), 363-369.

Moon, K. H., Falchetto, A. C., Wistuba, M. P., & Jeong, J. H. (2015). Analyzing aggregate size distribution of asphalt mixtures using simple 2D digital image processing techniques. *Arabian Journal for Science and Engineering*, *40*(5), 1309-1326.

NCHRP Report 704. (2011). *A performance-related specification for hot-mixed asphalt* (NCHRP Report 704). Transportation Research Board.

Ozen, M., & Guler, M. (2014). Assessment of optimum threshold and particle shape parameter for the image analysis of aggregate size distribution of concrete sections. *Optics and Lasers in Engineering*, *53*, 122-132.

Onal, O. (2008). *Development and use of digital image analysis techniques for analyzing sectional characteristics of some geomaterials* (Doctoral dissertation, DEÜ Fen Bilimleri Enstitüsü).

Peng, Y., & Sun, L. J. (2009). Towards an index of asphalt mixture homogeneity. *Road Materials and Pavement Design*, *10*(3), 545-567.

Peng, Y., & Sun, L. J. (2009). Towards an index of asphalt mixture homogeneity. *Road Materials and Pavement Design*, *10*(3), 545-567.

Peng, Y., & Sun, L. J. (2011). Application of statistical methods in evaluating asphalt mixture homogeneity. *Journal of Testing and Evaluation*, *39*(3), 327-334.

Peng, Y., & Sun, L. J. (2016). Micromechanics-based analysis of the effect of aggregate homogeneity on the uniaxial penetration test of asphalt mixtures. *Journal of Materials in Civil Engineering*, *28*(11), 04016119.

Peng, Y., Harvey, J. T., & Sun, L. J. (2017). Three-Dimensional Discrete-Element Modeling of Aggregate Homogeneity Influence on Indirect Tensile Strength of Asphalt Mixtures. *Journal of Materials in Civil Engineering*, *29*(11), 04017211.

Peng, Y., & Sun, L. J. (2017). Aggregate distribution influence on the indirect tensile test of asphalt mixtures using the discrete element method. *International Journal of Pavement Engineering*, *18*(8), 668-681.

Roberts, F. L., Kandhal, P. S., Brown, E. R., Lee, D. Y., & Kennedy, T. W. (1991). Hot mix asphalt materials, mixture design and construction, Second Edition, NAPA Education Foundation Lanham, Maryland.

Schneider, C. A., Rasband, W. S., & Eliceiri, K. W. (2012). NIH Image to ImageJ: 25 years of image analysis. *Nature methods*, *9*(7), 671-675, PMID 22930834.

Sun, L. (2016). Structural Behavior of Asphalt Pavements, Elsevier Inc., 978-0-12-849908-5, 821.

Tashman, L., Masad, E., Peterson, B., & Saleh, H. (2001). Internal structure analysis of asphalt mixes to improve the simulation of Superpave gyratory compaction to field conditions. In *Association of Asphalt Paving Technologists Technical Sessions, 2001, Clearwater Beach, Florida, USA* (Vol. 70), 605-634.

Williams, R. C., Duncan Jr, G., & White, T. D. (1996). Hot-mix asphalt segregation: measurement and effects. *Transportation Research Record*, *1543*(1), 97-105.

Witczak, M. W., Kaloush, K., Pellinen T., El-Basyouny, M., & Von Quintus, H (2002). *Simple performance test for superpave mix design* (NCHRP Report 465). Transportation Research Board.

Witczak, M. W. (2005). *Simple performance tests: Summary of recommended methods and database* (NCHRP Report 547). Transportation Research Board.

Wu, W., Wang, D., & Zhang, X. (2011). Estimating the gradation of asphalt mixtures using X-ray computerized tomography and stereology method. *Road Materials and Pavement Design*, *12*(3), 699-710.

Yue, Z. Q., Bekking, W., & Morin, I. (1995). Application of digital image processing to quantitative study of asphalt concrete microstructure. *Transportation Research Record*, *1492*, 53-60.

Yue, Z. Q., & Morin, I. (1996). Digital image processing for aggregate orientation in asphalt concrete mixtures. *Canadian Journal of Civil Engineering*, *23*(2), 480-489.

Zhang, K., Zhang, Z., Luo, Y., & Huang, S. (2017). Accurate detection and evaluation method for aggregate distribution uniformity of asphalt pavement. *Construction and Building Materials*, *152*, 715-730.

Zhou, F., Scullion, T., & Sun, L. (2004). Verification and modeling of three-stage permanent deformation behavior of asphalt mixes. *Journal of Transportation Engineering*, *130*(4), 486-494.

APPENDICES

A. COMPARISON OF AGGREGATE SHAPE PARAMETERS USING VERTICAL AND HORIZONTAL SECTION IMAGES

The size distribution of aggregates was estimated by using the maximum Feret diameter and the equivalent circle diameter of aggregate particles to evaluate success of the parameters. Both the horizontal and vertical cross sections of laboratory prepared specimens were used for the size distribution analyses. For each mixture, only one vertical section image and one horizontal section image were used in the image analyses.

In the particle shape analysis, maximum Feret diameter is a line segment connecting the two perimeter points with the farthest distance between them. The diameter of an equal area circle is called equivalent circle diameter as shown in Figure A.1.

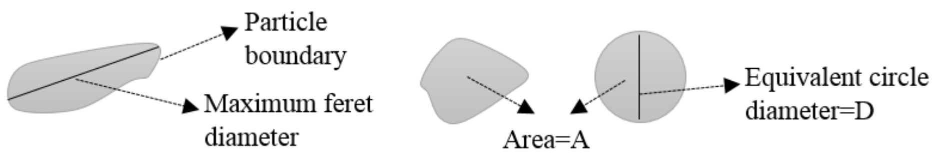

Figure A.1. Maximum Feret diameter and equivalent circle diameter of aggregate particles

For the calculation of percent passing from each size fraction, maximum Feret diameters and equivalent circle diameters were calculated and compared with the standard diagonal sieve sizes and square sieve sizes, respectively. Results of the 2D image based gradation are shown in Table A.1.

Table A.1. *Actual and estimated gradations*

Sieve Size (mm)	Actual	Percent Passed							
		Horizontal Sec.		Vertical Sec.		Horizontal Sec.		Vertical Sec.	
		Max. Feret	Eq. Dia.	Max. Feret	Eq. Dia.	Max. Feret	Eq. Dia.	Max. Feret	Eq. Dia.
		Mix-1				Mix-3			
19	100	100.0	100.0	100.0	100.0	100.0	100.0	100.0	100.0
12.5	88	89.9	84.1	89.7	90.7	90.8	89.6	95.1	94.8
9.5	72	71.3	71.4	76.7	76.7	78.6	76.4	86.1	82.4
4.75	42	40.6	42.2	43.7	44.7	44.1	41.4	45.9	44.6
2	25	23.1	24.1	23.4	24.7	24.1	23.7	25	25.3
0.425	10	10.0	10.0	10.0	10.0	10.0	10.0	10.0	10.0
		Mix-2				Mix-4			
12.5	100	100.0	100.0	100.0	100.0	100.0	100.0	100.0.	1000
9.5	90	89.6	88.3	92.1	94.4	90.9	89.2	94.6	95.1
4.75	72	70.3	71.1	72.9	74.5	72.3	72.4	77.6	76.9
2	53	48.9	49.9	51	53.4	52.8	53.4	54.1	54.4
0.425	28	28.0	28.0	28.0	28.0	28.0	28.0	28.0	28.0

The graphical comparison of the gradation analyses is given in Figure A.2 (a-d). In these graphs; H: horizontal cut surface, V: vertical cut surface, F: maximum Feret diameter and E: equivalent circle.

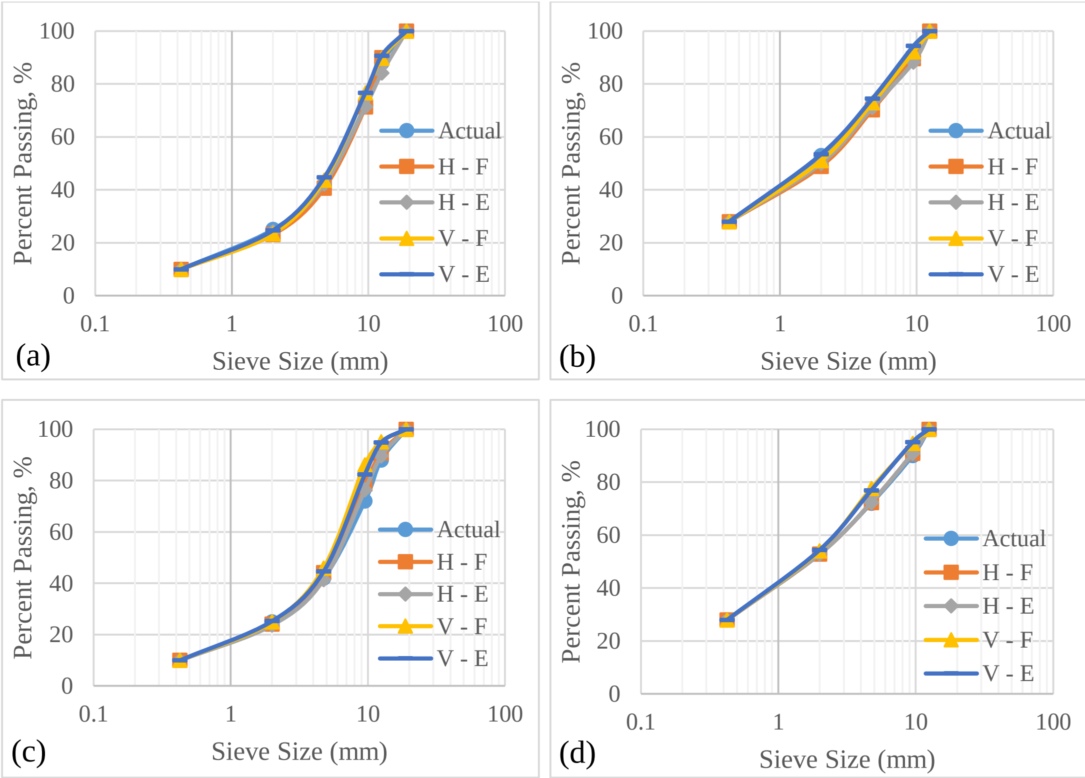

Figure A.2. Actual and estimated gradations; a) Mix-1, b) Mix-2, c) Mix-3, d) Mix-4

Analysis results show that maximum ferret diameter and equivalent circle diameter can be used to estimate the actual size distribution asphalt mixture specimens. However, maximum Feret diameter was selected as an optimal shape parameter to estimate actual gradations and implement homogeneity evaluation.

B. REDISTRIBUTION ALGORITHM FOR CIRCULAR CROSS SECTIONS

The developed redistribution algorithm has been modified to analyze inhomogeneity of horizontal cut sections. The algorithm detects all the particles located on the cross section and similar procedure to rectangular sections is applied. Figure B.1 shows obtained horizontal cross section image in RGB format and its binary format after image processing steps.

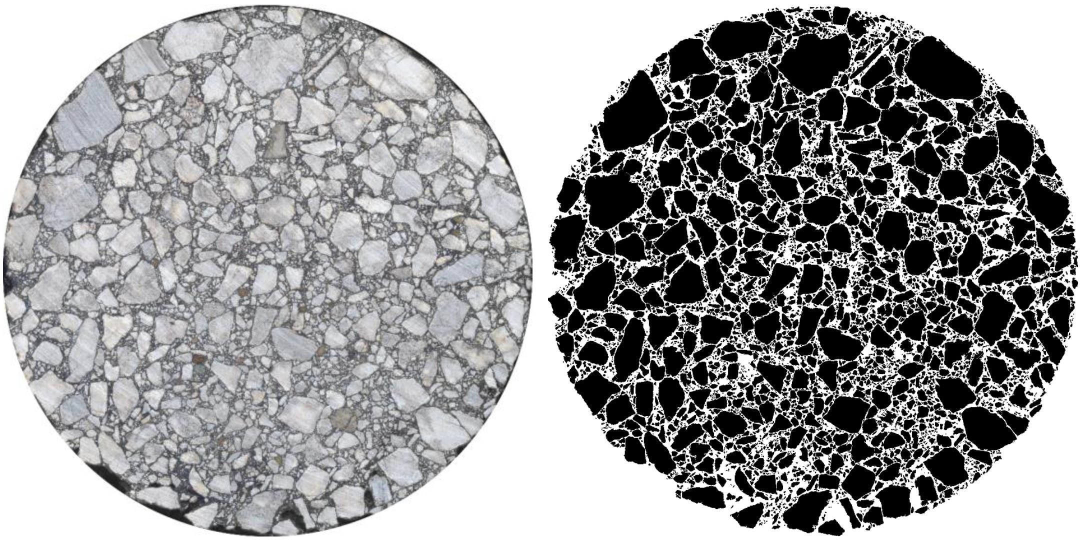

(a) (b)

Figure B.1. Horizontal section image; a) Original image, b) Binary image

Similar to the vertical sections, particle redistribution algorithm is implemented. Because the diameter of gyratory compacted specimens is 100 mm or 150 mm, image border is defined according to initial size. Figure B.2 shows the original image and an example synthetic image created using the redistribution algorithm.

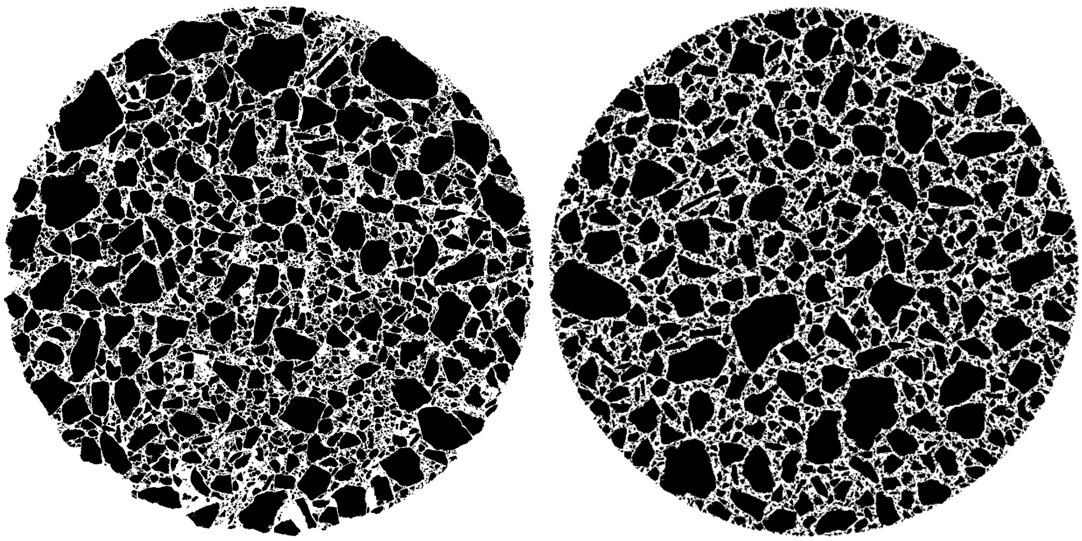

(a) (b)

Figure B.2. Aggregate redistribution; a) Original image, b) Synthetic image

Using the developed algorithm, inhomogeneity analysis can be conducted for circular cross sections.

C. SPECIMEN CROSS SECTIONAL IMAGES USED IN THE INHOMOGENEITY INDEX DEVELOPMENT STEP

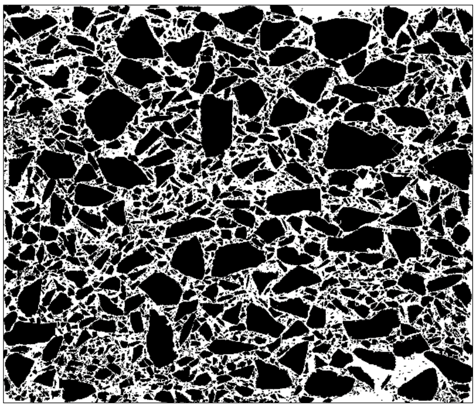

(a)

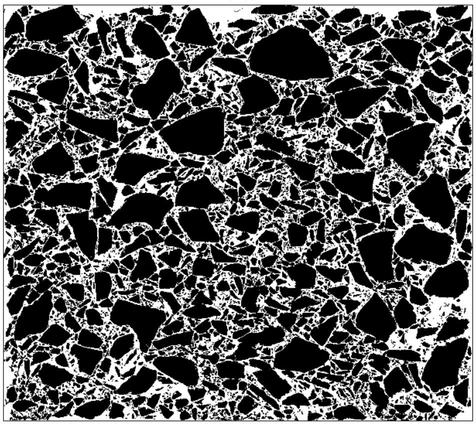

(b)

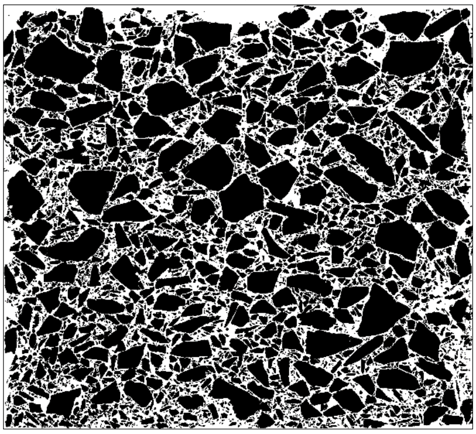

(c)

Figure C.1. Binary images for mix-1; a) S-1, b) S-2, c) S-3

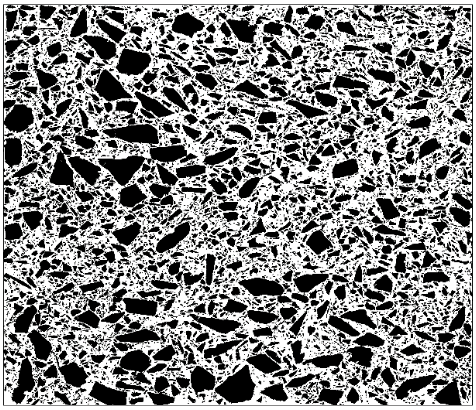
(a)
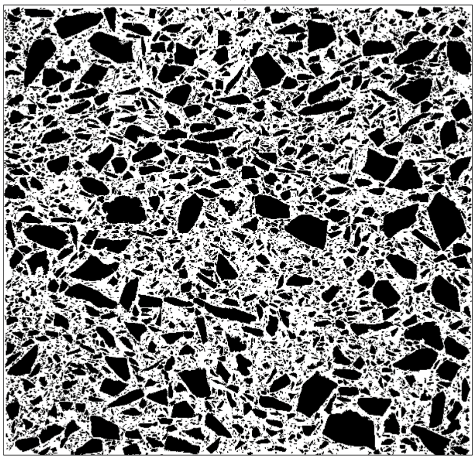
(b)
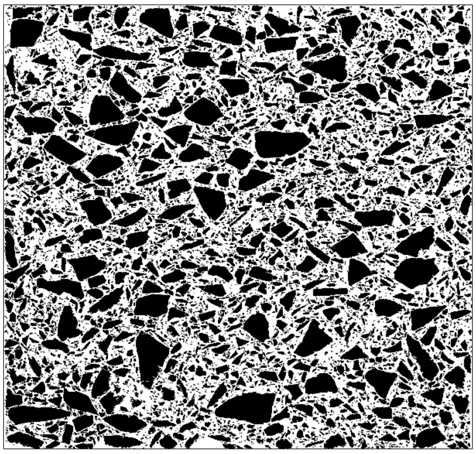
(c)

Figure C.2. Binary images for mix-2; a) S-1, b) S-2, c) S-3

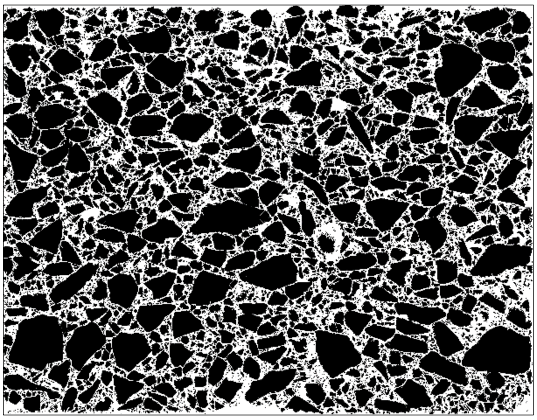
(a)

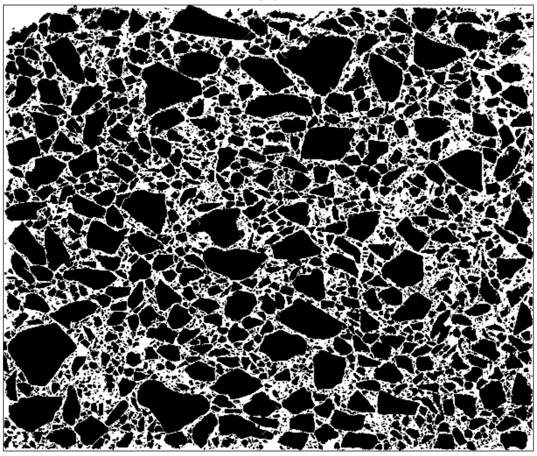
(b)

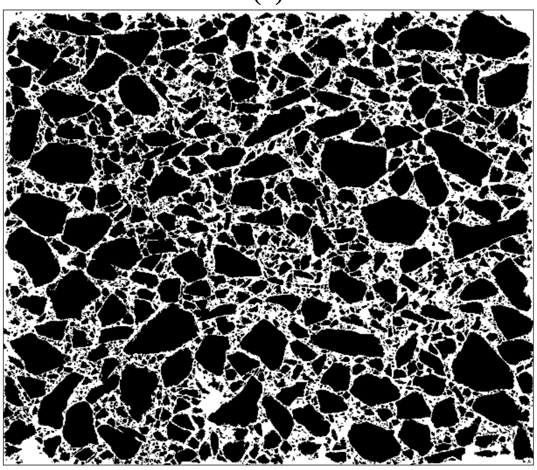
(c)

Figure C.3. Binary images for mix-3; a) S-1, b) S-2, c) S-3

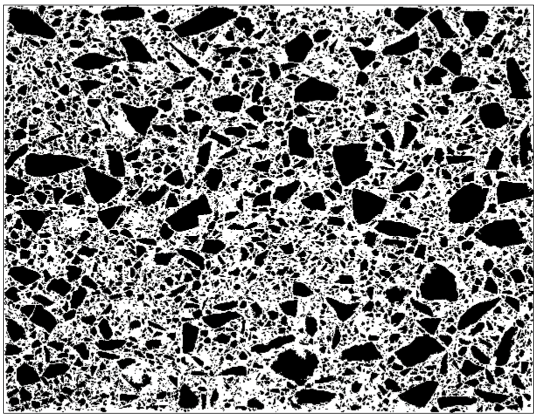
(a)
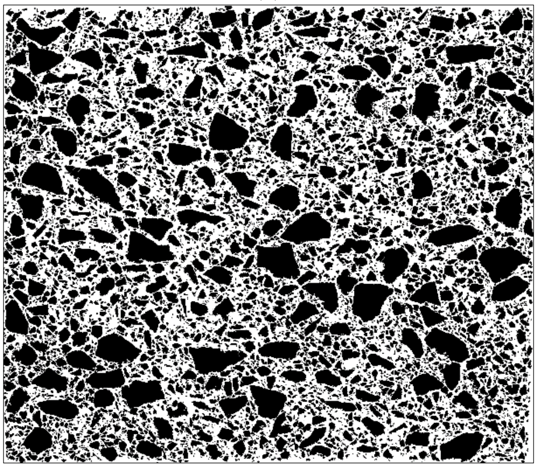
(b)
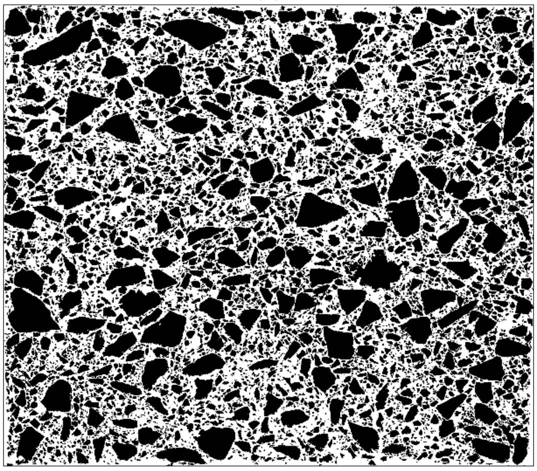
(c)

Figure C.4. Binary images for mix-4; a) S-1, b) S-2, c) S-3

D. COMPACTION CURVES OF THE SPECIMENS

Compaction curves for the group-1 and group-2 specimens are given below.

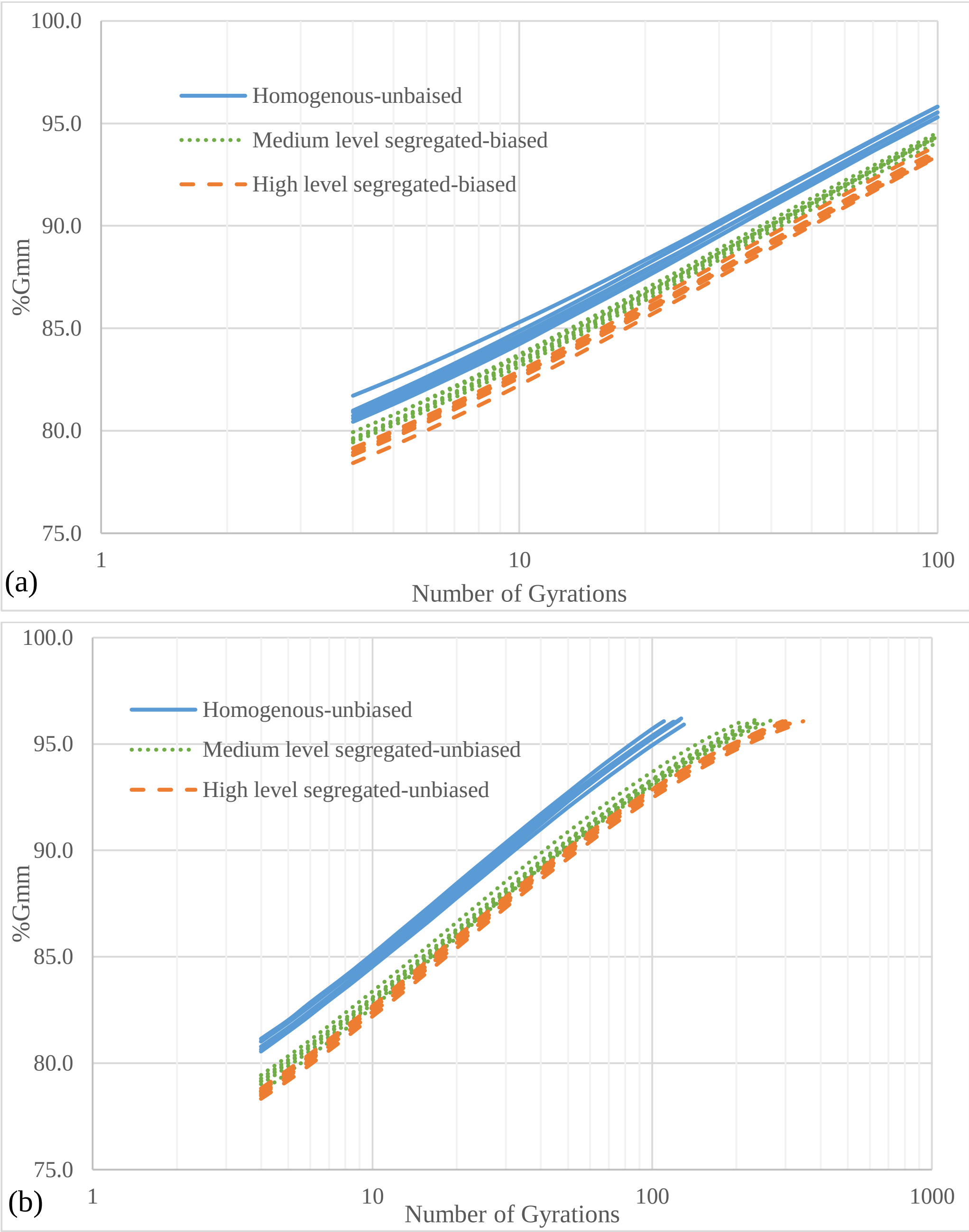

Figure D.1. Number of gyrations-Gmm%; a) Group-1 specimens, b) Group-2 specimens

E. END TREATMENT

To reduce friction between end platens and specimens, end treatments were placed. Latex membrane with approximately 0.5 mm thickness was used in this study. Silicone grease oil with 12500 cSt viscosity at room temperature was applied between the specimen and latex membrane to reduce friction. Viscosity test result obtained from rotational viscometer test of the silicone oil is given in Figure D.1.

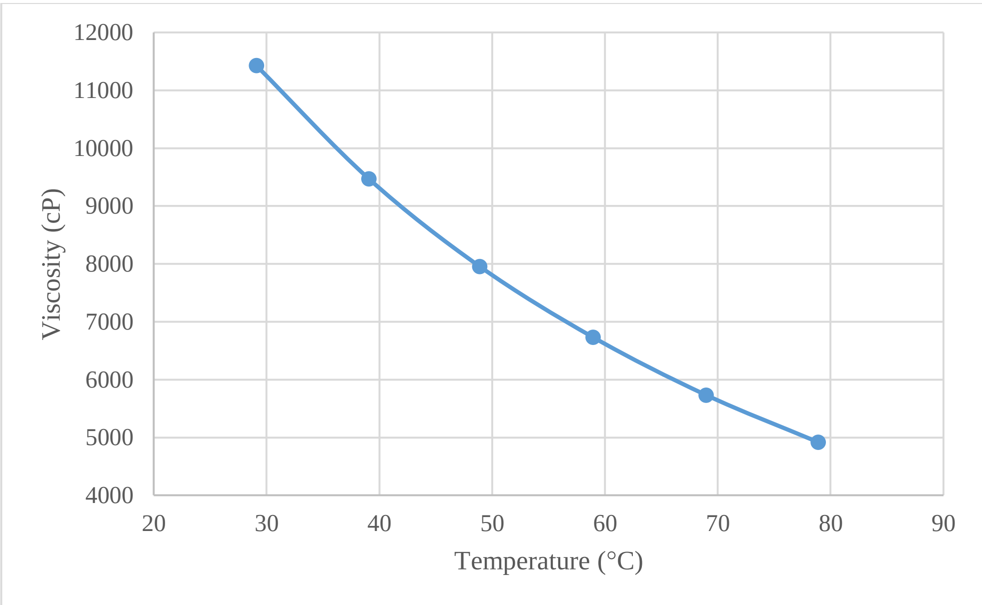

Figure E.1. Viscosity versus temperature graph for silicone oil

The test temperature for repeated creep test was selected as 42ºC in this study. Viscosity value of the silicone grease oil at this temperature was measured as approximately 9000 cP.

F. ASPHALT CONCRETE SPECIMENS AFTER REPEATED CREEP TEST

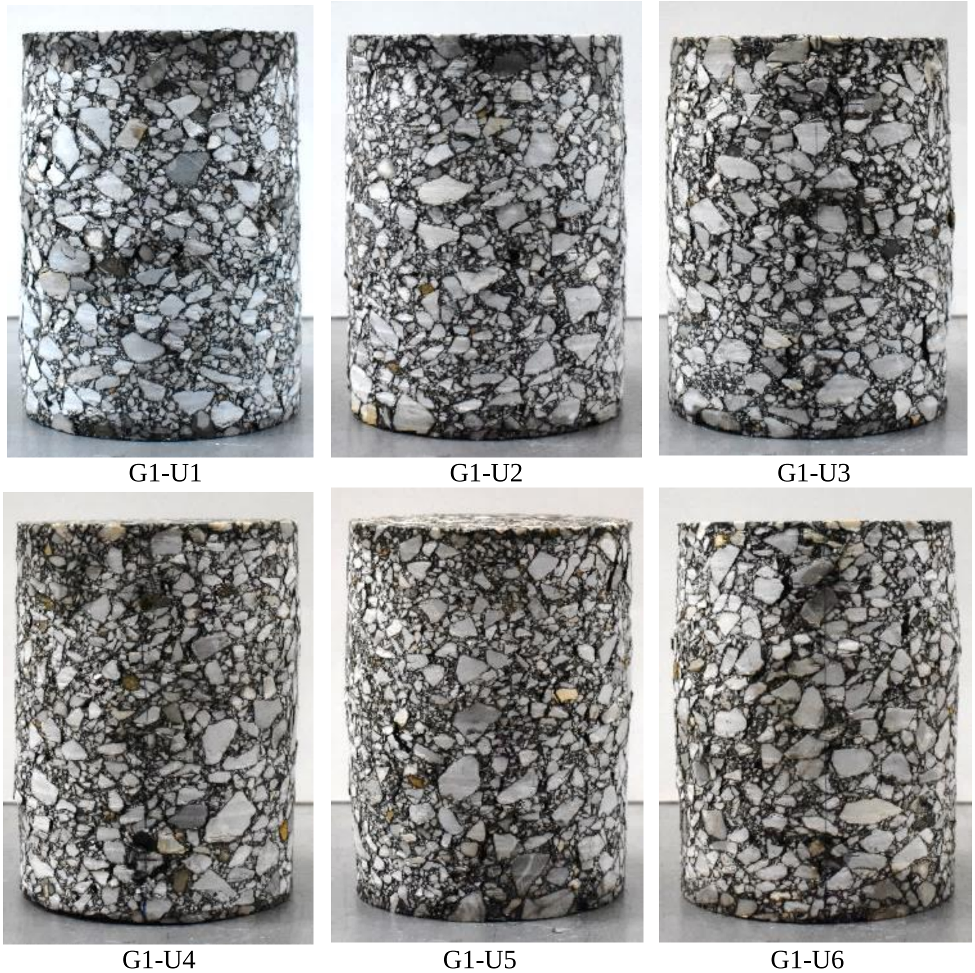

Figure F.1. Group-1 homogenous-unbiased test specimens after the test


G1-BM1


G1-BM2


G1-BM3


G1-BM4


G1-BM5


G1-BM6

Figure F.2. Group-1 medium level segregated-biased test specimens after the test

G1-BH1

G1-BH2

G1-BH3

G1-BH4

G1-BH5

G1-BH6

Figure F.3. Group-1 high level segregated-biased test specimens after the test

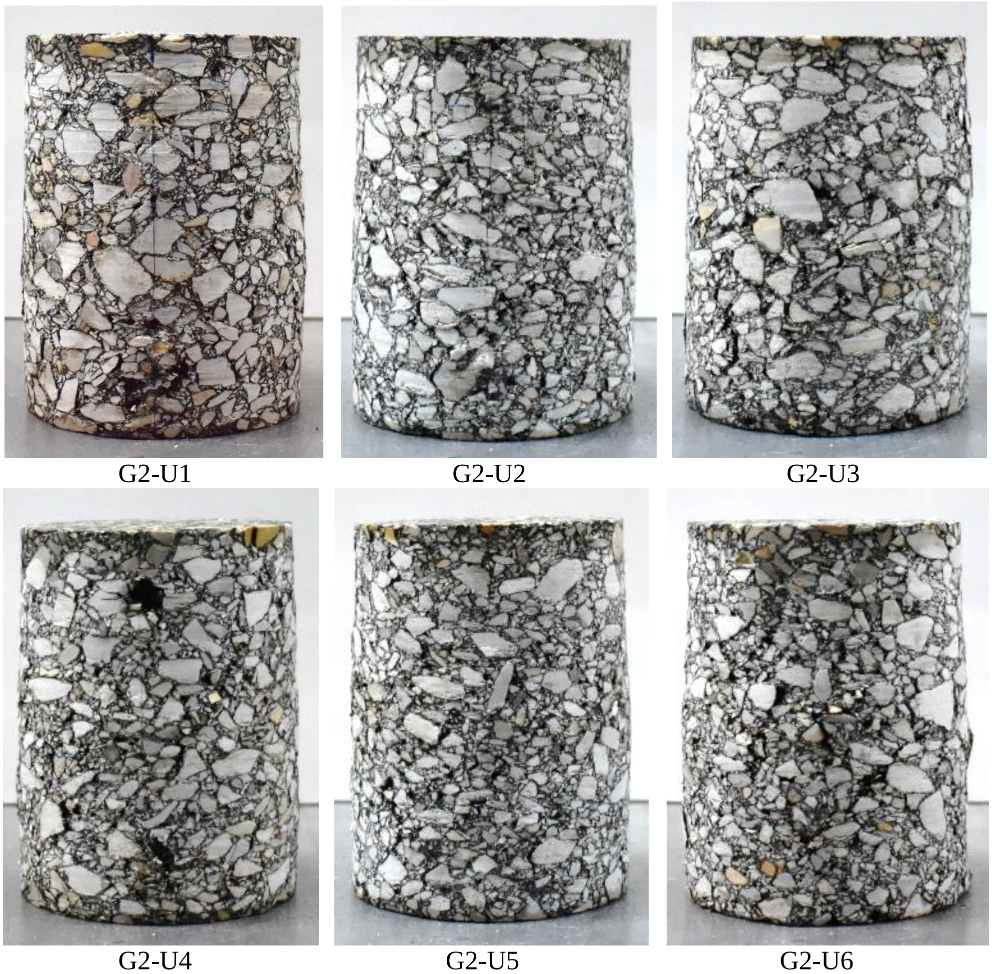

Figure F.4. Group-2 homogenous-unbiased test specimens after the test

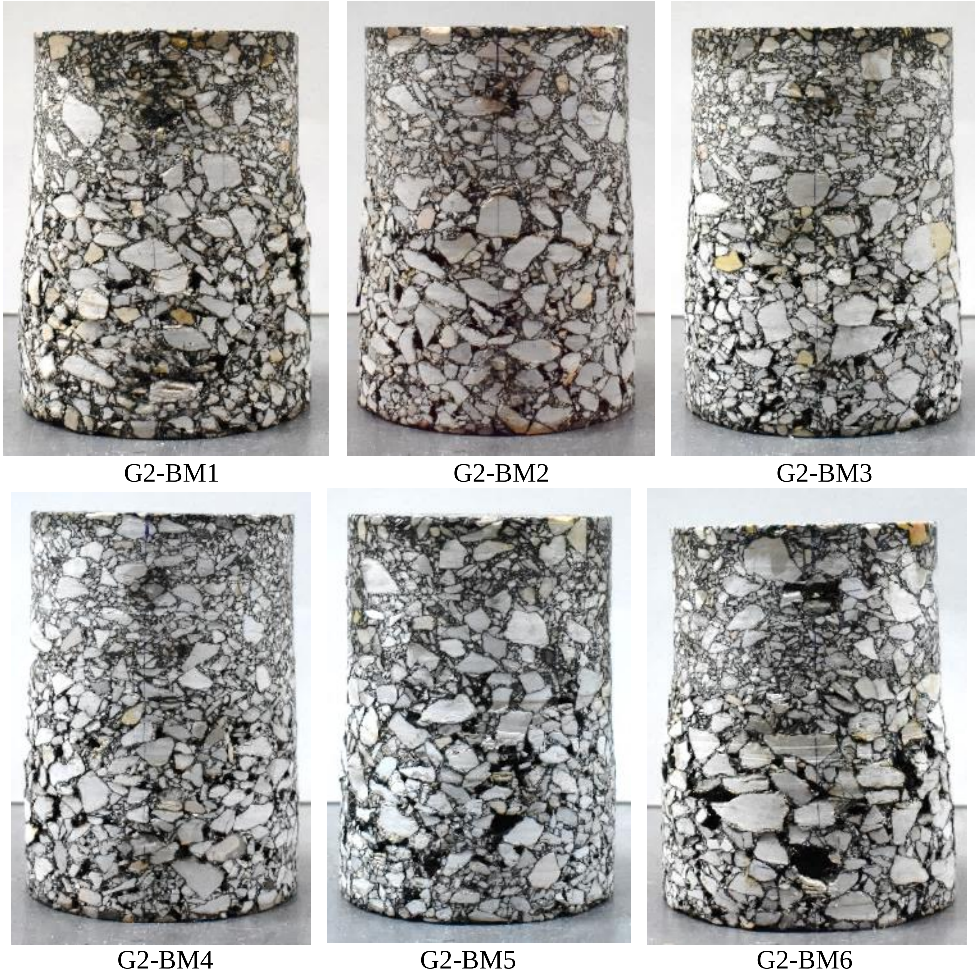

Figure F.5. Group-2 medium level segregated-biased test specimens after the test

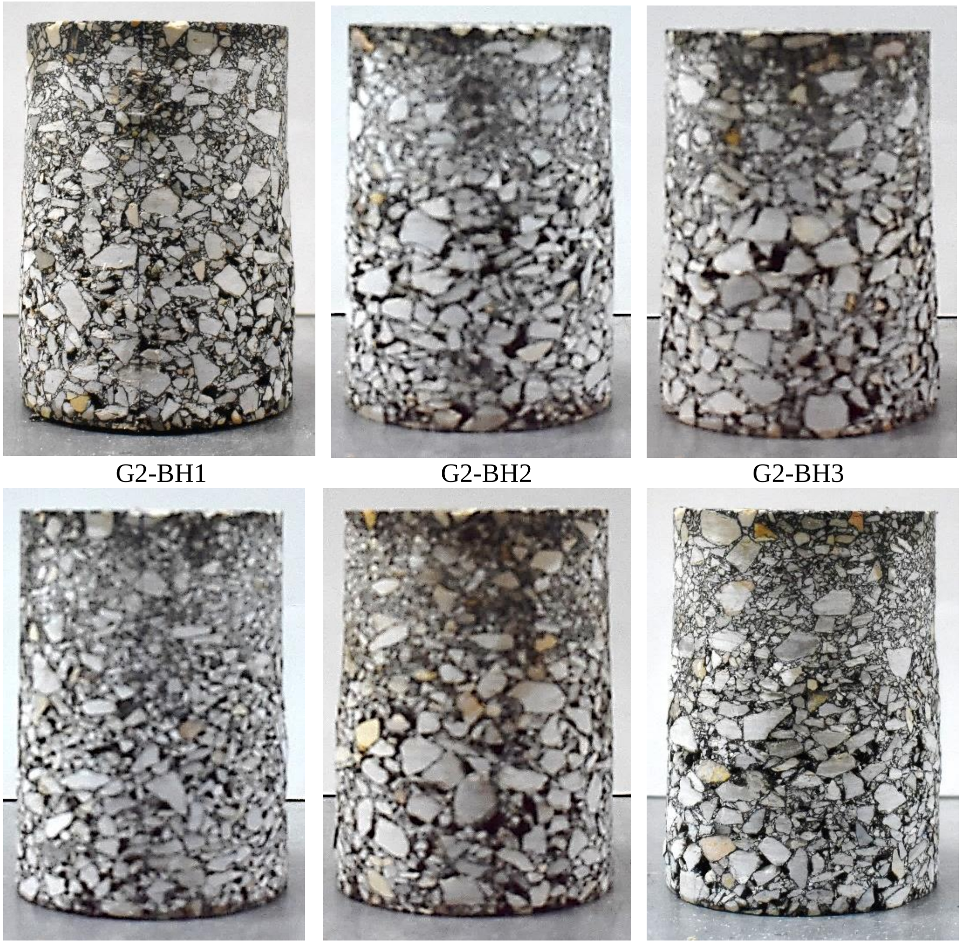

G2-BH1 G2-BH2 G2-BH3

G2-BH4 G2-BH5 G2-BH6

Figure F.6. Group-2 high level segregated-biased test specimens after the test

G. BINARY IMAGES OBTAINED FROM TESTED SPECIMEN CROSS SECTIONS

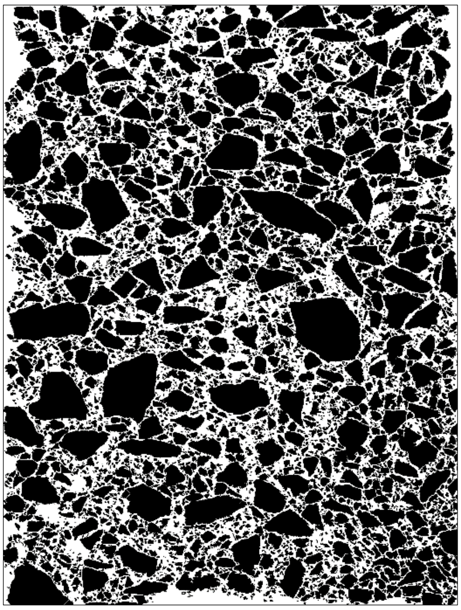

G1-U1

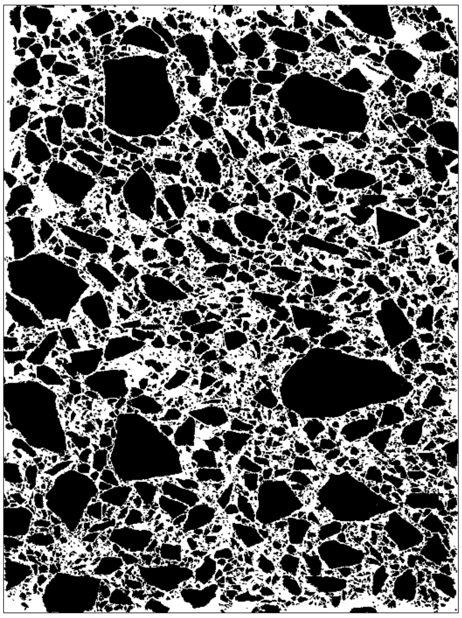

G1-U2

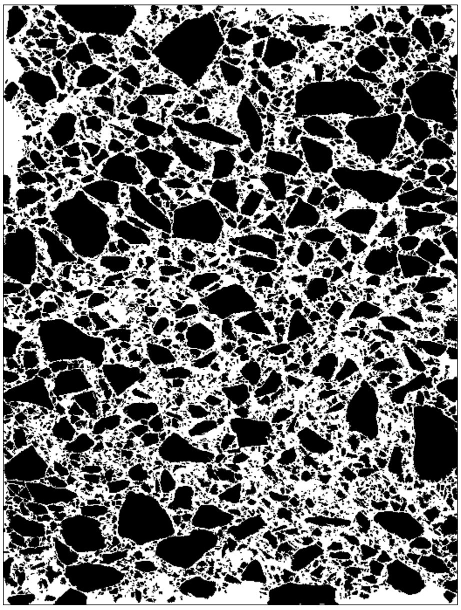

G1-U3

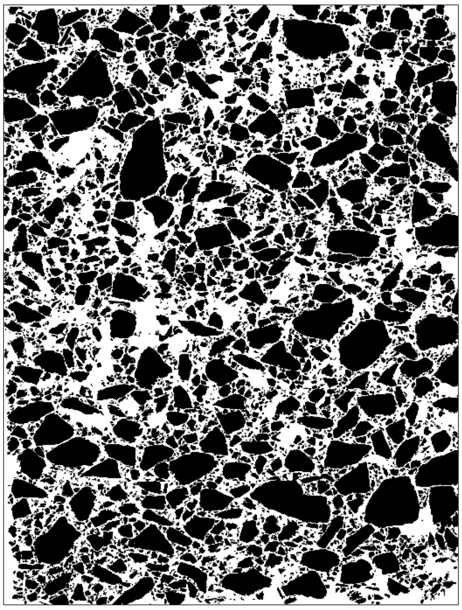

G1-U4

Figure G.1. Binary images for the tested specimens

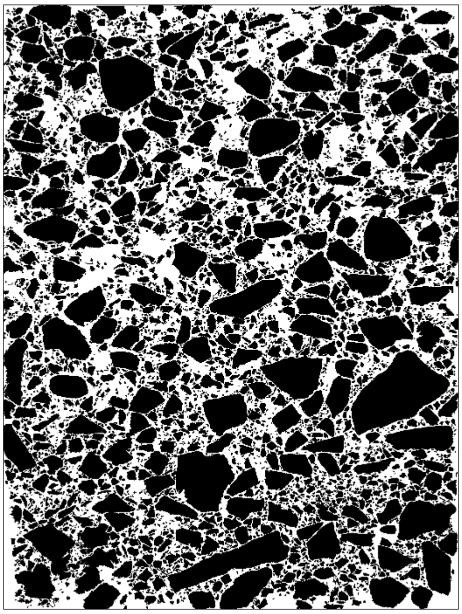

G1-U5

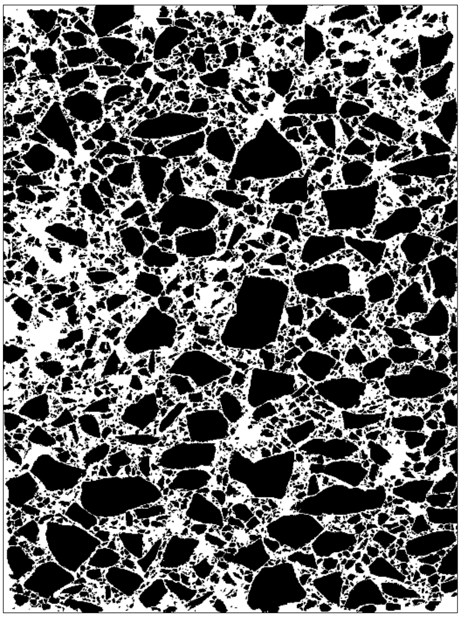

G1-U6

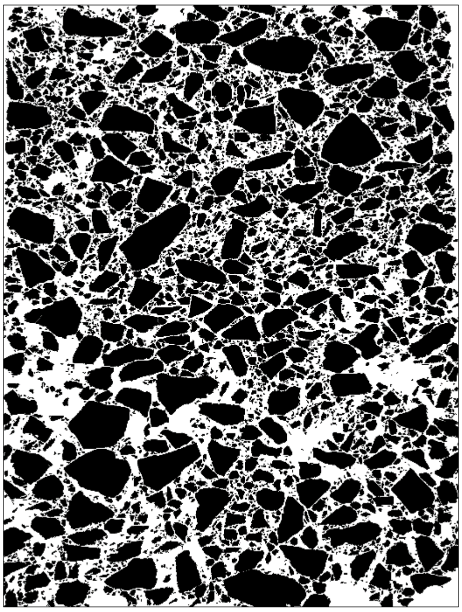

G1-M1

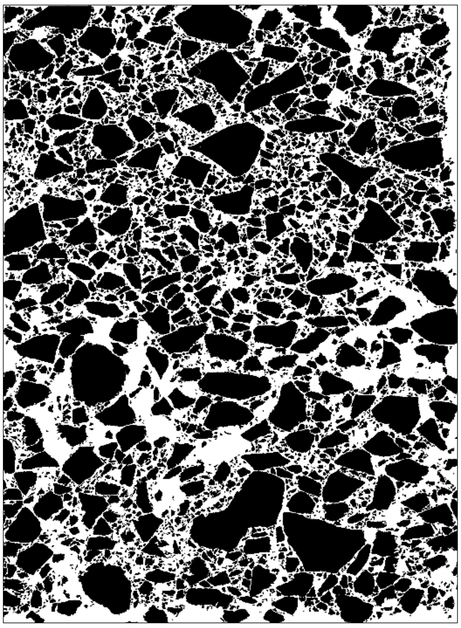

G1-M2

Figure G.1. (Continued)

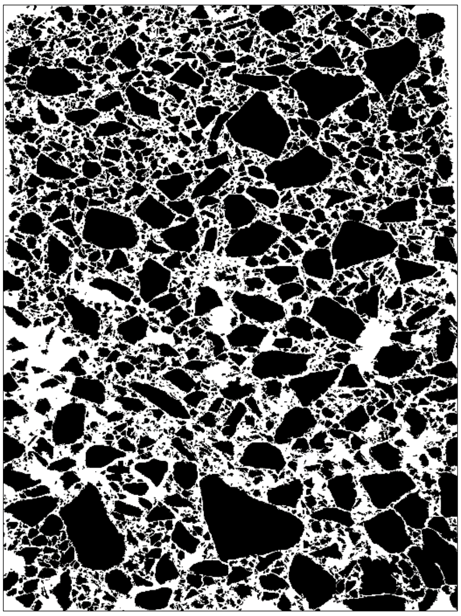

G1-M3

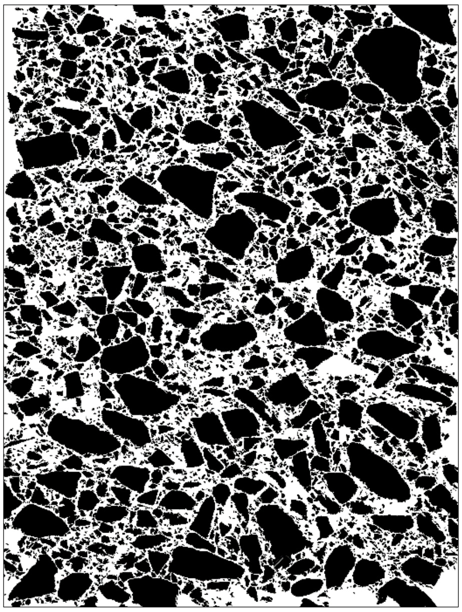

G1-M4

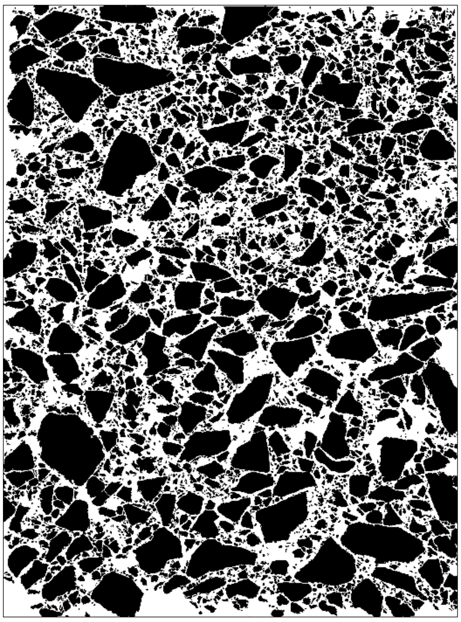

G1-M5

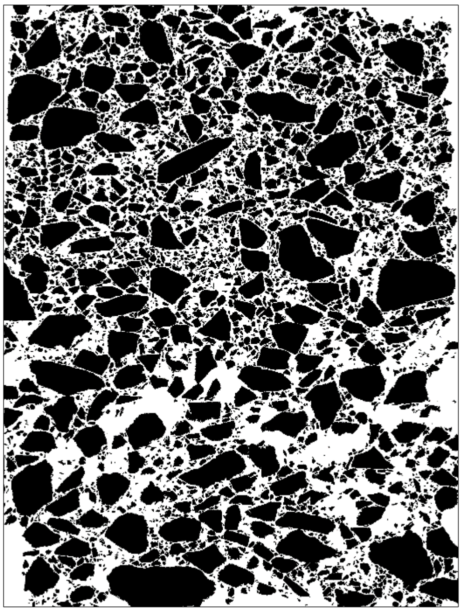

G1-M6

Figure G.1. (Continued)

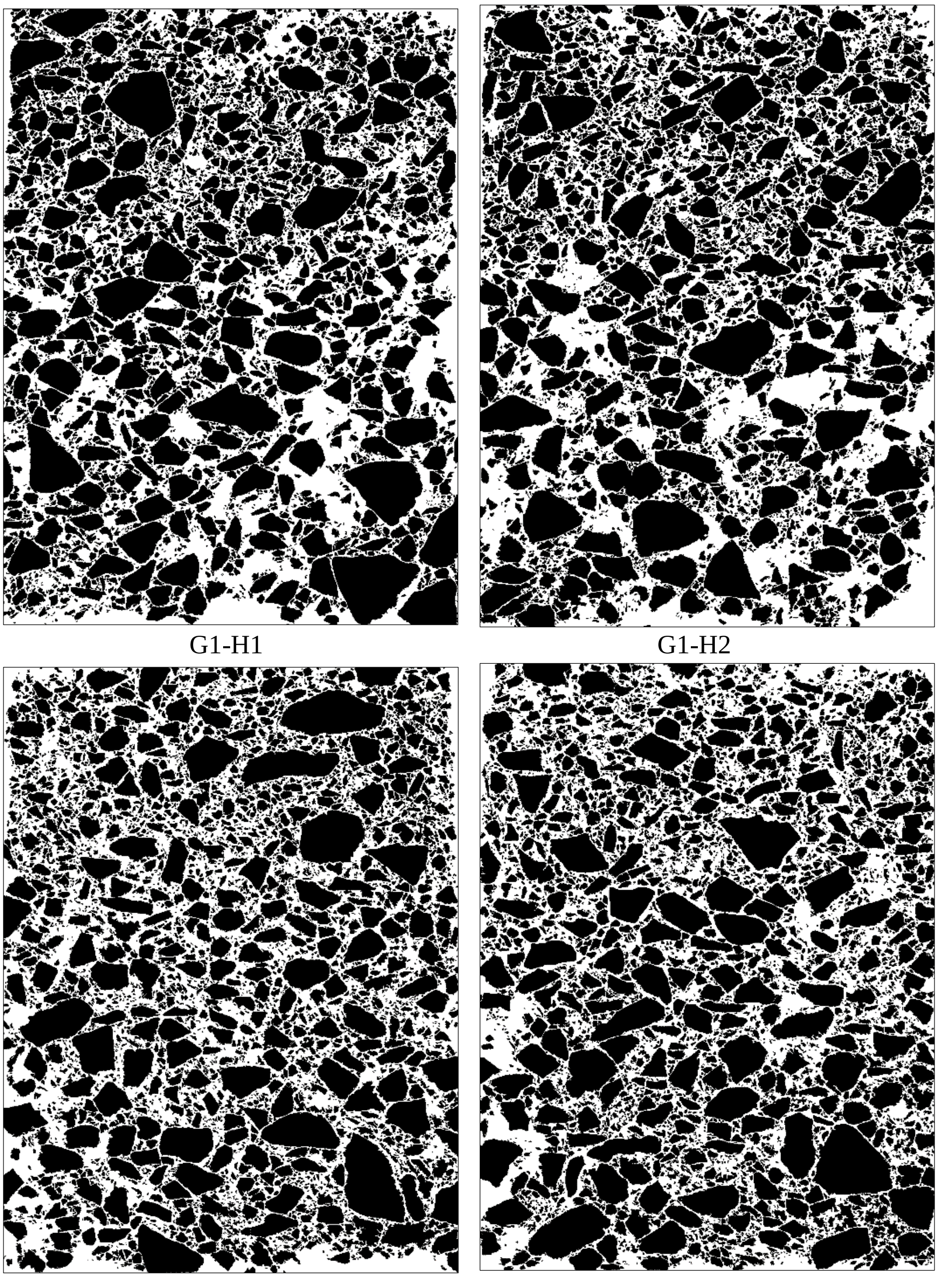

G1-H1 G1-H2

G1-H3 G1-H4

Figure G.1. (Continued)

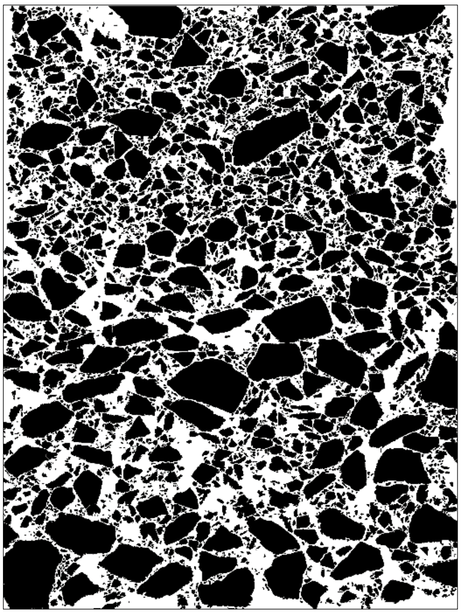

G1-H5

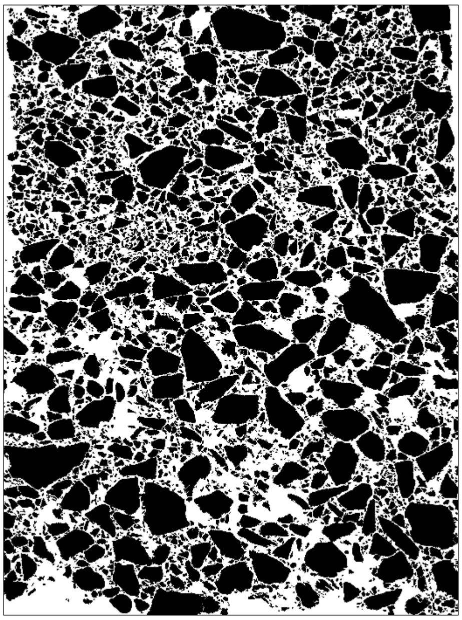

G1-H6

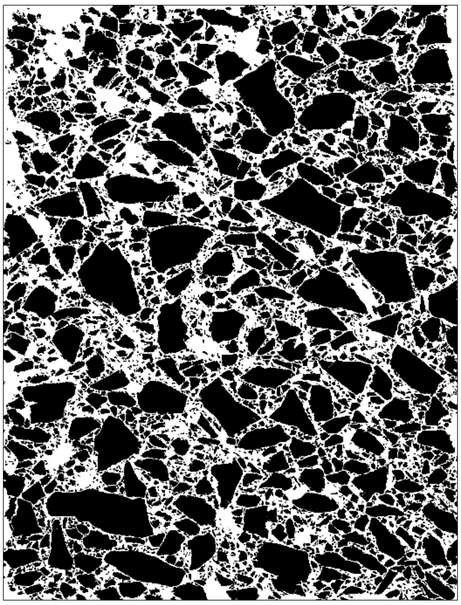

G2-U1

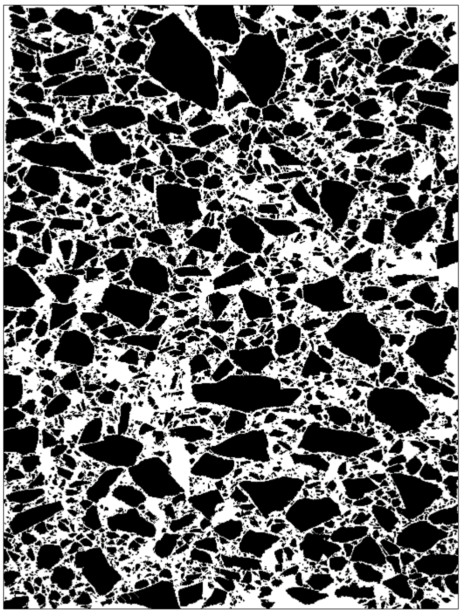

G2-U2

Figure G.1. (Continued)

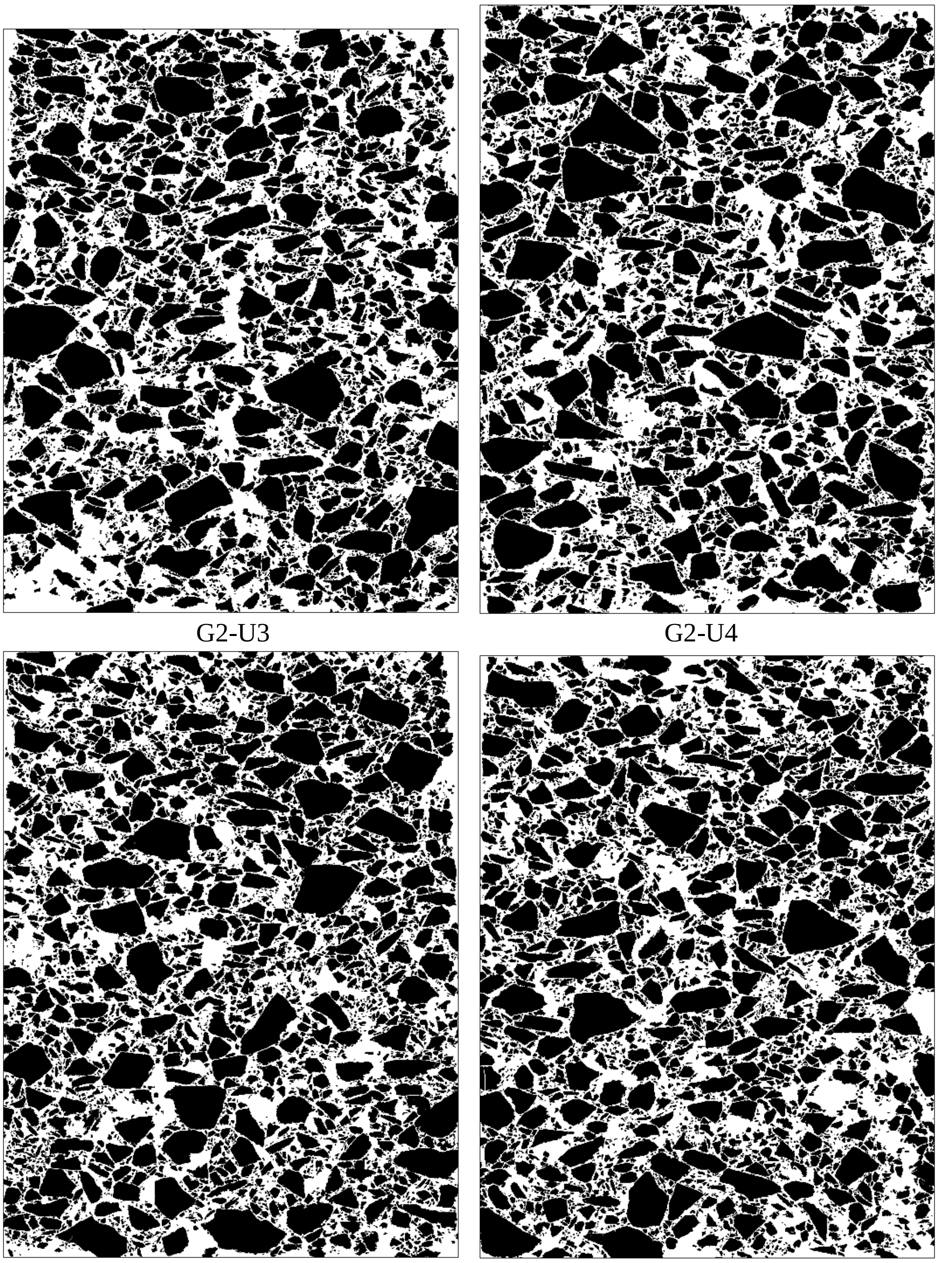

Figure G.1. (Continued)

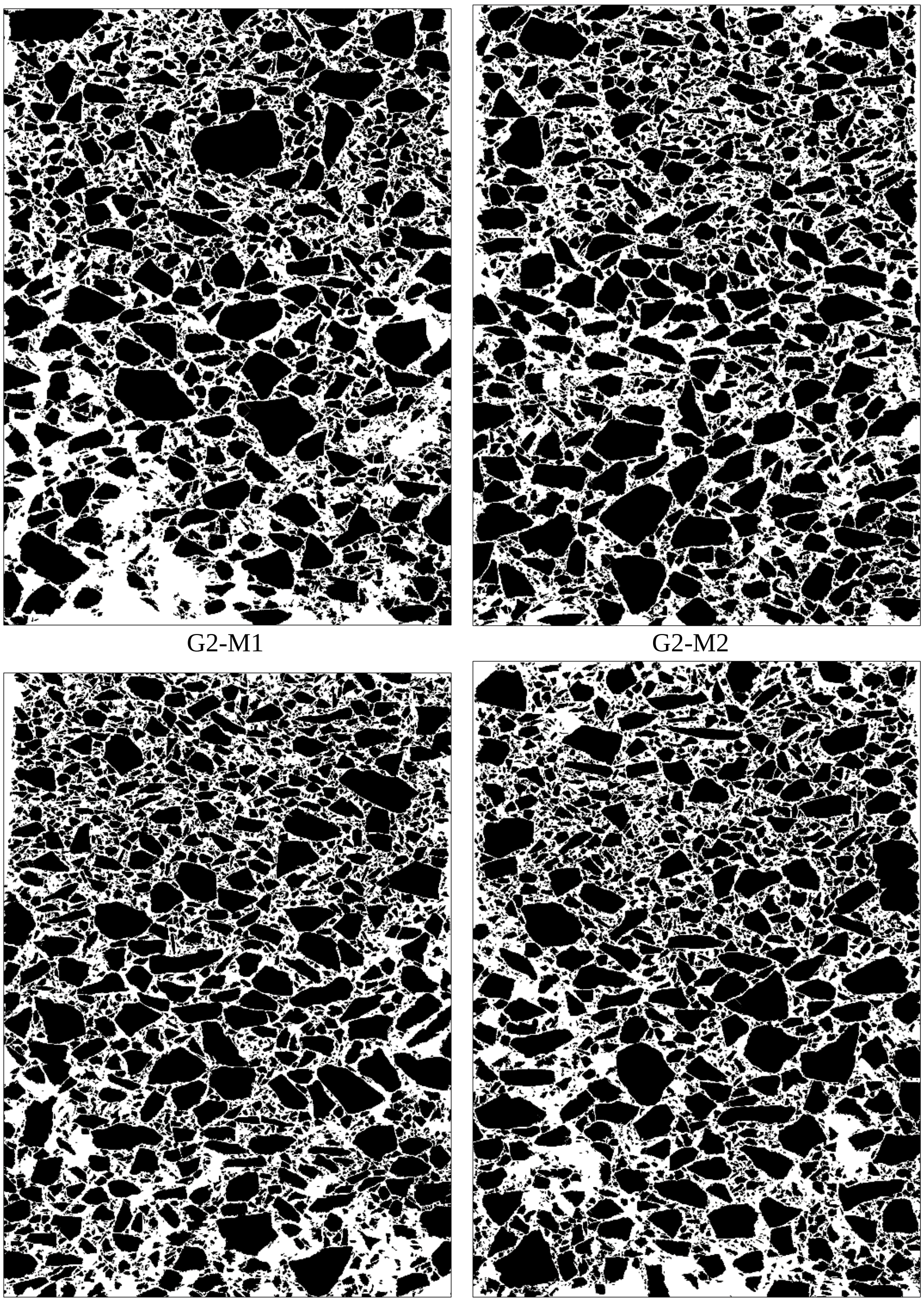

G2-M1 G2-M2

G2-M3 G2-M4

Figure G.1. (Continued)

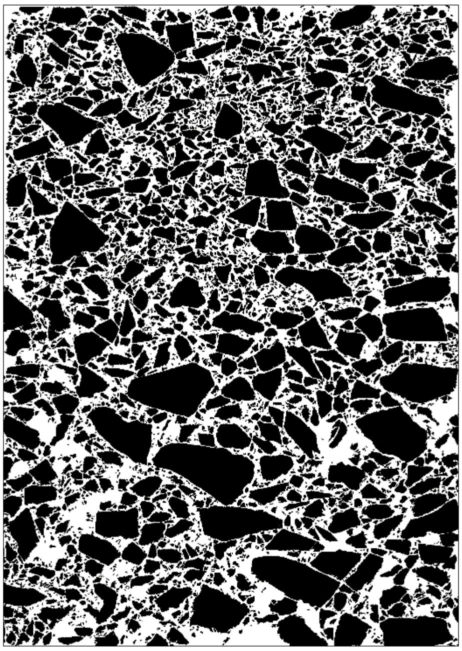

G2-M5

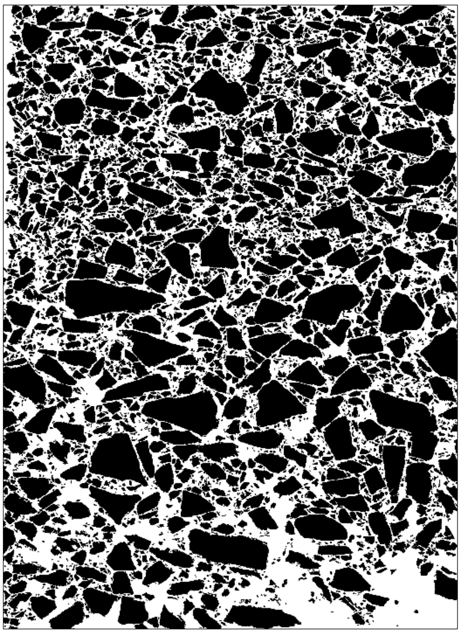

G2-M6

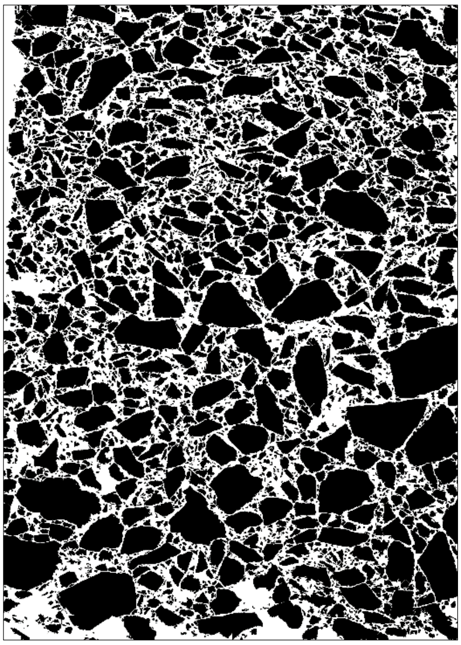

G2-H1

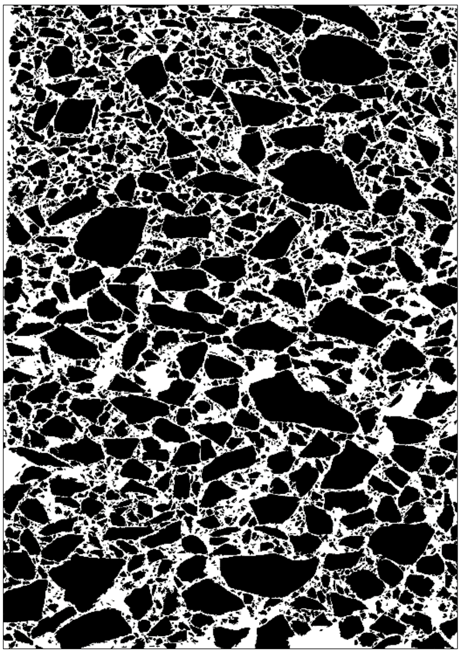

G2-H2

Figure G.1. (Continued)

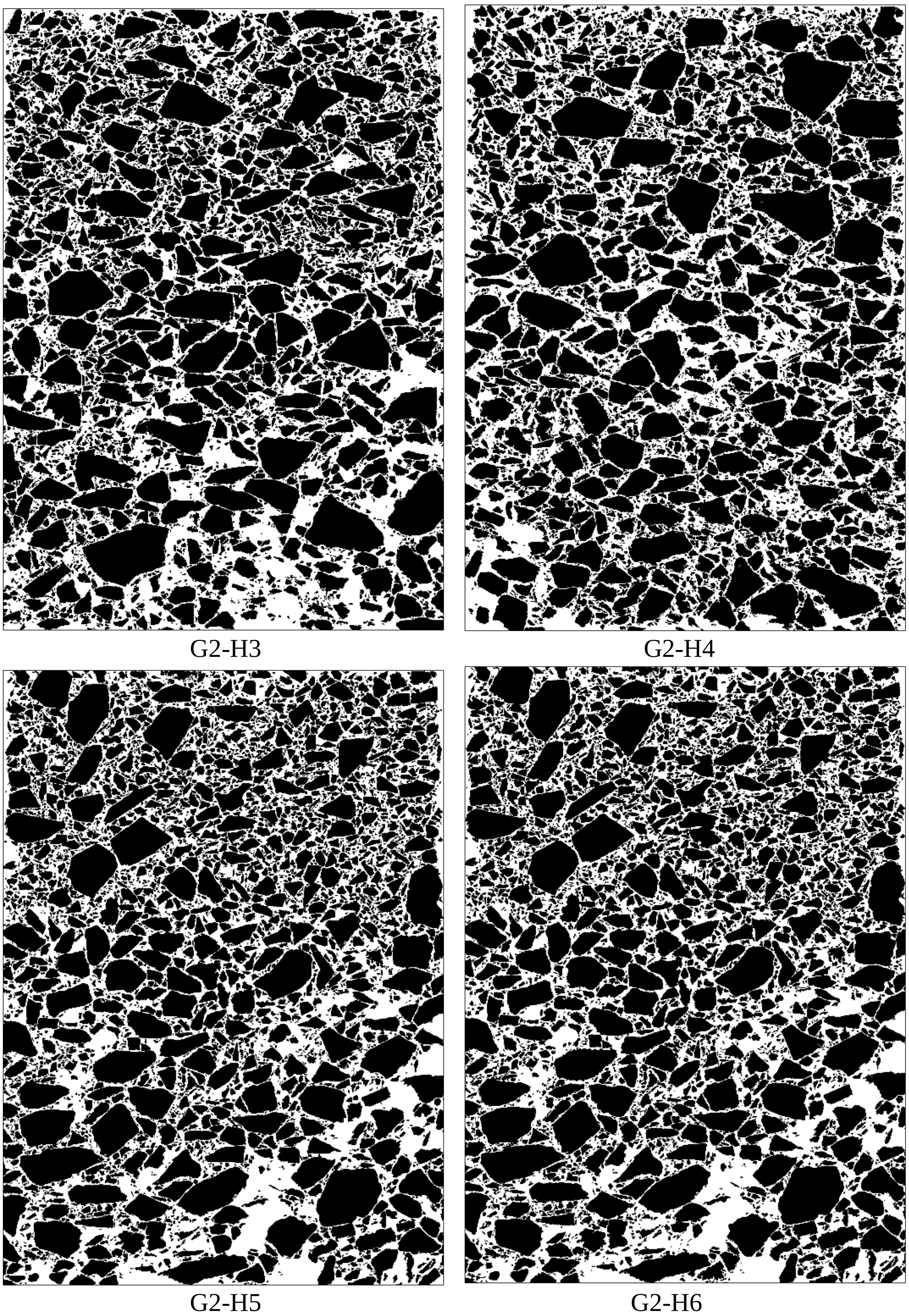

Figure G.1. (Continued)

CURRICULUM VITAE

PERSONAL INFORMATION

Surname, Name : Yücel, Ayhan Öner
Nationality : Turkish (TC)
Date and Place of Birth : 28 November 1989, Gemerek
E-mail : aoyucel@adu.edu.tr

EDUCATION

Degree	**Institution**	**Year of Graduation**
MS	MKU Civil Engineering	2012
BS	MKU Civil Engineering	2010

WORK EXPERIENCE

Year	**Place**	**Enrollment**
2019-Present	Aydın Adnan Menderes University Civil Engineering	Research Assistant
2013-2019	Middle East Technical University Civil Engineering	Research Assistant
2012-2013	Aydın Adnan Menderes University Civil Engineering	Research Assistant

FOREIGN LANGUAGES

Advanced English

PUBLICATIONS

Journal Articles / Book Chapters

1. Yucel, A. O., & Guler, M. (2019). Characterization of Homogeneity of Asphalt Concrete Using 2D Cross-Sectional Images. In: Pradhan B. (eds) GCEC 2017. GCEC 2017. *Lecture Notes in Civil Engineering*, vol 9. Springer, Singapore

2. Yücel, A., Atahan, A., Arslan, T., & Sevim, U. (2018). Traffic safety at median ditches: steel vs. concrete barrier performance comparison using computer simulation. *Safety*, *4*(4), 50.

3. Atahan, A. O., Yücel, A. Ö., & Erdem, M. M. (2014). Crash testing and evaluation of a new generation L1 containment level guardrail. *Engineering Failure Analysis, 38,* 25-37.

4. Atahan, A. O., & Yucel, A. O. (2013). Laboratory and field evaluation of recycled content sign posts. *Resources, Conservation and Recycling, 73,* 114-121.

5. Atahan, A. O., & Yücel, A. Ö. (2012). Crumb rubber in concrete: static and dynamic evaluation. *Construction and Building Materials*, *36*, 617-622.

Conferences

1. Yucel, A. O., & Guler, M. (2018). Evaluation of Aggregate Size Effect on Asphalt Mixture Homogeneity Using Image Analysis. 13th International Congress on Advances in Civil Engineering, October 12-14, Çeşme-İzmir, Turkey.

2. Yucel, A. O., & Guler, M. (2017). Characterization of Homogeneity of Asphalt Concrete Using 2D Cross-Sectional Images. 1st Global Civil Engineering Conference (GCEC 2017), July 25-28, Kuala Lumpur, Malaysia.

3. Atahan, A. O., Yucel, A. O., & Guven, O. (2013). Development of N2–H1 Performance-Level Guardrail: Crash Testing and Simulation. *Transportation Research Circular*, (E-C172).

4. Atahan, A. O., Yucel, A. O., & Guven, O. (2012). Risks of Unprotected Median Drainage Ditches on Vehicle Stability. *Proceedings of the Roadside Safety Design and Devices, Milan, Italy*, 135-142.